Spring 12-12-2022

Angiogenesis and Endothelial Dysfunction: Insights of Autophagy Machinery in Regulating Endothelial cell Biology

Hongmin Yao

Angiogenesis and Endothelial Dysfunction: Insights of Autophagy Machinery in Regulating Endothelial cell Biology

by

Hongmin Yao

Under the Direction of Zhonglin Xie, PhD

A Dissertation Submitted in Partial Fulfillment of the Requirements for the Degree of

Doctor of Philosophy

in the College of Arts and Sciences

Georgia State University

2022

ABSTRACT

Autophagy is an intracellular degradation system that delivers cytoplasmic components to the lysosome for degradation. Autophagy is essential for cellular homeostasis and provides a mechanism to adapt to metabolic and stress cues. Endothelial autophagy regulates the response of ECs to a variety of stress factors related to EC homeostasis and plasticity. However, the precise role of autophagy in angiogenesis requires more detailed research. Although autophagy-related 7 (ATG7) is essential for classical degradative autophagy and cell cycle regulation, whether and how ATG7 influences endothelial cell (EC) function and regulates post-ischemic angiogenesis remain unknown. Endothelial dysfunction is a potential contributor to the pathogenesis of diabetic cardiovascular complications. However, little is known about disruptions of endothelial autophagy contributing to diabetes-induced endothelial dysfunction. This dissertation aims to address how ATG7 influences endothelial cell (EC) function and regulates post-ischemic angiogenesis, and to determine the role of autophagy in the development of endothelial dysfunction.

EC-specific deletion of *Atg7* significantly impaired angiogenesis, delayed the recovery of blood flow reperfusion, and displayed reduction in hypoxia inducible factor 1 subunit alpha (HIF1A) expression. Mechanistically, lack of ATG7 in the cytoplasm disrupted the association between ATG7 and transcription factor ZNF148/ZBP-89 that is required for STAT1 (signal transducer and activator of transcription1) constitutive expression, increased the binding between ZNF148/ZBP-89 and importin-β1 (KPNB1), which promoted ZNF148/ZBP-89 nuclear translocation, and increased STAT1 expression. STAT1 bond to *HIF1A* promotor and suppressed *HIF1A* mRNA expression, thereby preventing ischemia-induced angiogenesis. These results demonstrate that *ATG7* deficiency is a novel suppressor of ischemia-induced angiogenesis.

In addition, streptozotocin (STZ)-induced type 1 diabetes inhibits autophagic flux and reduced protein levels of autophagy gene related protein, including ULK1, ATG7, ATG5, and Beclin1, which was accompanied by an impairment of acetylcholine-induced relaxation of isolated mouse aortas. Inhibition of endothelial autophagy by the deletion of endothelial ULK1 exacerbated diabetes-induced endothelial dysfunction, reactive oxygen species (ROS) overproduction and impeded endothelial nitric oxide synthase (eNOS) phosphorylation. Mechanistically, suppression of autophagy by diabetes aggravated ROS overproduction. Downregulation of ULK1 reduced eNOS phosphorylation. Thus, promoting autophagy activity may be a potential strategy to prevent endothelial dysfunction in diabetes.

INDEX WORDS: Autophagy, Angiogenesis, ATG7, Endothelial dysfunction, ULK1, Type 1 diabetes

Angiogenesis and Endothelial Dysfunction: Insight of Autophagy Machinery in Regulating Endothelial Biology

by

Hongmin Yao

Committee Chair: Zhonglin Xie

Committee: Deborah Baro

Andrew Ted Gewirtz

Minghui Zou

Electronic Version Approved:

Office of Graduate Services

College of Arts and Sciences

Georgia State University

December 2022

DEDICATION

To my husband Hao Xing, who loves me and takes care of me like a child.

To my mother Jianyun Sun and my father Jianjie Yao, who wish me the best and love me the most.

To families and friends in China, I always remember the lovely time we spent together.

ACKNOWLEDGEMENTS

Number one, I would like to express my grateful to my advisor, Dr. Zhonglin Xie. He is an accommodating advisor and mentor, who is always not pushing me and understanding all the mistakes I made. Thank him for all the help and sharing his precious experience with me.

Secondly, I would like to thank Dr. Minghui Zou, who dedicated his effort to build up the center of Center for Molecular and Translational Medicine and provided the extraordinary experimental environment for the researchers and thank him for improving my presentation skill and encouraging me to graduate. Thank for all the research seminars you held for us.

Thirdly, I would like to thank my dissertation committee members, Dr. Deborah Baro and Dr. Andrew Ted Gewirtz for providing their thoughts and suggestions in the dissertation proposal and the final dissertation defense.

I am also willing to thank some faculty member I met at GSU. I want to thank Dr. Bingzhong Xue, Dr. Andrew Ted Gewirtz and Dr. Hang Shi to be the committee members in my qualifying examination. They contributed priceless and far-reaching advice in my writing and presentation. Sharon Leigh Cavusgil, an English speaking and writing teacher in GSU, taught me how to present on the stage with no fear and to write in a professional manner. Thanks Dr. Chun Jiang, who showed the true love in science and teaching that will affect me in a long period of my life. Dr. Julia Hilliard, I took her Graduate Survival Skill class, and I learnt multiple grant-writing methods and knew the true logic of research from her. Dr. Blaustein and Drew presented their knowledge of teaching and shaped me as a qualified teaching assistant. Dr. Ping Song, who always enthusiastically discusses the projects in the group meeting and raises many key questions in my research to clear my mind. Dr. Chunying Li, who provides helps without a doubt and broaden my mind by introducing other scientists in the research seminar.

I would also like to thank the staff at GSU. Larialmy Marteace Allen, Tameka Hudson and Kristanna Chanel Barnes, the coordinators of graduate student, they offered their expertise in administrative assistance. Dr. Charles Hampton recovered one portable hard disk and one USB flash drive and I am astonished by his technology background. Members from biology core facility, Jesse M Gardner, Sonja Young, and Debby Walthall, helped me with DNA sequencing and trained me to use core facility instruments. Members from animal core facility, Joi Darcel McNair, Kim Bryant, and Courtnye D. Billingsley, I want to thank you for taking care of the mice and showed me the professional way to do animal surgery.

I would also like to thank the colleagues in Center for Molecular and Translational Medicine, including but not limited to Dr. Qiulun Lu, who trained me animal surgery, cardiac function measurement by echocardiography, retina isolation and muscular tissue dissection; Dr. Shengnan Wu, taught me to do immunoprecipitation experiment and take images by confocal microscopy and shared her experience in scientific study; Dr. Jian Li, inspires me by endeavoring his efforts on research and always provides helps in my projects; Dr. Zhixue Liu, is a knowledgeable researcher and has excellent memory, who I can always get valuable suggestions for my projects from him; Yu Qiu, thank for her hard work in genotyping. Thank Ms. Zhengxing Zhao, who burdens the management of the whole lab and takes care of everyone in the lab. My researching work could not proceed that smooth without her help. Thanks for the experimental consumption preparation from Hsinying Tammy Ku, Zeidy Rivera Morales and Xicong Tang. Thanks for the help from Izaura Karmen Garrison, Fa'Tima Geeston, Kay Gilstrap. Thanks to Junqing An, Dr. Tatiana Bedarida, Sean Michael Carr, Dr. Ye Ding, Dr.Young-min Han, Dr. Haingo Fransky Mitchell Hantelys, Dr. Jing Mu, Dr. Liu Ouyang, Dr. Yao Qu, Dr. Gloria Andrea Torres Rivera, Dr. Ganesh Satyanaraya, Sanjiv Shrestha, Dr.

Ramprasath Tharmarajan, Dr. Yunli Tian, Dr. Cheng Wang, Dr. Qilong Wang, Dr. Yang Wu, Dr. Shaojin You, Dr. Changjiang Yu, Dr. Fujie Zhao, Dr. Qiang Zhao, Dr. Donghong Zhang, Dr. Xiaoxu Zheng. It is my luck to know all of you in GSU and I deeply appreciate the valued tips, which were sedimented by your years of experimental experience and your glowing characters will light me in the future of my life.

TABLE OF CONTENTS

LIST OF TABLES

LIST OF FIGURES

LIST OF ABBREVIATIONS

ATF3	activating transcription factor 3
3-MA	3-methyladenine
AMPK	AMP activated protein kinase
ATG1	autophagy-related 1
ATG5	autophagy related 5
ATG7	autophagy related 7
Atg14L	Atg14-like
AP-1	activator protein 1
apoE	apolipoprotein E
atg7 KO	endothelial cell-specific *atg7* knockout
ATGs	autopha*g*y-related genes
BECN1	Beclin-1
BH4	tetrahydrobiopterin
CAD	coronary artery disease
ChIP	chromatin immunoprecipitation
CMA	chaperone-mediated autophagy
cNOS	constitutive NOS
CQ	chloroquine
EC(s)	endothelial cell(s)
eNOS	endothelial nitric oxide synthase
EP300	E1A binding protein p300
EPO	erythropoietin

FAD	flavin adenine dinucleotide
FGF	fibroblast growth factors
FMN	flavin mononucleotide
G6PDH	glucose-6-phosphate dehydrogenase
GS-eNOS	glutathionylation of eNOS
HEK293	human embryonic kidney 293 cells
HIF1A	hypoxia inducible factor 1 subunit alpha
HIFs	hypoxia-inducible factors
HR	hormone receptor
HUVECs	human umbilical vein endothelial cells
IFN-γ	interferon gamma
IL-6	interleukin 6
IRF9	interferon regulatory factor 9
ISGF3	interferon stimulated gene factor 3 complex
KPNB1	karyopherin (importin) beta 1
LPS	lipopolysaccharide
MAP1LC3A	microtubule associated protein 1 light chain 3 alpha
3-MA	3-Methyladenine
MCF7	Michigan Cancer Foundation-7 cells
ECM	extracellular matrix
MEFs	mouse embryonic fibroblasts
MLECs	mouse lung endothelial cells
MMP1	matrix metallopeptidase 1

MTORC1	mechanistic target of rapamycin complex 1
NAC	N-acetyl-l-cysteine
NADPH	nicotinamide adenine dinucleotide phosphate
NO	nitric oxide
NOS3	nitric oxide synthase 3
NOX	NADPH oxidase
NRP-1	neuropilin-1
NFKB1/NFκB	nuclear factor kappa B
PAD	peripheral artery diseases
PARP1	phosphorylating DNA damage repair protein poly (ADP-ribose) polymerase 1
PAS	phagophore assembly site
P5CS	pyrroline-5-carboxylate-synthetase
PDGFB	platelet-derived growth factor B
PE	phosphatidylethanolamine
PECAM-1/CD31	platelet endothelial cell adhesion molecule
PI3KC3	class III phosphatidylinositol 3 kinase
PLGF	placental growth factor
PPP	pentose phosphate pathway
PtdI3P	phosphatidylinositol 3-phosphate
RA	rheumatoid arthritis
RB1CC1	RB1-inducible coiled-coil protein 1
ROS	reactive oxygen species

SDF-1	stromal-derived factor 1
SP1	specificity protein 1
SQSTM1/p62	sequestosome 1
STAT1	signal transducer and activator of transcription 1
STZ	streptozocin
T1D	type 1 diabetes
TGF	transforming growth factor
TSP-1	thrombospondin-1
Ubl	ubiquitin-like
ULK1	unc-51 like kinase 1
ulk1 KO	endothelial cell-specific *Ulk1* knockout
VEGF	vascular endothelial growth factor
VPS34	vacuolar protein sorting 34
VSMCs	mouse aortic smooth muscle cells
WT	wild type
ZNF148/ZBP-89	zinc finger protein 148

1 INTRODUCTION

1.1 Endothelium

The endothelium is a single layer of endothelial cells (ECs) lining the entire vascular system (Kruger-Genge, Blocki, Franke, & Jung, 2019). Unlike smooth muscle cells, they also cover the blood and the lymphatic capillaries. Endothelium possesses a wide range of functions, including regulation of vascular tone, angiogenesis, thrombosis, smooth muscle cell proliferation, and inflammatory response.

Endothelium allows molecules ranging from 0.1 nm to 11.5 nm in diameter to pass through it (Sukriti, Tauseef, Yazbeck, & Mehta, 2014). Under physiological conditions, the molecules smaller than 6 nm in diameter can pass passively through endothelial cell-cell junctions, whereas the larger molecules must be transported by endocytosis of ECs. Precise regulation of endothelial permeability is crucial for maintaining endothelial barrier function and preventing tissue edema.

Endothelium not only serves as a barrier between vessels and tissues but also functions as sensor to monitor the surrounding environment. In respond to shear stress and chemical stimuli, endothelium secretes diverse molecules, among them, nitric oxide (NO) is one of the most crucial molecules, which induces vasodilation, promotes angiogenesis, inhibits platelet aggregation, prevents inflammatory response, inhibits smooth muscle cell proliferation, and delivers the distress signal to different organs (Alderton, Cooper, & Knowles, 2001; Daiber et al., 2019; Tousoulis, Kampoli, Tentolouris, Papageorgiou, & Stefanadis, 2012). Thus, NO production is essential for maintaining endothelial homeostasis.

The evidence collected from human beings indicates that risk factors associated with endothelial dysfunction (also called endothelial activation), including smoking, hypertension,

hyperglycemia, hyperlipidemia, and diabetes etc., also correlates with the progression of vascular diseases and forecasts the incidence of cardiovascular events (Deanfield, Halcox, & Rabelink, 2007; Grover-Paez & Zavalza-Gomez, 2009). Endothelial dysfunction is characterized by switching endothelial cells from a quiescent status toward one that promotes inflammation and coagulation. Thus, it is associated with most forms of cardiovascular disease, such as hypertension, coronary artery disease, chronic heart failure, peripheral vascular disease, diabetes, chronic kidney failure, and severe viral infections (Almourani, Chinnakotla, Patel, Kurukulasuriya, & Sowers, 2019; L. Chen & Hao, 2020; Dong et al., 2019; Haffner, 2006; Jankowski, Floege, Fliser, Bohm, & Marx, 2021; Sowers, Epstein, & Frohlich, 2001). Endothelial dysfunction precedes damaged endothelial cell integrity, senescence, and apoptosis. The dysfunctional ECs might detach from blood vessels and be flushed into the circulation, serving as a biomarker of endothelial dysfunction (Deanfield et al., 2007). Here, I focus on the regulatory effects of endothelium on angiogenesis and vasodilation.

1.2 Endothelium and angiogenesis

Angiogenesis is the formation of new blood vessels from the existing vasculature. Until recently, two forms of angiogenesis have been described, such as sprouting angiogenesis and intussusceptive angiogenesis (Burri, Hlushchuk, & Djonov, 2004). The new blood vessel formation supplies the tissues with oxygen and nutrients, which are critical for wound healing and the successful treatment of cardiovascular diseases. On the other hand, tumor angiogenesis promotes tumor growth and enables tumor cell invasion and dissemination. The basic steps of sprouting angiogenesis include: (1) endothelial cells receive pro-angiogenic signals, resulting in degradation of vascular basement membrane and activation of endothelial cells; (2) endothelial

cells sprouts, proliferates, and migrates within extracellular matrix; (3) formation of lumen within the vascular sprouts, thereby creating vascular tubes; and (4) vascular tubes are encircled by vascular basement membrane and pericytes, thereby stabilizing the new vessels (Senger & Davis, 2011).

Intussusceptive angiogenesis is characterized by extending the capillary wall into the lumen of an existing vessel and splitting a single vessel into two vessels. It occurs in three distinct phases: (1) formation of contact zone between two capillary walls; (2) the ECs are reorganized and allow cells enter the lumen; (3) the contact zone is filled by migrating pericytes and fibroblasts, creating an extracellular matrix (ECM) network for vessel lumen formation, subsequently it is reorganized to generate two vessels (Burri et al., 2004). Therefore, in intussusceptive angiogenesis, new vessels develop without increasing endothelial cell proliferation (Mentzer & Konerding, 2014). Another mechanism of new blood vessel formation is arteriogenesis, in which pre-existent arterio-arteriolar anastomoses are remodeled into much larger conductance artery. Unlike angiogenesis, arteriogenesis is mainly induced by physical forces, most importantly fluid shear stress. It is characterized by an increase in the diameter of existing arterial vessels without altering vessel number (van Royen et al., 2001).

Physiologically, angiogenesis is crucial for embryonic development, tissue and organ growth, and normal wound healing. In pathological conditions, angiogenesis is associated with tumor growth, invasion, and metastasis. In normal condition, a balance between angiogenic inductors and inhibitors maintains the quiescent capillary vasculature. The major pro- and anti-angiogenic factors are listed in the **Table 1-1**. One of the most important triggers initiating angiogenesis is the lack of oxygen. Hypoxia stabilizes hypoxia-inducible factors (HIFs) and prevents its degradation, resulting in the accumulation of HIFs, which sequentially activates

transcription of a variety of genes encoding proteins involved in regulating each step of angiogenesis (Semenza, 2003).

Table 1.1 Partially listed factors implicated in angiogenesis

Stimulator	**Mechanism**
Shear stress	Initiation of angiogenesis (Wragg et al., 2014)
Exercise	Capillaries increased and enlarged (Gorski & De Bock, 2019)
VEGF	Increase permeability, devastating extracellular matrix, promote EC proliferation, migration, and survival (Przybylski, 2009)
HIF1A	Promote VEGF, transforming growth factor-β3 expression
FGF	Stimulate ECs proliferation, migration and extracellular matrix rearrangement (Przybylski, 2009)
VEGFR and NRP	Transducer of survival signals, expressed on endothelial tip cells and guide tip cells
peroxisome-proliferator-activated receptor-γ coactivator-1α (PGC-1α)	Induce VEGF expression by HIF independent pathway (Arany et al., 2008)
Ang1 and Tie2	Stabilize vessels, prim bone marrow-derived progenitor cells, increase adhesion molecule production
PDGF and PDGFR	Induce new vessel formation, mature neovascularized vessels by recruiting smooth muscle cells
TGF-β and TGF-β receptors	Increase extracellular matrix components expression, activate EC proliferation and migration, active growth factors (Pardali & ten Dijke, 2009)
CCL2	Activate monocytes and promote VEGF expression (Pardali and ten Dijke 2009)
Integrins	Bind matrix macromolecules and proteinases
VE-cadherin and CD31	Endothelial junctional molecules
ephrin	Determine formation of arteries or veins
plasminogen activators	remodels extracellular matrix, releases and activates growth factors
SEMA3A, 3B, 3C	Retain tumor-associated macrophage in hypoxia, promote EC survival (B. Jiao et al., 2021)
Nogo-A	Promote vasculature formation in the insult of stroke
MMPs	Facilitate matrix degradation, activate integrin
Placental growth factor (PLGF)	Stimulate EC growth and migration, recruit and activate monocytes (Carmeliet & Jain, 2011)

Integrin	Facilitate EC migration and survival(Avraamides, Garmy-Susini, & Varner, 2008)
Inhibitor	**Mechanism**
Thrombospondin-1 (TSP-1)	Antagonize of VEGF(Hanahan & Folkman, 1996; P. R. Lawler & Lawler, 2012) (Hanahan & Folkman, 1996)
Epigallocatechin-3-gallate	Inhibit MMP-2, prevent EC invasion and growth (Cao & Cao, 1999)
Angiostatin	Inhibit EC proliferation, promote EC apoptosis
Endostatin	Inhibit EC proliferation, promote EC apoptosis
Vasostatin	Inhibit EC attachment to laminin (Ribatti, 2009), inhibit of VEGFR signaling (Wei et al., 2021)
Tumstatin	Inhibit activation of focal adhesion kinase, inhibitEC protein synthesis (Yamamoto et al., 2004)
Arresten, Canstatin	Inhibit EC proliferation, migration, inhibit integrin/focal adhesion kinase (FAK) and Akt signaling pathway
MMP inhibitors	Inhibit EC migration and proliferation
IFN-α, β, γ	Inhibit FGF, inhibit MMPs, induce cell apoptosis
SEMA3A, 3B, 3C, 3E, 3F	Inhibit VEGF secretion or signaling pathways, destruct integrin-related adhesion, prohibit EC proliferation, migration and sprouting (B. Jiao et al., 2021)
Nogo-A	Inhibited spreading, migration, and sprouting of primary brain microvascular ECs, retract lamellipodia and filopodia in developmental CNS (Walchli et al., 2013)

In adult individuals, the endogenous angiogenesis inhibitors counteract pro-angiogenic signals and prevent new vessel formation. Angiogenesis occurs when the total angiogenic stimulation overwhelms the total angiogenic inhibition, conversely, angiogenesis is inhibited once pro-angiogenic factors are overcame by anti-angiogenic ones. Correspondingly, enhanced angiogenesis ensures blood supply to all cells within an organ, whereas impaired angiogenesis diminishes blood flow.

The imbalance between pro-angiogenesis and anti-angiogenesis factors in implicated in cancer and various ischemic and inflammatory diseases. For example, cancer and age-related macular degeneration are characterized by excessive angiogenesis. In contrast, reduced angiogenic activity leads to ischemia and worsens the prognosis in patients with cardiac

infarction and peripheral artery occlusions. Recent progress in understanding the roles of extracellular matrix remodeling and ECs metabolic adaptation in angiogenesis makes them attractive anti-angiogenic targets. Pathological shear stress reduces the expression of extracellular matrix proteins, including glycosaminoglycans and proteoglycans, potentiating angiogenesis (Russo, Banuth, Nader, & Dreyfuss, 2020). Further study shows that shear stress above the 10 dyn/cm^2 induces sprouting angiogenesis specifically up-regulates the expression of matrix metallopeptidase 1 (MMP1) (Galie et al., 2014), which breaks down the extracellular matrix and is important in step 1 of angiogenesis. ECs produces ATP relying on glycolysis rather than on oxidative phosphorylation, which is required for angiogenesis, inhibition of glycolysis in ECs impairs vessel formation (De Bock et al., 2013). By comparing murine choroidal ECs with choroidal neovascularization ECs, researchers find that two genes, Aldh18a1 and Sqle, encoding pyrroline-5-carboxylate-synthetase (P5CS) and squalene monooxygenase respectively, have higher expression in choroidal neovascularization ECs. P5CS is the key enzyme that catalyzes synthesis of proline from glutamate, while squalene monooxygenase is a rate-limiting enzyme responsible for cholesterol synthesis (Rohlenova et al., 2020). Thus, the regulation of glycolysis and extracellular matrix (ECM) degradation and remodeling plays a critical role in controlling new vessel formation, stabilization, and maturation.

1.2.1 Angiogenesis in cancers

Angiogenesis occurs before a tumor can grow to larger than 1-2 mm in size. Unlike the temporary activation of angiogenesis in wound healing and menstrual cycle, the angiogenesis activation in cancer seems to be permanent. During tumor angiogenesis, overexpression of pro-angiogenic factors leads to the development of disorganized blood vessel networks. Tumor vasculature is characterized by hemorrhage, hyper-permeability, and disorganized branching

(Schaaf, Garg, & Agostinis, 2018). The abnormality of angiogenesis in tumors contribute to the formation of an acidic microenvironment due to the inefficiency in removing metabolic wastes, such as carbon dioxide and lactic acid (Nagy, Chang, Shih, Dvorak, & Dvorak, 2010).

In response to the increased requirement of nutrients and oxygen, tumor cells or stroma cells release angiogenic molecules, such as VEGF-A, that contribute to formation of new vasculature. In solid tumor, the hypoxic environment is considered as the major stimulators of VEGF expression. Additionally, other mechanisms may also participate in regulation of VEGF-A generation, such as expression of oncogenes, deletion of tumor suppressor genes, and stimulation by either cytokines or hormones (Palazon et al., 2017). Since VEGF-A is a well-known HIF1A target that is up-regulated under hypoxic conditions in solid tumors, HIF1A has been highly appreciated in tumor progression, and treatment of tumor by targeting HIF1A warrants further studied.

1.2.2 Angiogenesis in ischemic cardiovascular diseases

Coronary artery disease (CAD) is the leading cause of death in the United States, killing 382,820 in 2020, about one in every ten deaths was due to CAD (Tsao et al., 2022). Atherosclerosis is the primary cause of CAD, in which the plaque formation in the wall of arteries narrows the arteries, leading to myocardial ischemia and impairing cardiac function (Benjamin et al., 2017).

The inflammatory response following myocardial ischemia is the first stage of repairing the infarcted myocardium, which is followed by myofibroblast activation and proliferation (Prabhu & Frangogiannis, 2016). During this cardiac repair period, inflammatory macrophages convert to an anti-inflammatory phenotype that reduces the production of inflammatory mediators, including IL-10, and transforming growth factor (TGF)-β, thereby promoting fibrosis

and angiogenesis (Hanna & Frangogiannis, 2019; Sziksz et al., 2015). This anti-inflammatory response can extend for a long time until the adverse signaling diminishes.

Current therapeutic strategies for CAD primarily focus on the development of antiplatelet agents, β-blockers, and statins. Besides treatment with drugs, restoring circulation to the affected heart muscle could be achieved by surgical interventions, including coronary artery bypass graft surgery and percutaneous coronary intervention. Unfortunately, some patients deem unsuitable to be treated with surgical interventions. For this group of patients, promoting angiogenesis seems to be a potential therapeutic strategy.

1.2.3 Angiogenesis in other diseases

Pathologic ocular angiogenesis occurs in many ocular disorders, including diabetic retinopathy, retinopathy of prematurity, and age-related macular degeneration, which constitutes most of the blindness in developed countries (Hartnett, 2014; Rajappa, Saxena, & Kaur, 2010). Thus, anti-angiogenic therapy has opened new possibilities for the prevention of visual impairment and blindness.

There were 236.62 million people older than 25 years suffered from peripheral artery diseases (PAD) worldwide in 2015. PAD is typically caused by atherosclerotic obstructions in the large arteries to the leg(s). Increasing evidence indicates that the leading risk factors for PAD include smoking, diabetes, hypertension, and hypercholesterolemia (Song et al., 2019). Diabetic patients have a greater incidence and severity of PAD, which is associated with 5 to 10 times more likely to undergo an amputation than nondiabetic individuals (Society for Vascular Surgery Lower Extremity Guidelines Writing et al., 2015). The prevalence of PAD tends to increase in the near future as 65-and-older population grows rapidly, obesity has become an epidemic, and a diabetes epidemic is underway, thus, PAD has become a serious health problem worldwide.

(Society for Vascular Surgery Lower Extremity Guidelines Writing et al., 2015) The patients with PAD have chronic lower extremity ischemia and manifest with no symptoms or claudication because of a severe blockage in the arteries of the lower extremities, which markedly reduces blood flow. Currently, medical therapies used to treat patients with PAD include lower cholesterol, antiplatelet, anticoagulation, and anti-hypertension. If these medical management is not suitable or effective in severe cases of PAD, endovascular and surgical interventions may be necessary. In addition to medical and interventional treatments, therapeutic angiogenesis is a novel therapy for PAD.

In addition, angiogenesis also plays a critical role in the pathogenesis of rheumatoid arthritis (RA). During RA, newly formed blood vessels transport inflammatory cells to the inflammatory joints and provide oxygen and nutrients to the inflamed tissue (Elshabrawy et al., 2015). Targeting angiogenesis in rheumatoid arthritis ameliorates symptoms. Thus, the blockade of angiogenesis appears to be a promising therapeutic strategy for rheumatoid arthritis

1.2.4 Angiogenesis-targeted treatments

VEGF inhibitor, bevacizumab, is the first antiangiogenic agent approved by FDA in 2004 (Ferrara, Hillan, Gerber, & Novotny, 2004). Due to the key role of angiogenesis in tumor growth and ocular diseases, numerous research groups have been engaged in the development of anti-angiogenic medications, and more angiogenesis inhibitors have been approved in the treatment of various cancers or age-related macular degeneration. Angiogenesis inhibitors may be used as either alone or in combination with other canonical anti-cancer medicines (Table 1-2). Preclinical and early clinical data suggest antiangiogenic reagents in combination with chemotherapy appear to be more effective therapies for patients with cancer. On the other hand, therapeutic angiogenesis for treatment of ischemic cardiac disease is still in its infancy.

Stimulation of new vessel growth by VEGF to compensate for tissue ischemia, remains an unfulfilled promise, although various approaches have been used to deliver VEGF to the ischemic myocardium to promote angiogenesis in ischemic cardiac diseases.

1.2.4.1 Pro-angiogenesis reagents

The concept of using growth factors as a therapeutic strategy for pro-angiogenesis evolved from the pioneering work by Folkman and colleagues in 1971 (Takeshita et al., 1994). The first clinical trial on patients with coronary artery diseases using pro-angiogenesis therapy was performed in Germany by targeting the patients with fibroblast growth factor 1 (FGF-1) (Stegmann, 1998). Currently, most studies focus on direct delivery of either angiogenic growth factors (eg. VEGF) or stem cells/progenitor cells to ischemic tissues.

Administration of VEGF-165 in rabbits undergone femoral artery ligation promotes the regeneration of collateral vessels and capillaries, which suggests that the single administration of VEGF is sufficiency to inducing angiogenesis (Takeshita et al., 1994; Tekabe et al., 2015).

Angiogenesis is a complex and multi-stage process. To ensure that developing or healing tissues receive an adequate supply of nutrients, pro-angiogenesis applications should generate a vasculature with normal structure and functions, and avoid unpropitious effects, such as excessive vessel growth, tortuous and dilated vessels, and hyperpermeability. Thus, identify the medicine and establishing the timing to induce angiogenesis is essential for the development of future and more effective therapies for ischemic heart disease.

Another promising strategy for treatment of ischemic diseases is to inhibit the production of anti-angiogenetic factors. As a potent endogenous inhibitors of angiogenesis, thrombospondin-1 (TSP-1) expression strongly increases during myocardial infarction, indicating an important role for TSP-1 in cardiac remodeling (Taraboletti, Rusnati, Ragona, &

Colombo, 2010).TSP-1 inhibits angiogenesis by inhibiting endothelial cell migration and proliferation, stimulating endothelial cell apoptosis, and antagonizing the activity of VEGF. Previous study shows that downregulation of TSP-1 ECs enhances angiogenesis in cultured cells, suggesting that TSP-1 may become potential therapeutic targets (J. Lawler, 2022). In addition, in the comparison with non- diabetic patients with coronary artery disease exhibit higher levels of anti-angiogenic factors, including angiostatin and endostatin, which inhibit coronary collateralization. This finding suggests new therapeutic targets for proangiogenic therapy in diabetes (Sodha et al., 2009).

1.2.4.2 Anti-angiogenesis medications

In 1971, Surgeon Judah Folkman proposed the concept that tumor growth and metastasis are dependent on angiogenesis and inhibition of angiogenesis might be a potential therapeutic strategy for cancer. Currently, clinical efforts to develop antiangiogenic therapies mainly focus on multiple growth factors, receptors, and intracellular signaling pathways. Since tumor growth requires increased new vessel formation, inhibiting angiogenesis by antiangiogenic drugs prevents tumor progression. However, the inhibitory effect of antiangiogenic drugs on angiogenesis can only persist for a limited time, and consequently tumors become resistant to antiangiogenic therapy, or reoccurs after retraction of anti-angiogenesis reagents. Given that the hypoxic tumor microenvironment stimulates tumor cells to express many growth factors, including VEGF, FGF, and PIFG, to confront the adverse environment, and enhances new vessel formation by bone marrow-derived stem cells (Carmeliet and Jain 2011). (Lee, Miwa et al. 2022) Targeting single growth factor might not be able to get a satisfactory outcome in tumor treatment.

Hypoxia-inducible factor-1 (HIF-1) has been recognized as a target for cancer therapy because it acts as the upstream of multiple genes encoding angiogenic growth factors and cytokines, including VEGF, erythropoietin (EPO), stromal-derived factor 1 (SDF-1), placental growth factor (PLGF), angiopoietin 1 and 2, and platelet-derived growth factor B (PDGFB) (Hirota & Semenza, 2006; Masoud & Li, 2015). Thus, targeting HIF-1 has attracted a lot of attention in the development of anti-angiogenesis treatment. The regulation of HIF activity is tightly modulated at multiple levels, such as regulation of HIF1A synthesis, HIF1A stability, and HIF1A transactivation. Although it is well documented that the regulation of HIF1A expression is mainly at the protein level by post-translational modifications and degradation, increasing evidence shows that regulation of HIF1A expression at the mRNA level by transcription factors is a rate-limiting step in modulating HIF1-A protein expression (Chamboredon et al., 2011). Recent study suggests that an antisense oligonucleotide targeted to *HIF1A* mRNA inhibits *HIF1A* mRNA transcription, downregulates HIF1A protein expression, suppresses angiogenesis and tumor growth. Indeed, EZN-2968, a new type of anti-cancer drug, composed of third-generation oligonucleotide, can specifically inhibits the expression of *HIF1A* mRNA, resulting in inhibition of angiogenesis, tumor cell proliferation, and tumor growth (Onnis, Rapisarda, & Melillo, 2009; J. Wu et al., 2019).

Antiangiogenic reagents approved by FDA are listed in **Table 1-2**.

Table 1.2 Antiangiogenic reagents approved by FDA

Anti-angiogenic agent	**Indication**	**Target**
Aflibercept	Metastatic colorectal carcinoma, wet macular degeneration, diabetic retinopathy	VEGF-A, VEGF-B, PlGF
Axitinib	Renal cell carcinoma	VEGFR1-3

Bevacizumab	Cervical cancer, colorectal cancer, glioblastoma, hepatocellular carcinoma, nonsquamous non-small cell lung cancer, ovarian epithelial, fallopian tube, primary peritoneal cancer, renal cell carcinoma	VEGF-A
Cabozantinib	Differentiated thyroid cancer, hepatocellular carcinoma, medullary thyroid cancer, renal cell carcinoma	MET (hepatocyte growth factor receptor), VEGFR
Everolimus	Breast cancer, pancreatic cancer, gastrointestinal cancer, renal cell carcinoma, subependymal giant cell astrocytoma	mTORC1, VEGFR-2 (Piguet et al., 2014)
Lenalidomide	Anemia, follicular lymphoma, mantle cell lymphoma, marginal zone lymphoma, multiple myeloma	HIF1A (L. Lu et al., 2009)
Lenvatinib mesylate	Endometrial carcinoma, hepatocellular carcinoma, renal cell carcinoma, thyroid cancer	VEGFR2
Pazopanib	Renal cell cancer, soft tissue sarcoma	VEGFR1-3, PDGFR, c-Kit
Ramucirumab	Colorectal cancer, hepatocellular carcinoma, non-small cell lung cancer, stomach adenocarcinoma, gastroesophageal junction adenocarcinoma	VEGFR2
Regorafenib	Colorectal cancer, gastrointestinal stromal tumor, hepatocellular carcinoma	VEGFR2, VEGFR3, PDGFR, Raf, Tet, Kit
Sorafenib	Hepatocellular carcinoma, thyroid cancer, renal cell cancer	VEGFR2, PDGFR, Raf
Sunitinib	Gastrointestinal stromal tumor, pancreatic cancer, renal cell carcinoma	VEGFR2, PDGFR-β, c-Kit, Fms-related tyrosine kinase 3 (FLT3)
Thalidomide	Multiple myeloma	TNF-α
Vandetanib	Medullary thyroid carcinoma	VEGFR2, EGFR
Ziv-aflibercept	Colorectal cancer	VEGFR

1.3 Diabetes and endothelial dysfunction

Diabetes is a chronic metabolic disease characterized by higher blood glucose levels and is closely associated with increased cardiovascular morbidity and mortality. There are two main forms of diabetes, type 1 (insulin-dependent diabetes mellitus) and type 2 (non-insulin-dependent diabetes mellitus). Type 2 diabetes is far more common than type 1 diabetes. Currently, around 90% of all adults with diabetes have type 2 diabetes. The International Diabetes Federation reports that the prevalence of diabetes in adult was estimated to be 537 million in 2021 worldwide (Y. Yan et al., 2022). The major complications of diabetes encompass heart attack, stroke, kidney disease, neuropathy, retinopathy, and lower-extremity amputation (Tao, Shi, & Zhao, 2015). Poorly controlled diabetes substantially increases the risk of diabetic complications and premature death.

Hypertension is more common in diabetic patients, and both diabetes and hypertension share similar etiology and pathologic processes, including obesity, inflammation, oxidative stress, and insulin resistance (Cheung & Li, 2012). Substantial clinical and experimental evidence suggest that diabetes causes endothelial dysfunction, which reduces release or availability of nitric oxide (NO), leading to impaired endothelium-dependent vascular relaxation (De Vriese, Verbeuren, Van de Voorde, Lameire, & Vanhoutte, 2000). Therefore, endothelial dysfunction has a close inter-relationship with hypertension in diabetes. Currently, it is wildly acknowledged that diabetes increases ROS release, which leads to endothelial dysfunction. Under diabetic conditions, there are several sources of ROS in cells, including nonenzymatic glycosylation reaction (Nowotny, Jung, Hohn, Weber, & Grune, 2015), electron transport chain in mitochondria (R. Z. Zhao, Jiang, Zhang, & Yu, 2019), membrane-bound NADPH oxidase (NOX) (Laddha & Kulkarni, 2020), nitric oxide synthases, xanthine oxidases, lipoxygenases,

cyclooxygenases, and peroxidase (Newsholme, Cruzat, Keane, Carlessi, & de Bittencourt, 2016; Newsholme et al., 2007).

NOXs are ROS-generating enzymes. Endothelial cells express four NOX isoforms, including the superoxide-generating enzymes NOX1, NOX2, and NOX5 and the hydrogen peroxide-generating enzyme NOX4 (Drummond & Sobey, 2014). Hyperglycemia enhances NOX level and activates the enzyme (Drummond & Sobey, 2014). The active NOX complex allows for the transfer of electrons to molecular oxygen to generate superoxide, but it is still not clear which isoform of NOX plays the leading role in hyperglycemia-induced ROS production. The mitochondrial respiratory chain is another major source of ROS production. Under diabetic conditions, the electron transport chain is activated to increase electron leak, which leads to production of larger amounts of ROS (Nishikawa & Araki, 2007).

Metabolic modifications are also implicated in the development of high glucose-induced ECs dysfunction. Hyperglycemia increases blood glucose level and inhibits glucose-6-phosphate dehydrogenase (G6PDH) activation by promoting cAMP-PKA phosphorylation, which causes pentose phosphate pathway (PPP) deviation and decreases NADPH levels (Z. Zhang, Apse, Pang, & Stanton, 2000). This mechanism in turn regulates ROS production through NOX catalyzation. It is proposed that glyceraldehyde-3-phosphate dehydrogenase (GAPDH) ADP-ribosylation blocks the conversion of glyceraldehyde-3-phosphate to 1,3-bisphosphoglycerate, which inhibits physical glycolytic pathway and induces upstream metabolites accumulation (J. Wu, Jin, Zheng, & Yan, 2016). There is almost 30% of glucose swerved to polyol pathway as the shutting down of glycolysis (L. J. Yan, 2018). In STZ-injected rat lung, polyol pathway is activated to replace glycolytic pathway. The activation of the polyol pathway induces the accumulation of sorbitol and fructose content, decreases the NADPH/NADP+ ratio and nitric

oxide production, and increases NADH/NAD+ ratio leading to ROS production and oxidative stress (J. Wu et al., 2016; L. J. Yan, 2018). These events cause endothelial dysfunction, consequently, accelerates diabetic vascular complications.

1.3.1 The role of ROS in endothelial injury

In general, potential sources of ROS production in ECs include NOX, xanthine oxidase, mitochondria and uncoupled eNOS. As the byproduct of mitochondrial aerobic respiration, ROS production is inevitable and ubiquitous in living creatures. Simultaneously, antioxidant enzymes convert ROS into H_2O_2 and finally generating H_2O and O_2 to prevent the detrimental effects of ROS. Thus, elaborate balancing the production and elimination of ROS is crucial for maintaining normal biological functions in ECs. NOX is a membrane bound enzyme complex participating in the reaction of electron transfer from NADPH to oxygen molecule to produce O_2^-, and H_2O_2. ECs contains several isoforms of NOX, including NOX1, 2, 4, and 5 isoforms. NOX1, 2, 5 mainly produce O_2^-, while NOX4 predominantly catalyzes H_2O_2 production.

Hyperglycemia is a major stimulus of endothelial NOX activation. In several Type 2 diabetes and insulin-resistant animal models, NOX1 and/or NOX2 are demonstrated as key generators of ROS in ECs and responsible for vascular dysfunction. High fat diet triggers NOX2 protein expression in aorta, whereas the deletion of NOX2 prevents diabetic-initiated ROS production and endothelial dysfunction (Drummond & Sobey, 2014; Lynch et al., 2013).

In contrast to the discoveries in type 2 diabetic animal models, NOX2 inhibition does not prevent ROS overproduction and endothelial dysfunction in STZ-treated type 1 diabetic animals. Moreover, NOX4 seems not to be important in type 1 diabetes-induced endothelial dysfunction, because deletion of NOX4 does not prevent artherogenesis in response to oxidative stress. By contrast, in cultured human retinal ECs and HUVECs, NOX4 may be an important source of

ROS and contributes to high glucose-induced endothelial dysfunction, because in high glucose-treated cells, NOX4 expression is upregulated, and inhibition of NOX4 significantly reduces ROS production and cell death (W. Jiao et al., 2019; Luo et al., 2019). However, NOX1 may play an essential role in the development of endothelial dysfunction in STZ-induced type 1 diabetes as NOX1 is upregulated in STZ-treated mice, which enhances ROS production and promotes eNOS uncoupling. Suppression of NOX1 improves endothelial function in STZ-induced type 1 diabetic mice (Youn, Gao, & Cai, 2012).

1.3.2 ENOS and endothelial homeostasis in diabetes

Nitric oxide (NO), a free-diffused gaseous and lipophilic molecule, is predominantly generated from the endothelial isoform of NO synthase (eNOS), also known as nitric oxide synthase 3 (NOS3) or constitutive NOS (cNOS), in normal condition, and is firstly identified as endothelium-generated factor for vasorelaxation (Deanfield et al., 2007). The biological effects of NO are involved in diverse cellular processes, including maintenance of vascular tone, angiogenesis, tissue remodeling, and anti-inflammation (Kruger-Genge et al., 2019). The production of eNOS and NO is stimulated by many factors, such as shear stress, insulin, and inflammatory cytokines (Michel & Vanhoutte, 2010). In response to the changes in metabolic demands and oxygen consumption rate, endothelium finely tunes vascular tension by release several vasoactive modulators, such as bradykinin and thrombin. For example, when cardiac output changes, endothelium produces vasoactive modulators to regulate vasoconstriction and vasodilation, thus maintaining normal blood pressure (Sandoo, van Zanten, Metsios, Carroll, & Kitas, 2010).

NO formation starts from converting L-arginine into NO and L-citrulline, which requires core enzyme, endothelial nitric oxide synthase (eNOS). ENOS is a dimer containing two

identical monomers. ENOS monomer is inactive, and the dimeric form is required for its function. Monomer eNOS is composed of a reductase domain and an oxidase domain. These two domains are bridged by a calmodulin-binding sequence. The reductase domain is the binding site for nicotinamide adenine dinucleotide phosphate (NADPH), flavin mononucleotide (FMN), and flavin adenine dinucleotide (FAD), while the oxidase domain contains the interacting sites for heme group, zinc, the cofactor tetrahydrobiopterin (BH4), and the substrate L-arginine (Alp & Channon, 2004). The bioavailability of L-arginine and enzymatic activity is responsible for NO production, while ROS are major determinants of NO degradation. The cofactor BH4 is a cofactor required for the synthesis of NO by eNOS (Alp & Channon, 2004). In the isolated rat heart, ischemia decreased BH4 content, and concurrently inhibits eNOS activity, resulting endothelial dysfunction. Administration of BH4 prevents endothelial dysfunction and improve cardiac function in ischemia stimulation (Cai, Khoo, Mussa, Alp, & Channon, 2005; Dumitrescu et al., 2007).

It is reported that eNOS activity is impaired in diabetic patients, because hyperglycemia downregulates eNOS expression, inhibits eNOS phosphorylation, increases oxidation of nitric oxide, and reduces BH4. ENOS expression is not always well correlated with the amount of NO production (C. Heiss, Rodriguez-Mateos, & Kelm, 2015). As constitutive endothelial overexpression of eNOS in apolipoprotein E (apoE) knockout mice reduces NO production, in association with increased oxidative stress (Ozaki et al., 2002). Conversely, reduction of NO is not certainly resulted from the loss of eNOS protein. Thus, regulation of NO production is complex, it is not only regulated by eNOS expression, but also modulated by eNOS substrate and cofactors, the phosphorylation status of eNOS, and ROS that can inactivate eNOS. Under pathological conditions, eNOS may become dysfunctional, which generates superoxide anion

instead of NO. This phenomenon is referred to as eNOS uncoupling that remarkably increases in the ratio of eNOS monomers to dimers.

During pathological conditions, overproduction of ROS reduces BH4 levels by converting it into BH3• radical leading to eNOS uncoupling. Uncoupled eNOS transfers electrons to O_2 instead of NO, resulting in generation of superoxide that can react with NO, consequently reducing cellular NO availability by converting NO to peroxynitrite ($ONOO^-$). Furthermore, peroxynitrite directly promotes eNOS uncoupling. In human aortic ECs, high glucose activates activator protein 1 (AP-1) by inducing ROS overproduction, which in turn inhibits eNOS mRNA transcription, and consequently downregulates the eNOS protein and inhibits its activity. In porcine aortic ECs, hypoxia-induced metabolic changes elevate NAD(P)H/NAD(P) ratio, which activates AP-1, leading to elevation of eNOS mRNA transcription (Hoffmann, Gloe, & Pohl, 2001).

In addition, eNOS activity is regulated by multiple sites of phosphorylation through different signaling pathways. For example, phosphorylation of eNOS at Ser 1179 and dephosphorylation at Thr 497 activates the enzyme, whereas phosphorylation at Thr 497 and dephosphorylation at Ser 1179 inactivates eNOS (E. H. Heiss & Dirsch, 2014). Low share stress inhibits eNOS activity depends on phosphorylation of eNOS-Thr495 via an ERK1/2 mechanism (X. Kong et al., 2017), and metabolic disorders in db/db mice diminishes eNOS phosphorylation at Ser1176 and inhibits its activity (Cheang et al., 2011). Thus, endothelial dysfunction occurring in diabetes contributes to diabetic complications, suggesting that the endothelium is a potential target for the therapy of diabetic cardiovascular complications.

1.4 Autophagy

1.4.1 Overview

Autophagy, meaning self-eating, is a cellular degradation process, in which cytoplasmic constituents are sequestered into double-membrane vesicles termed autophagosomes, and delivered to the lysosome for breakdown. Autophagy has been divided into three general types that are macroautophagy, microautophagy, and chaperone-mediated autophagy (CMA) (Parzych & Klionsky, 2014). The term "autophagy" usually refers to macroautophagy. Under normal conditions, basal-level autophagy is very low and functions as a cellular quality control mechanism to turnover intracellular components and maintain cellular energetic balance and serves as a stress adaptation pathway that promotes cell survival. Thus, basal autophagy might play a protective role in many fundamental physiological processes, including development, differentiation, and tissue remodeling. While malfunction of autophagy might contribute to the development of many diseases including neurodegeneration, cardiovascular diseases, liver disease, diabetes, and cancer. Autophagy consists of several sequential steps: (1) induction by an autophagic stimulator, (2) double membrane isolation or phagophore assembly, (3) expansion and sealing the double membrane structure to develop an autophagosome, (4) fusion the autophagosome with lysosome to form autolysosome, and (5) degradation and recirculation of autophagosome contents (Mizushima, 2007; Nakatogawa, 2020).

The molecular machinery of autophagy has been identified in both yeast and mammals, and more than 40 genes encoding components of autophagy machinery, named autopha*g*y-related genes (*ATGs*), have been identified (Mizushima, 2020; Yin, Pascual, & Klionsky, 2016). In mammalian cells, autophagy induction is controlled by the serine/threonine protein kinase ULK1 (unc-51-like kinase 1, a homologue of yeast ATG1) complex, which is comprised of

ULK1, ATG13, RB1-inducible coiled-coil protein 1 (RB1CC1, also known as FIP200) and ATG101. ULK1 is directly regulated by nutrient and energy sensors MTORC1 (mechanistic target of rapamycin complex 1) and AMPK (AMP activated protein kinase). MTORC1 is an inhibitor of autophagy in mammalian cells. Under nutrient rich environment, MTORC1 interacts, phosphorylates, and inactivates ULK1 and ATG13 to suppress autophagy. In contrast to phosphorylation by MTORC1, AMPK-mediated phosphorylation of ULK1 activates ULK1 to induce autophagy (Kim, Kundu, Viollet, & Guan, 2011). Upon ULK1 activation, the ULK1 complexes translocate to the phagophore assembly site (PAS) to trigger the nucleation of the phagophore by phosphorylating and activating class III phosphatidylinositol 3 kinase (PI3KC3) complexes. The PI3K complex consists of VPS34 (vacuolar protein sorting 34), Beclin1, VPS15, and Atg14L (Atg14-like), and is responsible for the production of the phospholipid phosphatidylinositol 3-phosphate (PtdI3P) and the recruitment of two ubiquitin-like (Ubl) conjugation systems, Atg12-Atg5-Atg16 and Atg8-PE (phosphatidylethanolamine), to the PAS (Suzuki et al., 2001), which are important in regulating the membrane nucleation process and autophagosome formation.

The expansion of the isolation membrane is controlled by two ubiquitin-like protein conjugation pathways, ATG12-ATG5 and the microtubule-associated protein light chain 3-phosphatidylethanolamine (LC3-PE). In the first case, E1 enzyme ATG7 and E2 ubiquitin-conjugating enzyme ATG10 are responsible for conjugating ATG12 onto ATG5. This is a prerequisite for the recruitment of Atg8 (LC3), which is catalyzed and covalently conjugated with PE in the phagophore membrane. When autophagosome formation is completed, it fuses with lysosomes. The inner membrane of the autophagosome and the cargo contained in the autophagosome are then degraded by lysosomal hydrolases (Denton, Nicolson, & Kumar, 2012).

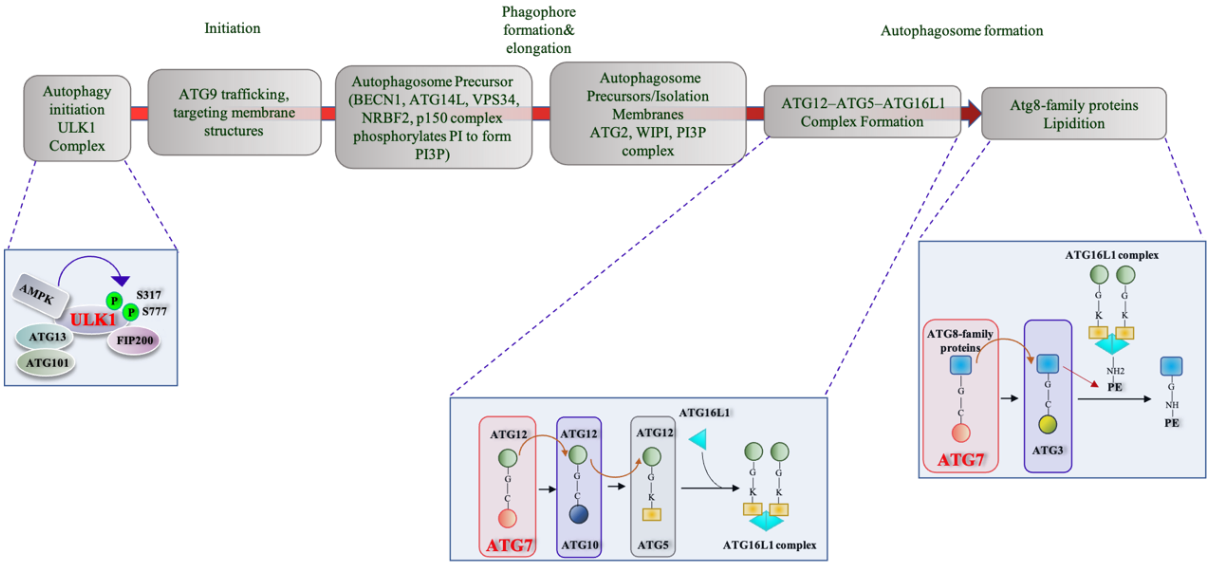

Figure 1.1 Overview of autophagy.
Schematic depicting the main autophagic pathways. Briefly, the induction of autophagy is mediated by the ULK1, VPS34, and ATG12-ATG5-ATG16 complexes. The formation mechanisms are described in the text.

1.4.2 ULK1

Autophagosome biogenesis is a dynamic membrane event, which is executed by the sequential function of ATG proteins. ULK1 (UNC-51-like kinase 1), the mammalian orthologue of the yeast ATG1 (autophagy-related 1), is the serine-threonine kinase and the autophagy initiator. Under nutrient-deficient condition, ULK1 is phosphorylated by AMPK, thereby activating autophagy. However, under over-nutrition conditions, activated mTOR phosphorylates ULK1 at multiple residues. The phosphorylation of ULK1 by mTORC1 results in suppression of autophagy initiation. Thus, ULK1 is the decisive hub for autophagy regulation in response to the metabolic stress (Kim et al., 2011).

ULK1 is also involved in hypoxia-induced mitophagy, a major mechanism involved in mitochondrial quality control via selectively removing damaged or unwanted mitochondria. Hypoxia activates AMPK, which in turn phosphorylates ULK1 at ser555 and promotes the

translocation of ULK1 to mitochondria and initiating mitophagy (Tian et al., 2015). Particularly, ULK1 engages in hydrogen peroxidase-induced non-apoptosis cell death by translocating to the nucleus and phosphorylating DNA damage repair protein poly (ADP-ribose) polymerase 1 (PARP1) (Joshi et al., 2016). Functioning as a serine/threonine kinase, ULK1 not only regulates glucose metabolism by phosphorylating glycolytic enzymes including hexokinase, phosphofructokinase 1, enolase 1, and the gluconeogenic enzyme fructose-1,6-bisphosphatase, but also mediates NADPH production by regulating pentose phosphate pathway (PPP) (T. Y. Li et al., 2016). Furthermore, ULK1 regulates ferritin turnover independent of autophagy (Goodwin et al., 2017). Dysregulation of ULK1 has been observed in many pathological conditions. For example, in transverse aortic constriction mouse model, ULK1activates mitophagy by a mechanism independent of ATG5/ATG7 in the myocardial ischemic stage of myocardial infarction, which enables selective removal of dysfunctional mitochondria. In obesity mouse model, ULK1 is down-regulated in the hearts, and ULK1-dependent mitophagy plays a critical role in maintaining cardiac function (D. F. Egan et al., 2011). However, the role of ULK1 in endothelial dysfunction remains unknown.

1.4.3 ATG7

ATG7 is an autophagy gene encoding E1-like enzyme in the two ubiquitin-like conjugation systems that are essential for the autophagosome biogenesis. Deficiency of ATG7 has been reported in mitochondrial dysfunction, ER stress, ROS overproduction, and inhibition of proteins secretion (Antonucci et al., 2015; Heinitz et al., 2019; Mortensen et al., 2010; Qiao et al., 2020; Y. Zhuang, Li, Li, Xie, & Wu, 2016). Overexpression of ATG7 activates autophagy that removes misfolded proteins and aggregated contents in cardiomyocytes, and recovers ER stress in autophagy-deficit hepatic cells (Pattison, Osinska, & Robbins, 2011) (L. Yang, Li, Fu,

Calay, & Hotamisligil, 2010). It is reported that vascular density in muscular tissue is indistinguishable between EC specific *atg7* knockout mice and wild-type mice (Torisu et al., 2013). However, microvascular density in the brain is significantly decreased (S. F. Zhuang et al., 2017) in *atg7* KO mice, indicating that ATG7 functions differently in muscle and brain vasculature. Additionally, ATG7 expression is downregulated in aged brain, contributing to the degeneration of neurons (Lipinski et al., 2010). However, whether ATG plays a role in angiogenesis remains elusive.

Recently, several autophagy-independent functions of ATG7 have been described. For example, ATG7 regulates G1-arrest by interacting with p53, and p53-mediated apoptosis is activated under autophagy-deficient conditions (I. H. Lee et al., 2012). Although there is result indicating that ATG7 is increased in hypoxia stimulation (J. Wu, Lei, & Yu, 2015), whether and how ATG7 affects EC function and regulates postischemic angiogenesis are still unveiled.

1.4.4 Autophagy-independent functions of autophagy related proteins

The core autophagy machineries essential for autophagosome formation and maturation contains more than 40 autophagy related proteins. In addition to functioning as critical regulators of autophagy machineries, some ATG proteins also mediate autophagy-independent functions including protein secretion, endocytosis, virus replication and release, and inflammasome activation.

Emerging evidence shows that ATGs are required for the production of inflammatory mediators, such as IL-1β and IL-18. In adipose tissue, ATG7 deletion inhibits chemerin secretion, which is a chemoattractant adipokine for immune cells such as dendritic cells and macrophages, and promotes adipocyte differentiation (Heinitz et al., 2019). In mouse ameloblasts, the epithelial cells that produce enamel, specific deletion of ATG7 prevents iron

transportation from ameloblasts into the mature enamel, resulting in white but not yellow surface of incisors (Sukseree et al., 2020). In addition, viruses use LC3 positive membranes to exit host cells via exocytic pathways rather than via lysosome degradation pathway. ATG16L1 gene mutant is found in Crohn's disease, a common type of inflammatory bowel disease characterized by mucosal ulceration and inflammation in ileum and abnormality in immune response to the gut microbiota. This mutation of ATG16L1 gene leads to imbalanced cytokine production and is linked to ER stress. Moreover, knockout of ATG16L1 promotes macrophages to generate more IL-1β to mediate intestinal inflammation (Cadwell & Debnath, 2018; Galluzzi & Green, 2019; Saitoh et al., 2008). Nevertheless, some questions remain: whether ATGs deficiency-inhibited secretion is the consequences of compromised autophagy or their non-autophagic function. If the secreted substances are enclosed in double membrane autophagosomes, and how they are transported to the cell membrane.

1.4.5 Autophagy and angiogenesis

Angiogenesis often occurs in hypoxic environment that triggers autophagy response.

Autophagy has been implicated in many pathophysiological processes, including cancer, metabolic diseases, neurodegenerative disorders, and cardiovascular diseases (Cheng, Ren, Hait, & Yang, 2013). Moreover, increasing evidence suggests a controversial correlation between angiogenesis and autophagy-that is both processes are regulated in a reciprocal fashion and autophagy has dual roles in regulation of angiogenesis. Inhibition of autophagy by 3-methyladenine (3-MA) or siRNA against autophagy related 5 (*Atg5*) reduces angiogenesis while induction of autophagy by overexpression of *Atg5* promotes angiogenesis (Du et al., 2012). In the myocardium, activation of autophagy during ischemia is essential for cell survival (Furman, 2015; Hamacher-Brady et al., 2007; Matsui et al., 2008). Elevated VEGF-A in ischemic

cardiomyocytes activates ROS-ER-initiated autophagy to trigger angiogenesis (Zou et al., 2019). Moreover, autophagy activation by mTOR inhibitor, rapamycin, enhances angiogenesis in the heat-denatured endothelial cells (P. Liang et al., 2018). This evidence suggests that autophagy positively regulates angiogenesis. On the contrary, some studies show that, autophagy negatively modulates angiogenesis. For example, mice deficient in autophagic protein Beclin1 (BECN1) display a pro-angiogenic phenotype. Kringle 5 of human plasminogen, a potent inhibitor of endothelial cell growth, induces autophagy and concurrently inhibits angiogenesis in absence of nutritional stress or hypoxia (Cho, Chen, Chang, Wu, & Shi, 2013). Activation of autophagy by Mebendazole is associated with inhibition of angiogenesis (Sung, Kim, Hong, & Joe, 2019). Endostatin, a well-characterized endogenous inhibitor of angiogenesis can also evoke autophagy (Nussenzweig, Verma, & Finkel, 2015).

The effects of autophagy on tumor angiogenesis also seems to be paradoxical as inhibition of autophagy by either genetic deletion of ATG5 or chloroquine treatment has different effects on tumor growth and angiogenesis. Blockage of autophagy by deleting ATG5 inhibits tumor growth with more chaotic and dysfunctional tumor vasculature, but does not prevent tumor metastasis, while CQ treatment produced opposite effect, it normalizes the vasculature, increases tissue oxygenation, and enhances medicine delivery. The results suggest that ATG5 may regulate vessel homeostasis through its autophagy-related function. However, CQ restrains tumor invasion and metastasis by normalization of vasculature independently of autophagy function (Maes et al., 2014). Thus, the precise role of autophagy in angiogenesis requires more detailed research.

1.4.6 Autophagy and endothelial dysfunction

The link between autophagy and vascular functions has been studied in vitro and in vivo. A basal level of autophagy is observed in laminar shear stress-stimulated ECs in human and murine arteries, which protects vessels from atherosclerosis, because activation of laminar shear stress fights against oxidative stress, promotes eNOS expression, and inhibits inflammation in ECs. However, ECs exposed to low shear stress that might induce intimal thickening and atherosclerosis development exhibit defective autophagy. In $Apoe^{-/-}$ mice with defective endothelial autophagy develops more severe atherosclerosis, which may attribute to endothelial dysfunction, immune cells infiltration, and lipid metabolism dysregulation (Guo et al., 2014; J. X. Zhang et al., 2018)

Undermined EC autophagy reduces shear-induced NO generation by impairing EC glucose metabolism and transportation, the compromised glycolysis inhibits purinergic pathway and ultimately inhibits eNOS phosphorylation at S1177 and NO generation (Bharath et al., 2017). Diabetic patients exhibit defective autophagy, inhibition of eNOS phosphorylation at S1177 in response to insulin stimulation, and impaired endothelial function. The positive effect of autophagy on NO production is supported by the evidence that enforced activation of autophagy in diabetic ECs restores eNOS activity and NO production (Fetterman et al., 2016).

Cardiac reperfusion injury leads to glutathionylation of eNOS (GS-eNOS) and prolongs the retention of GS-eNOS in cytosol, which promotes GS-eNOS degradation by CMA, and simultaneously decreases NO production and diminishes the eNOS bioavailability. Noteworthy, the macroautophagy is not involved in the degradation of GS-eNOS (Subramani, Kundumani-Sridharan, & Das, 2021). In type 2 diabetic mouse model, autophagy is suppressed, concurrent with elevation of eNOS monomerization. The impairment of autophagy intensifies mitochondrial

ROS generation, which adversely regulates dimerization of eNOS and suppresses NO formation (L. Zhao et al., 2022). It is well known that various environmental stresses potentiate ROS production, leading to oxidative stress and autophagy activation.

Extracellular oxidants or mitochondrial generated ROS directly activate lysosomal Ca^{2+} channel to release more Ca^{2+} into cytosol, which promotes TFEB nuclear translocation to activate the expression of autophagy and lysosomal biogenesis-related genes, thereby promoting autophagosome formation, autophagosome-lysosome fusion, and the degradation of autophagy substrates, which would feedback to initiate autophagy to clean damaged mitochondria and ROS, and to maintain intracellular homeostasis (X. Zhang et al., 2016).

1.5 Potential therapeutic strategies of autophagy for endothelial-related diseases

1.5.1 Potential therapeutic action of autophagy in angiogenesis

Anti-angiogenic drugs, such as bevacizumab and sunitinib, shrink tumor vascular network and induce hypoxia, which in turn increases autophagic flux. The role of activated autophagy in tumor development is debatable, although it generally serves as a mechanism of tumor suppression, by maintaining genomic integrity and preventing proliferation and inflammation. Accumulating evidence suggests that enhanced autophagy activity facilitates tumor cells to avoid energy deficiency and contributes to the resistance to chemotherapy (Yun & Lee, 2018). Autophagy inhibitor, hydroxychloroquine, combined with chemotherapy with Gemcitabine/Nab-Paclitaxel significantly inhibits the development of resectable pancreatic adenocarcinoma (Zeh et al., 2020).

However, some studies report that autophagy inhibition promotes the development of tumors. For example, Beclin-1 is downregulated in human breast carcinoma. Overexpression of

autophagic gene suppresses tumor growth (X. H. Liang et al., 1999). Administration of Pelareorep, a non-enveloped dsRNA virus that selectively lyses *KRAS*-mutated colorectal tumors cells, triggers tumor cell apoptosis, and inhibits tumor growth, which is associated with autophagy induction, suggesting that pelareorep treatment together with autophagy activator may enhance its anti-cancer effect (Jiffry et al., 2021). Moreover, autophagy-related proteins are elevated after endocrine therapy in hormone receptor (HR)-positive breast cancer, in which autophagy is considered as a positive signal that contributes to reducing tumor size (Ueno et al., 2019). Thus, combination of autophagy activators with anti-angiogenesis reagents may stand an effective strategy to inhibit tumor development (Y. Y. Li, Lam, Mak, Zheng, & Ho, 2013; Liu, Fan, Wang, & Sun, 2016).

1.5.2 Potential therapeutic action of autophagy in diabetic complications

Previous studies show that autophagy is suppressed in diabetic mouse heart (Ouyang, You, & Xie, 2014), alterations of autophagy genes are associated with certain cardiometabolic traits, including blood pressure, lipid levels and proinsulin levels (Portilla-Fernandez et al., 2019), and autophagy activation augments redox iron level by releasing ferritin-trapped iron, which worsens anemia and glucose utilization in diabetic patients (Zacharski, Shamayeva, & Chow, 2018). Moreover, multiple clinical studies demonstrate that inhibition of autophagy by acetylation of Beclin1 ameliorates podocyte impairment (Xu et al., 2022; D. Yang et al., 2018). In either HFD- or STZ-induced diabetic rat model, metformin treatment protects against acute kidney injury by upregulating autophagy (S. Zhang, Xu, Yu, Wu, & Sui, 2017). Also, administration of metformin prevents diabetic cardiomyopathy. Thus, understanding of autophagy in diabetic complications will facilitate the discovery of a new therapeutic target for the prevention and treatment of these life-threatening diabetes complications.

2 HYPOTHESES AND SPECIFIC AIMS

Endothelial cells cover the whole vasculature and form an interface between circulating blood and nearby tissues, which ensures optimal nutrients and oxygen delivery to organs. Thus, endothelial dysfunction is deeply involved the pathophysiology of many disease states, including cardiovascular disease and cancer. Autophagy is a catabolic process that degrades intracellular components in lysosome, and functions as an essential pathway to maintain cellular homeostasis. Recent studies reveal a role for deregulated endothelial autophagy in vascular senescence and vascular diseases. However, many unanswered questions remain, such as what is the non-autophagic functions of autophagy proteins in endothelial homeostasis? What are the underlying mechanisms by which ATG proteins impact endothelial function independently of their autophagy function? Can modulating a specific autophagic gene be a potential therapeutic target for pro-angiogenesis or anti-angiogenesis? Whether autophagy contributes to hyperglycemia-induced endothelial dysfunction? What are the mechanisms by which autophagy suppression contributes hyperglycemia-induced endothelial dysfunction? This dissertation seeks to answer the above questions by using biochemical, cellular, and in vivo models, and physiological and molecular biological techniques. My **hypothesis** is that lack of ATG protein (such as ATG7) inhibits ischemia-induced angiogenesis independently of its autophagy activity, and inhibition of autophagy mediates hyperglycemia-induced endothelial dysfunction, understanding the basic mechanisms of autophagy and ATG proteins in endothelial biology may provide novel strategies for clinical treatment of cardiovascular disease and cancer. Two animal models are applied to evaluate the hypothesis. One is hindlimb ligation induced angiogenesis and another one is

3 RESULT 1: ATG7 REUGATES ANGIOGENESIS IN AN AUTOPHAGY INDEPENDENT METHOD

Ablation of endothelial *Atg7* inhibits ischemia-induced angiogenesis by upregulating *Stat1* that suppresses *Hif1a* expression

Hongmin Yao[1], Jian Li[1], Zhixue Liu[1], Changhan Ouyang[2], Yu Qiu[1], Xiaoxu Zheng[1], Jing Mu[1], Zhonglin Xie[1#]

3.1 Acknowledgements

This study was supported by grants from The National Heart, Lung, and Blood Institute (NHLBI) (HL128014, HL132500, HL137371, and HL142287) to Zhonglin Xie and Ming-Hui Zou.

3.2 Abstract

Ischemia-induced angiogenesis is critical for blood flow restoration and tissue regeneration, but the underlying molecular mechanism is not fully understood. ATG7 (autophagy related 7) is essential for classical degradative macroautophagy/autophagy and cell cycle regulation. However, whether and how ATG7 influences endothelial cell (EC) function and regulates post-ischemic angiogenesis remain unknown. Here, we showed that in mice subjected to femoral artery ligation, EC-specific deletion of Atg7 significantly impaired angiogenesis, delayed the recovery of blood flow reperfusion, and displayed reduction in HIF1A (hypoxia inducible factor 1 subunit alpha) expression. In addition, in cultured human umbilical vein endothelial cells (HUVECs), overexpression of HIF1A prevented ATG7 deficiency-reduced tube formation. Mechanistically, we identified STAT1 (signal transducer and activator of transcription 1) as a transcription suppressor of HIF1A and demonstrated that ablation of Atg7 upregulated STAT1 in an autophagy independent pathway, increased STAT1 binding to HIF1A promoter, and suppressed

HIF1A expression. Moreover, lack of ATG7 in the cytoplasm disrupted the association between ATG7 and the transcription factor ZNF148/ZBP-89 (zinc finger protein 148) that is required for STAT1 constitutive expression, increased the binding between ZNF148/ZBP-89 and KPNB1 (karyopherin subunit beta 1), which promoted ZNF148/ZBP-89 nuclear translocation, and increased STAT1 expression. Finally, inhibition of STAT1 by fludarabine prevented the inhibition of HIF1A expression, angiogenesis, and blood flow recovery in atg7 KO mice. Our work reveals that lack of ATG7 inhibits angiogenesis by suppression of HIF1A expression through upregulation of STAT1 independently of autophagy under ischemic conditions, and suggest new therapeutic strategies for cancer and cardiovascular diseases.

3.3 Abbreviations:

ATG5: autophagy related 5; ATG7: autophagy related 7; atg7 KO: endothelial cell-specific atg7 knockout; ChIP: chromatin immunoprecipitation; CQ: chloroquine; ECs: endothelial cells; EP300: E1A binding protein p300; HEK293: human embryonic kidney 293 cells; HIF1A: hypoxia inducible factor 1 subunit alpha; HUVECs: human umbilical vein endothelial cells; IFNG/IFN-γ: Interferon gamma; IRF9: interferon regulatory factor 9; KPNB1: karyopherin subunit beta 1; MAP1LC3A: microtubule associated protein 1 light chain 3 alpha; MEFs: mouse embryonic fibroblasts; MLECs: mouse lung endothelial cells; NAC: N-acetyl-l-cysteine; NFKB1/NFκB: nuclear factor kappa B subunit 1; PECAM1/CD31: platelet and endothelial cell adhesion molecule 1; RELA/p65: RELA proto-oncogene, NF-kB subunit; ROS: reactive oxygen species; SP1: Sp1 transcription factor; SQSTM1/p62: sequestosome 1; STAT1: signal transducer and activator of transcription 1; ULK1: unc-51 like autophagy activating kinase 1; ulk1 KO: endothelial cell-specific ulk1 knockout; VSMCs: mouse aortic smooth muscle cells; WT: wild type; ZNF148/Zfp148/ZBP-89: zinc finger protein 148.

3.4 Introduction

Angiogenesis, the growth and proliferation of blood vessels from an existing vascular network, is essential for many physiological processes, such as embryogenesis, tissue repair, and organ regeneration (Potente, Gerhardt, & Carmeliet, 2011). This process needs to be finely balanced, because excessive or insufficient angiogenesis contributes to a number of pathologies, including myocardial infarction, diabetic retinopathy, rheumatoid arthritis, cancer, etc. (Folkman, 1995; Inampudi, Akintoye, Ando, & Briasoulis, 2018). The mechanisms that control angiogenesis are regulated by several pro- and anti-angiogenic factors that are mainly stimulated by oxygen deficiency, including VEGF (vascular endothelial growth factor) and EPO (erythropoietin) (Melincovici et al., 2018; Zhu et al., 2010). Most transcriptional responses to oxygen deficiency are mediated by HIFs (hypoxia-inducible factors) that control the expression of numerous angiogenic, metabolic, and cell cycle genes (Ke & Costa, 2006; Pugh & Ratcliffe, 2003). Accordingly, the HIF pathway is currently considered as a master regulator of angiogenesis. It is essential to gain an accurate and deep understanding of HIF transcriptional machineries related to angiogenesis in vascular disorders such as peripheral arterial disease, cerebral ischemia, and heart attack.

Autophagy is an intracellular degradation system that delivers cytoplasmic constituents to the lysosome for degradation (Rabinowitz & White, 2010; Xie, He, & Zou, 2011). Autophagy has been implicated in many pathophysiological processes, including cancer, metabolic and neurodegenerative disorders, cardiovascular and pulmonary diseases (Cheng et al., 2013). Moreover, increasing evidence suggests a controversial correlation between angiogenesis and autophagy. For example, Kringle 5 of human plasminogen, a potent inhibitor of endothelial cell growth, induces autophagy and concurrently inhibits angiogenesis in absence of nutritional stress

or hypoxia (Cho et al., 2013). Mice deficient in the autophagic protein BECN1/ Beclin1 display a pro-angiogenic phenotype. Inhibition of autophagy by 3-methyladenine (3-MA) or siRNA against *Atg5* (autophagy related 5) reduces angiogenesis while induction of autophagy by overexpression of *Atg5* promotes angiogenesis (Du et al., 2012). In the myocardium, activation of autophagy during ischemia is essential for cell survival (Furman, 2015; Hamacher-Brady et al., 2007; Matsui et al., 2008). However, the precise role of autophagy in angiogenesis requires more detailed research.

The molecular machinery of autophagy has been identified in both yeast and mammals, and a number of genes encoding components of autophagy machinery, named *ATG* (autopha*g*y related), have been characterized (Mizushima, 2020; Yin et al., 2016). Among these proteins, several core proteins, including ATG5 and ATG7, have long been believed to be essential for autophagy (Glick, Barth, & Macleod, 2010). The absence of ATG5 leads to functional inhibition of the autophagy machinery. Previous work has shown that endothelial-specific deficiency of ATG5 attenuates pathological hypoxia/reoxygenation-related neovascularization through suppression of autophagy (Sprott et al., 2019). ATG7 is required for the conjugation of ATG12 to ATG5 as an E1-like enzyme, and is specifically involved in autophagosome formation (Komatsu et al., 2005). Deletion of *ATG7* severely impairs autophagy, leading to mitochondrial dysfunction, endoplasmic reticulum stress, reactive oxygen species overproduction, and inhibition of protein secretion (Antonucci et al., 2015; Heinitz et al., 2019; Mortensen et al., 2010; Qiao et al., 2020; Torisu et al., 2013; Y. Zhuang et al., 2016). In addition, several autophagy-independent functions of ATG7 have been described. Upon starvation, ATG7 interacts with TP53/p53 to inhibit the expression of pro-apoptotic genes. Accordingly, *Atg7* deletion increases DNA damage and promotes apoptotic cell death (I. H. Lee et al., 2012). Another study also shows that ATG7

represses the pro-apoptotic properties of caspase 9 (Han et al., 2014). This E1 enzymatic independent function of ATG7 might be implicated in other pathological conditions (Mauthe & Reggiori, 2016; Rosenfeldt et al., 2013). It is reported that under normoxic conditions, vascular density in skeletal muscle is indistinguishable between wild-type (WT) and EC-specific *atg7* knockout (*atg7* KO) mice, but brain microvessel density of *atg7* KO mice is significantly decreased (Torisu et al., 2013; S. F. Zhuang et al., 2017), which is accompanied by inhibiting nuclear translocation of NFkB subunit RELA/p65 that reduces IL6 (interleukin 6) production (S. F. Zhuang et al., 2017). However, it is not clear whether the regulation of RELA/p65 nuclear translocation by ATG7 is dependent or independent of autophagy. Since ATG7 is induced by hypoxia (J. Wu et al., 2015), induction of endothelial cell apoptosis may limit unwanted neovascularization of tumors, and prevention of endothelial cell apoptosis may improve angiogenesis and vasculogenesis in patients with ischemia (Dimmeler & Zeiher, 2000), it is important to understand whether and how the autophagy-independent functions of ATG7 influence endothelial cell function and regulate post-ischemic angiogenesis.

In the current study, using a mouse hindlimb ischemia model, we show inhibition of angiogenesis and impairment of post-ischemic blood flow recovery in EC-specific *atg7* KO mice. The loss of *Atg7* reduces HIF1A expression by upregulating *Stat1* in an autophagy-independent manner. Our findings uncover a novel direct link between ATG7 and post-ischemic angiogenesis and may lead to novel therapeutic strategies in the treatment of cancer or ischemic cardiovascular disorders.

3.5 Results

3.5.1 Angiogenesis is inhibited in endothelial-specific atg7 knockout mice subjected to femoral artery ligation.

To determine the role of ATG7 in angiogenesis, we generated endothelial *atg7*-specific knockout mice by mating female *Atg7*$^{flox/flox}$ mice with male *Cdh5*-Cre mice, and the offspring was genotyped by PCR (Komatsu et al., 2005). The mice with genotype *Atg7*$^{flox/flox}$/*Cdh5*-Cre^{+} were referred as to *atg7* KO, and the littermates with genotype *Atg7*$^{flox/flox}$/*Cdh5*-Cre^{-} were used as wild-type (WT) control (Figure 3.1 A). We examined ATG7 protein expression in isolated mouse lung endothelial cells (MLECs) and mouse aortic smooth muscle cells (VSMCs) by western blotting and found that endothelial ATG7 protein expression was abolished in *atg7* KO mice. However, deletion of endothelial *Atg7* gene did not affect ATG7 protein expression in VSMCs isolated from *atg7* KO mouse aortas, confirming specific knockout of *Atg7* in endothelial cells (Figure 3.1 B). To determine the effects of endothelial *Atg7* deletion on angiogenesis *in vivo*, we performed femoral artery ligation in WT and *atg7* KO mice at the age of 8 to 10 weeks and monitored blood flow restoration on 1, 3, 7, 14, 21, and 28 days after surgery by Laser Doppler Imaging (Figure 3.1 C). Four weeks post-surgery, the blood flow ratio returned to 1.04 ± 0.14 in WT mice, however, the blood flow ratio only recovered to 0.70 ± 0.11 in *atg7* KO mice (Figure 3.1 D), indicating an obvious impairment in perfusion recovery in *atg7* KO mice.

We further assessed angiogenesis by immunostaining of PECAM1/CD31 (platelet and endothelial cell adhesion molecule 1) in ischemic tissues. There was no obvious difference in the number of PECAM1/CD31-positive capillaries surrounding the gastrocnemius muscle fibers between *atg7* KO mice and their WT littermates in sham-operated condition (Figure 3.1 E and

F). Four weeks post ischemic insult, there was a significant increase in the number of PECAM1/CD31-positive capillaries in WT mice. However, the increase in the PECAM1/CD31-positive capillary was attenuated in *atg7* KO mice (Figure 3.1 E and F). Thus, *Atg7* deficiency delayed the ischemia-induced angiogenesis *in vivo*.

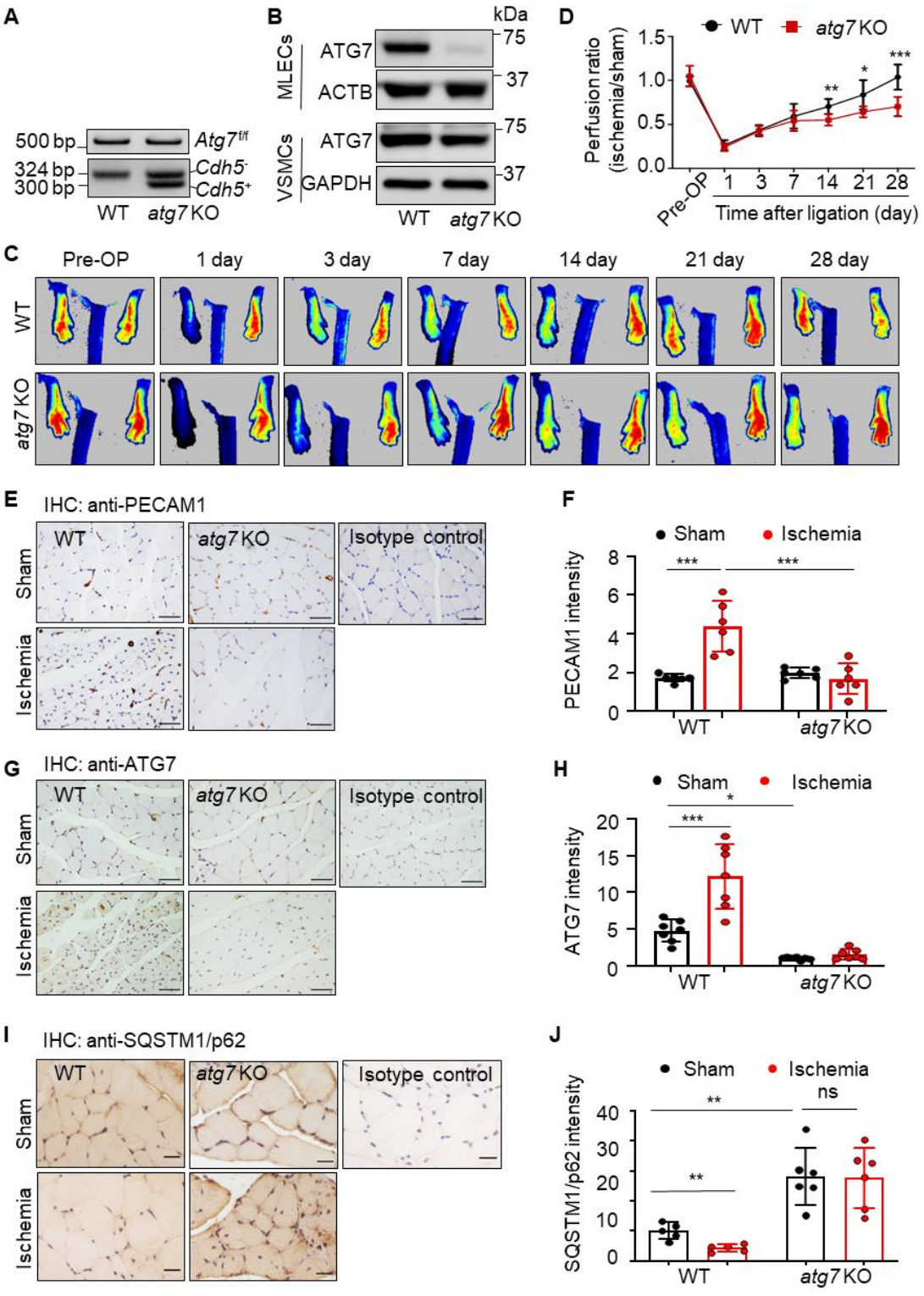

Figure 3.1 Endothelial Atg7 deletion impairs blood perfusion recovery and angiogenesis in mouse ischemic hind limbs

(**A**) Genotyping of WT (wild-type, *Atg* $^{f/f}$*/cdh5*$^{-}$) and *atg7* KO (*atg7* endothelial cell specific knockout, *Atg7* $^{f/f}$*/cdh5*$^{+}$) mice. (**B**) Western blot analysis of ATG7 in mouse lung endothelial cells (MLECs) and arterial smooth muscle cells (VSMCs) isolated from WT and *atg7* KO mice. (**C** and **D**) Femoral artery ligation was performed on 8–10-week-old WT and *atg7* KO mice. Representative images showing blood flow reperfusion assessed by Doppler laser ultrasound after ischemic injury (C). Blood flow was detected by laser Doppler at the indicated time points. The ratio of ischemic/non-ischemic perfusion, N = 7 for each group. * $P < 0.05$, ** $p < 0.01$; *** $p < 0.001$ (D). (**E**) Representative images of immunostaining for PECAM1/CD31 in gastrocnemius muscles of mice subjected to femoral artery ligation. Scale bar: 50 μm. (**F**) Quantification of immunohistochemistry staining for PECAM1/CD31. N = 6 for each group, *** $p < 0.001$. (**G**) Representative images of immunostaining for ATG7 in gastrocnemius muscles of mice subjected to femoral artery ligation. Scale bar: 50 μm. (**H**) Quantification of immunohistochemistry staining for ATG7. N = 7 for each group, * $p < 0.05$, *** $p < 0.001$. (**I**) Representative images of immunostaining for SQSTM1/p62 in gastrocnemius muscles of mice subjected to femoral artery ligation. Scale bar: 20 μm. (**J**) Quantification of immunohistochemistry staining for SQSTM1/p62. N = 5-6 for each group, ** $p < 0.01$, ns, not significant.

We also determined the effect of ischemia on autophagy activity. In WT mice, femoral artery ligation significantly increased the immunostaining intensity of ATG7 compared with sham surgery. Deletion of *Atg7* prevented femoral artery ligation-increased ATG7 protein expression (Figure 3.1 G and H). Concomitantly, in WT mice, protein level of SQSTM1/p62 (sequestosome 1), an autophagic flux marker, was significantly lower ($P < 0.05$) in the femoral artery ligation group than that in the sham-operated group. Lack of *Atg7* enhanced SQSTM1/p62 in sham-operated mice and prevented femoral artery ligation-reduced SQSTM1/p62 protein expression (Figure 3.1 I and J), suggesting that femoral artery ligation increases autophagic flux. Similarly, in cultured HUVECs, compared with normoxic treatment, hypoxia upregulated ATG7 protein expression and activated autophagy, as indicated by increased MAP1LC3A/LC3 (microtubule associated protein 1 light chain 3 alpha)-II:MAP1LC3A/LC3-I ratio and decreased SQSTM1/p62 protein level (Figure 3.2 A and B).

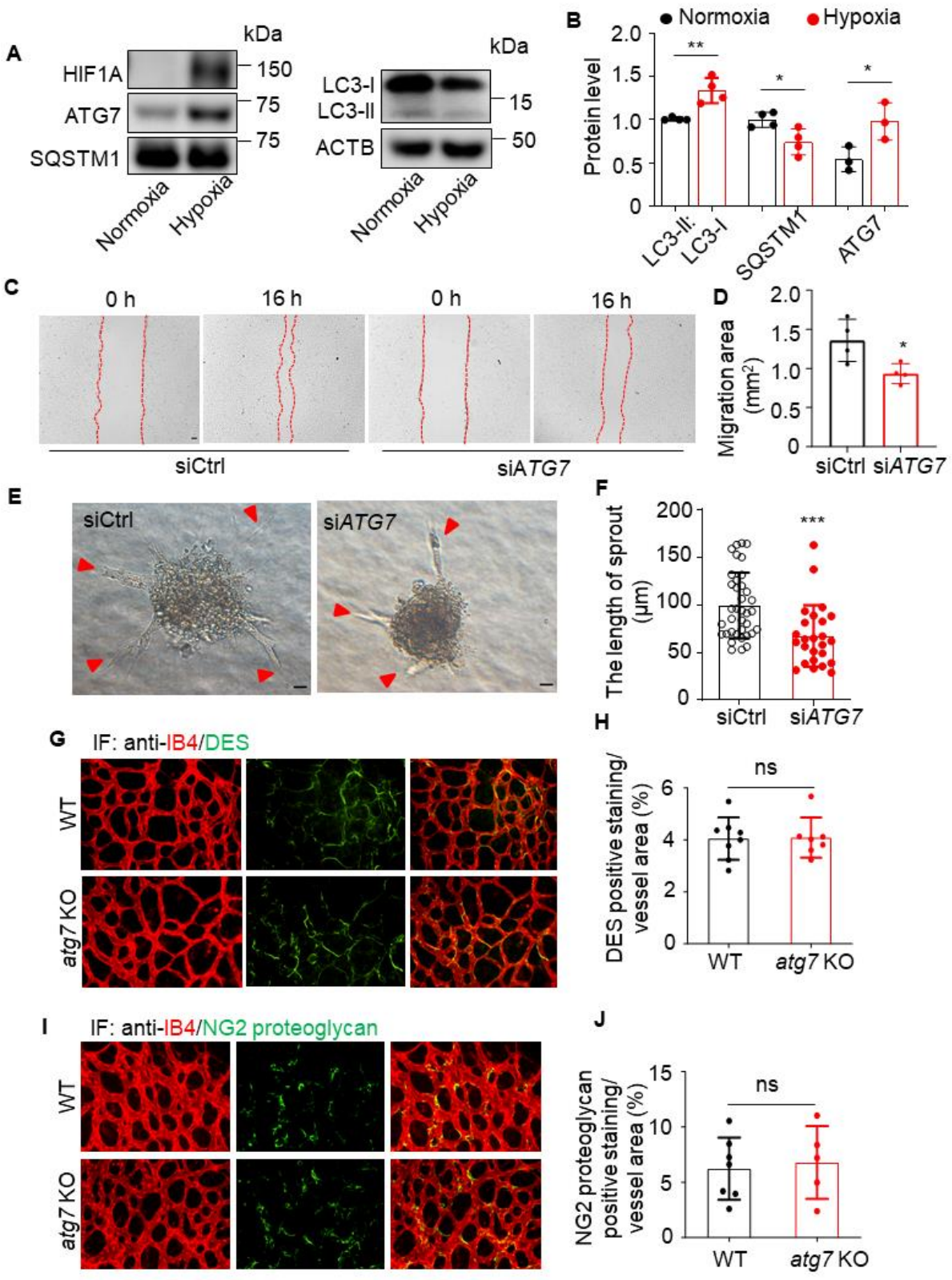

Figure 3.2 Hypoxia activates autophagy in cultured HUVECs and Atg7 deficiency inhibits endothelial cell migration.

(A and B) HUVECs were cultured in hypoxic chamber for 16 h, protein levels of HIF1A, ATG7, SQSTM1/p62, and MAP1LC3A/LC3-II:MAP1LC3A/LC3-I were determined by western blot (A) and densitometry (B). N = 3-4, * $p < 0.05$, ** $p < 0.01$. (C) HUVECs were transfected with siCtrl or siATG7 for 48 h, cell migration was determined by wound healing assay. Scale bar: 500 μm. (D) Migration area was quantified. N = 4, * $p < 0.05$. (E and F) HUVECs were transfected with siCtrl or siATG7 for 24 h. Three-dimensional spheroids were generated in rat tail collagen I for another 24 h and representative images of spheroids sprouting were analyzed. N = 27-35 spheroids, *** $p < 0.001$. Scale bar: 20 μm. (G) Representative images of immunofluorescence staining for pericyte marker DES (desmin) in WT and atg7 KO retina. (H) Quantification of DES staining. WT = 8 retinas, atg7 KO = 7 retinas, 3-8 views were analyzed in each retina. (I) Representative images of immunofluorescence staining for pericyte marker NG2 proteoglycan. (J) Quantification of NG2 proteoglycan staining. WT = 7 retinas, atg7 KO = 5 retinas, 5-8 views were analyzed in each retina. ns: no significance.

Next, we assessed the effects of *Atg7* deficiency on ECs migration *in vitro*. Wound healing assay showed that HUVECs transfected with *ATG7* siRNA exhibited impaired migration compared with the HUVECs transfected with control siRNA (Figure 3.2 C and D). In addition, spheroid-sprouting assay revealed a reduction in sprout length in *Atg7*-deficient endothelial cells (Figure 3.2 E and F), suggesting that ATG7 deficiency inhibits EC migration. Given that pericytes are critically involved in angiogenic response (Kang et al., 2019), we determined whether deletion of *Atg7* affects pericyte function by immunofluorescence staining of pericyte markers, DES (desmin) and NG2 proteoglycan, in WT and *atg7* KO retinas. The staining of both DES (Figure 3.2 G and H) and NG2 proteoglycan (Figure 3.2 I and J) was comparable between WT and *atg7* KO retinas, suggesting lack of *Atg7* has no effect on pericyte coverage.

To determine whether suppression of endothelial autophagy regulates angiogenesis *in vivo*, we knocked out endothelial *ulk1* (unc-51 like autophagy activating kinase), an important molecule in regulating autophagy initiation (Egan, Kim, Shaw, & Guan, 2011), to generate *ulk1* endothelial cell-specific knockout (*ulk1* KO) mice. Western blot analysis of ULK1 protein expression in MLECs demonstrated that endothelial ULK1 protein expression was abolished in *ulk1* KO mice, indicating knockout of *Ulk1* in endothelial cells (Figure 3.3 A). To determine the

effect of *Ulk1* deletion on autophagy, we detected protein level of SQSTM1/p62 and MAP1LC3A/LC3-II:MAP1LC3A/LC3-I ratio. In *ulk1* KO MLECs, SQSTM1/p62 protein level was significantly ($P < 0.05$) increased whereas MAP1LC3A/LC3-II:MAP1LC3A/LC3-I ratio was reduced Figure 3.3 B and C), indicating autophagic flux suppression. We then determined the effect of autophagy suppression on angiogenesis by performing femoral artery ligation in WT and *ulk1* KO mice at the age of 8 to 10 weeks, and monitored blood flow restoration on 1, 3, 7, 14, 21, and 28 day after surgery by Laser Doppler Imaging (Figure 3.3 E). Four weeks post-surgery, the blood flow ratios were comparable between WT and *ulk1 KO* mice (Figure 3.3 D), indicating that suppression of autophagy by *ulk1* deletion had no significant effect on perfusion recovery.

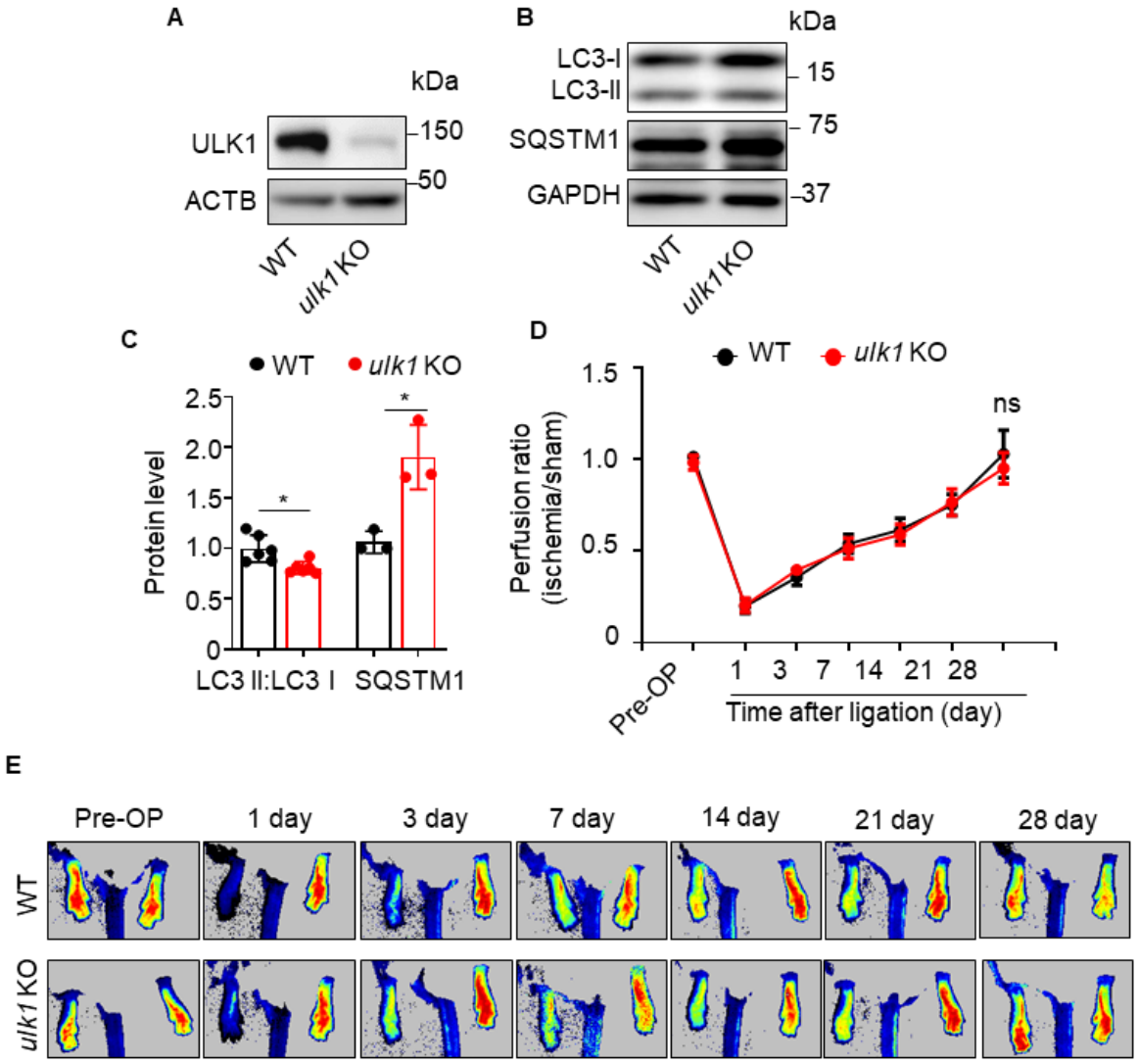

Figure 3.3 Endothelial Ulk1 deletion has no effect on blood perfusion recovery in mouse ischemic hind limbs.
(A) Western blot analysis of ULK1 in mouse lung endothelial cells (MLECs) isolated from WT and ulk1 KO mice. (B) Western blot analysis of MAP1LC3A/LC3-II:MAP1LC3A/LC3-I and SQSTM1/p62 expression in MLECs isolated from WT and ulk1 KO mice. (C) Quantification of protein levels of MAP1LC3A/LC3-II:MAP1LC3A/LC3-I and SQSTM1/p62. N = 3-6, * $p < 0.05$. (D) Femoral artery ligation was performed on 8–10-week-old WT and ulk1 KO mice. Blood flow was detected by Laser Doppler Imaging at the indicated time points. The ratio of ischemic/non-ischemic perfusion, N = 5-6 for each group. (E) Representative images showing blood flow reperfusion assessed by Laser Doppler Imaging after ischemic injury.

3.5.2 Lack of ATG7 inhibits HIF1A expression and tube formation.

Given that HIF1A is a key modulator of the transcriptional response to hypoxic stress and plays a critical protective role in ischemic cardiovascular diseases by regulating angiogenesis and vascular remodeling (Semenza, 2014), we detected HIF1A expression using immunohistochemistry in gastrocnemius muscles of WT and *atg7* KO mice subjected to femoral artery ligation (Fig. 2A). The result showed that the ligation significantly increased HIF1A expression in ischemic limbs of WT mice, while the ligation failed to upregulate HIF1A expression in *atg7* KO mice (Figure 3.4 A and B), suggesting that *Atg7*-deficiency inhibits ischemia-induced HIF1A expression. We further investigated whether hypoxia regulates HIF1A expression in MLECs isolated from WT and *atg7* KO mice. Deletion of *Atg7* significantly reduced *Hif1a* mRNA expression (Figure 3.4 C), and hypoxia increased HIF1A protein level in WT MLECs, whereas the hypoxia-induced HIF1A expression was attenuated in *atg7* KO MLECs (Figure 3.4 D and E). Similarly, treatment of MLECs with cobalt chloride ($CoCl_2$), a well-known hypoxia mimetic mediator (Ciafre, Niola, Giorda, Farace, & Caporossi, 2007; Dai et al., 2008), increased HIF1A expression in WT MLECs, and deletion of *Atg7* lessened the $CoCl_2$-upregulated HIF1A expression **(**Figure 3.4 F and G). Similar results were observed in HUVECs transfected with control siRNA (siCtrl) or *ATG7* siRNA (si*ATG7*) (Figure 3.5 A, B, C and D). However, overexpression of ATG7 did not influence HIF1A expression in both normoxic and hypoxic conditions (Figure 3.5 E and F). Notably, *ATG7* deficiency did not prevent hypoxia-upregulated HIF2A protein expression (Figure 3.5 G and H). Since *HIF1A* is an early response gene (Bartoszewska et al., 2015), we examined *HIF1A* mRNA expression in HUVECs transfected with siCtrl or si*ATG7* at 30, 60, and 120 min after exposure to hypoxia. The results showed that *ATG7* deficiency depressed hypoxia-induced *HIF1A* mRNA expression at these

time points (Figure 3.4 H). To determine whether reduction in HIF1A mediates *ATG7*-deficiency-inhibited angiogenesis, we analyzed tube formation in HUVECs co-transfected with *HIF1A* plasmid and *ATG7* siRNA. As depicted in Figure 3.4 I and J, hypoxia upregulated HIF1A expression in siCtrl-treated cells. The transfection of *HIF1A* plasmid increased HIF1A in normoxic condition and induced a further increase in HIF1A in hypoxic condition. However, in the cells transfected with si*ATG7*, HIF1A expression was significantly suppressed in both normoxic and hypoxic conditions. In line with the expression of HIF1A, silencing *ATG7* reduced tube formation in both normoxic and hypoxic conditions. By contrast, overexpression of *HIF1A* in *ATG7*-silenced cells attenuated the reduction in tube formation under both normoxic and hypoxic conditions (Figure 3.4 K and L). These data suggest that ATG7 deficiency downregulates HIF1A expression at the transcriptional level and inhibits angiogenesis *in vitro*.

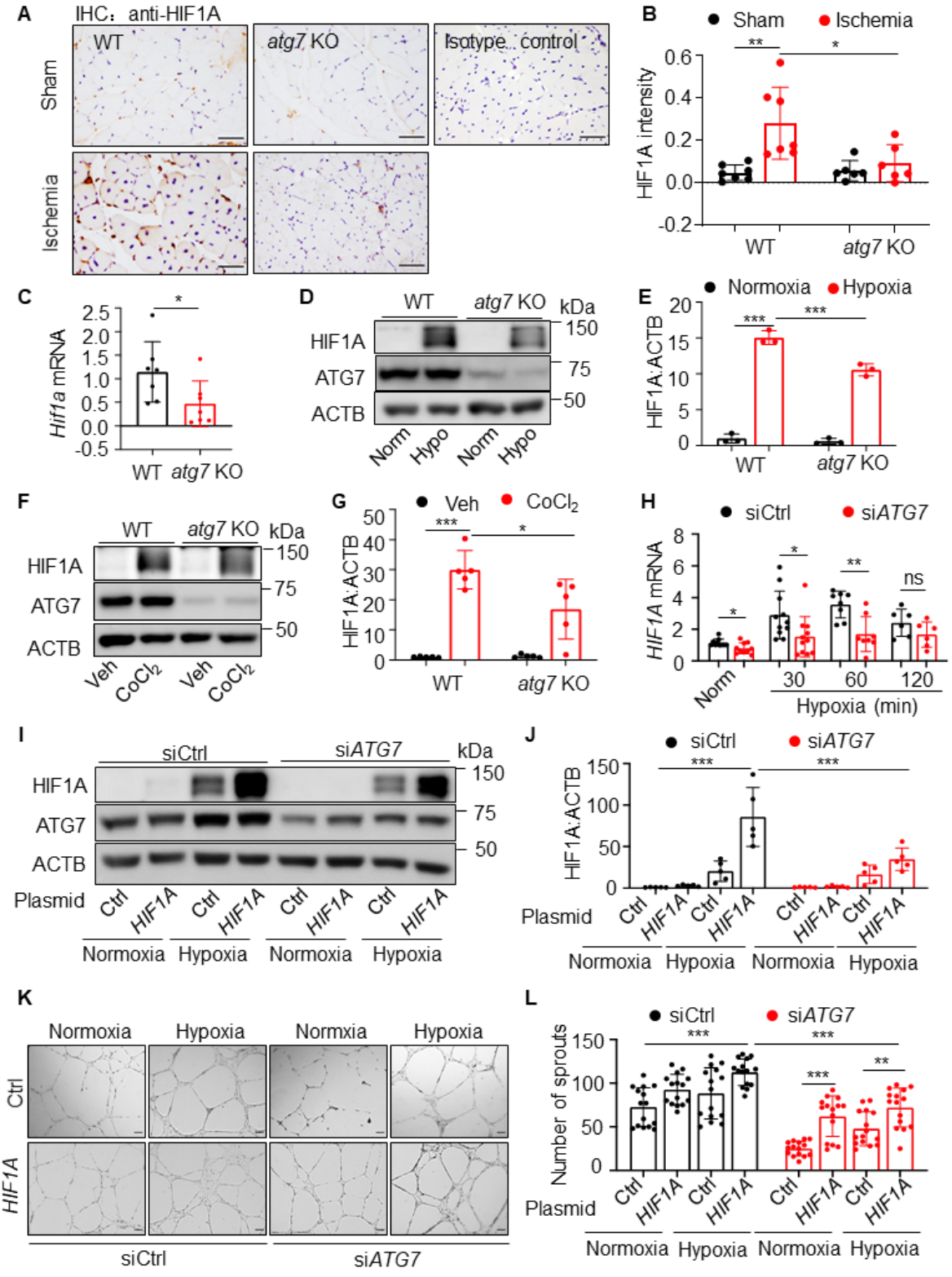

Figure 3.4 Lack of ATG7 inhibits hypoxia-induced HIF1A expression.

(A) Representative images of immunostaining for HIF1A in gastrocnemius muscles of mice subjected to 4-week femoral artery ligation. Scale bar: 50 μm. (B) Quantification of the HIF1A staining area in gastrocnemius muscle. N = 6-7, * $p < 0.05$, ** $p < 0.01$. (C) *Hif1a* mRNA level was determined by RT-PCR. N = 7, * $p < 0.05$. (D and E) MLECs were cultured in hypoxic chamber (1% O_2, 5% CO_2, 94% N_2) for 24 h, HIF1A protein expression was determined by western blot (D) and densitometry (E). N = 3, *** $p < 0.001$. (F and G) MLECs were treated with $CoCl_2$ for 24 h. HIF1A protein expression was determined by western blot (F) and densitometry (G). N = 5, * $p < 0.05$, *** $p < 0.001$. (H) *HIF1A* mRNA level in HUVECs transfected with siRNA (siCtrl) or ATG7 siRNA (si*ATG7*) was determined by RT-PCR at indicated time points. N = 6-11, * $p < 0.05$, ** $p < 0.01$; ns, not significant. (I and J) HUVECs were transfected with siCtrl, si*ATG7* and MYC-control (Ctrl) or MYC-HIF1A (*HIF1A*) plasmid for 24 h and then incubated in hypoxia chamber for another 16 h. HIF1A protein expression was analyzed by western blotting (I) and densitometry (J). N = 5, *** $p < 0.001$. (K) Representative images of tube formation assay from three independent experiments. Scale bar: 500 μm. (L) Quantitative analysis of the number of sprouts. N = 15 fields, ** $p < 0.01$, *** $p < 0.001$.

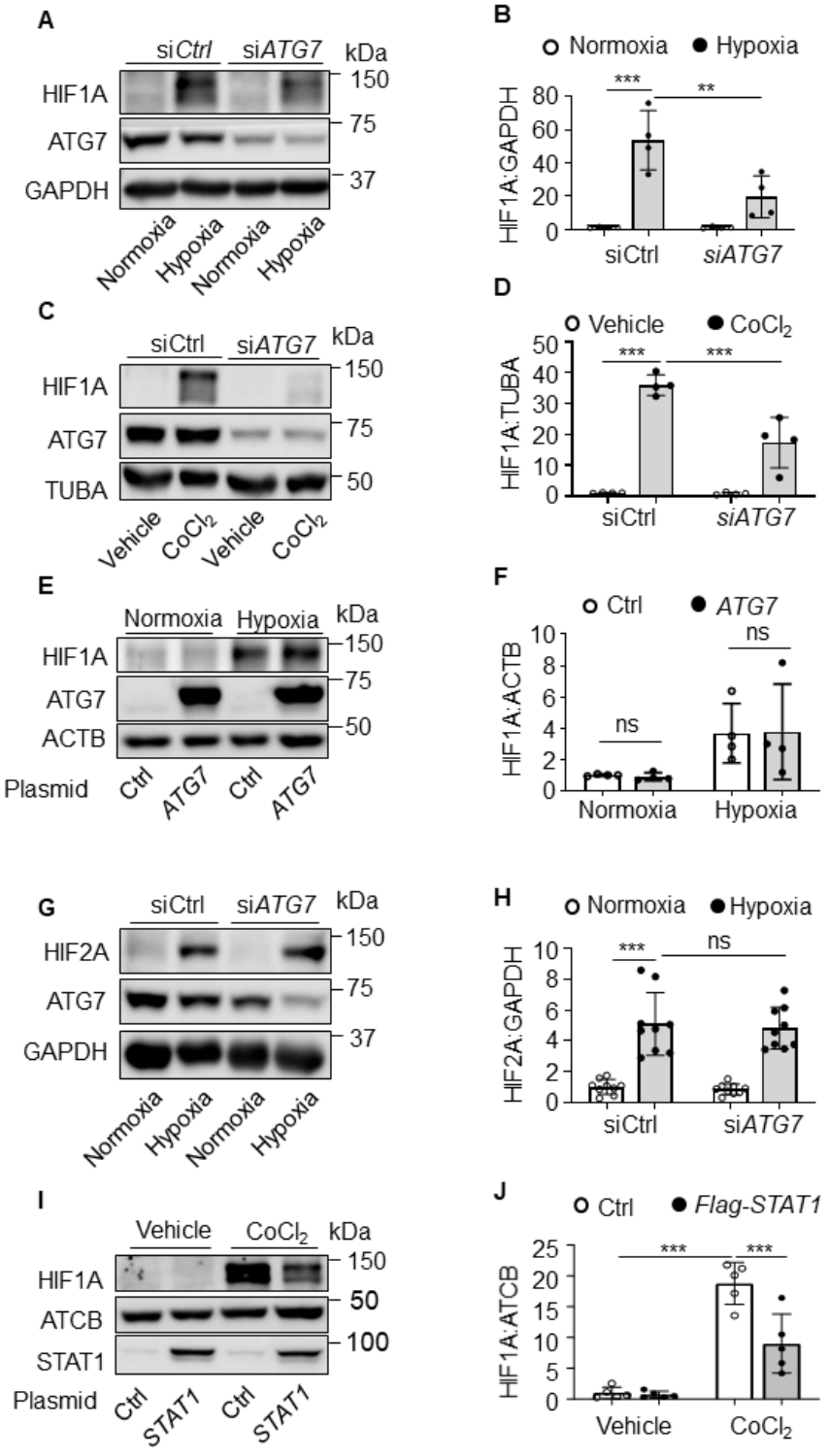

Figure 3.5 ATG7 deficiency inhibits hypoxia-induced HIF1A expression, but has no impact on HIF2A expression.

(A and B) HUVECs were transfected with siCtrl or siATG7 for 24 h, and then incubated in hypoxic chamber (1% O_2, 5% CO_2, 94% N_2) for another 16 h. HIF1A protein expression was analyzed by western blot. N = 4, ** $p < 0.01$, *** $p < 0.001$. (C and D) HUVECs were transfected with siCtrl or si*ATG7* for 24 h and treated with vehicle or $CoCl_2$ for another 16 h. ATG7 and HIF1A protein expression was measured by western blot and densitometric analysis. N = 4, *** $p < 0.001$. (E and F) HUVECs were transfected with Ctrl or ATG7 (*MYC-ATG7*) plasmid for 24 h, and then incubated in hypoxic chamber for another 16 h. ATG7 and HIF1A protein expression was measured by western blot and densitometric analysis. N = 4, ns, not significant. (G and H) HUVECs were transfected with siCtrl or si*ATG7* for 24 h, and then incubated in hypoxic chamber for another 16 h. ATG7 and HIF2A protein expression was measured by western blot and densitometric analysis. N = 9, ns, not significant. (I) Overexpression of STAT1 inhibits HIF1A expression in hypoxic conditions. HUVECs were transfected with STAT1 (Flag-*STAT1*) or control (Ctrl) plasmid for 24 h, and then treated with vehicle or $CoCl_2$ for another 16 h. Protein levels of STAT1 and HIF1A were determined by western blot. (J) Quantitative analysis of HIF1A protein levels. N = 5, *** p < 0.001.

3.5.3 Upregulation of STAT1 inhibits HIF1A expression in ATG7-deficient conditions.

Increasing evidence shows that HIF1A expression can be regulated at the mRNA level by transcription factors under hypoxic conditions (Galban & Gorospe, 2009). Transcription factors, such as the ISGF3 (interferon stimulated gene factor 3) complex, which is composed of STAT1, STAT2, IRF9 (interferon regulatory factor 9), STAT3, NFKB1/NFκB (nuclear factor kappa B subunit 1), NRF1 (nuclear respiratory factor 1), and BCLAF1 (BCL2 associated transcription factor 1), can bind to the *HIF1A* gene promoter to regulate *HIF1A* transcription (Gerber & Pober, 2008; Koyasu, Kobayashi, Goto, Hiraoka, & Harada, 2018; Park et al., 2017; Rius et al., 2008; Wen et al., 2019). Therefore, we identified the potential transcriptional factors that mediate the inhibition of *HIF1A* expression in *ATG7*-deficient condition by analyzing the expression of the six transcriptional factor genes using RT-PCR. In si*ATG7*-transfected HUVECs, *STAT1* mRNA had the highest expression with an increase of 13.3 folds, and that was followed by the increase in *IRF9* gene expression (4.8 folds). However, silencing *ATG7* did not affect the expression of *STAT3*, *NFKB1/NFκB*, *NRF1*, and *BCLAF1* genes (Figure 3.6 A).

To determine whether STAT1 engages in *ATG7*-deficiency-inhibited HIF1A expression, we first silenced both *ATG7* and *STAT1* in HUVECs and assessed *HIF1A* mRNA expression in normoxic condition. We found that silencing *ATG7* reduced *HIF1A* mRNA expression, and *STAT1* knockdown enhanced *HIF1A* mRNA expression as compared with siCtrl and prevented the reduction in *HIF1A* mRNA expression in si*ATG7*-transfected HUVECs (Figure 3.6 B). We further assessed the effect of STAT1 on *ATG7* deficiency-reduced HIF1A expression in normoxic and hypoxic conditions. The results demonstrated that hypoxia increased HIF1A protein expression, silencing *ATG7* attenuated hypoxia-enhanced HIF1A protein level, and *ATG7* deficiency-induced HIF1A reduction was prevented by silencing *STAT1* (Figure 3.6 C and D). Conversely, transfecting a plasmid encoding *STAT1* significantly suppressed *HIF1A* mRNA expression and attenuated hypoxia-upregulated HIF1A protein expression (Figure 3.6 E, F and G). Similarly, treatment of HUVECs with $CoCl_2$ to induce hypoxia increased HIF1A protein level in the cells treated with control plasmid, and the increase in HIF1A protein expression was attenuated by overexpression of *STAT1* (Figure 3.5 I and J).

To determine that STAT1 mediates the transcriptional regulation of *HIF1A* by ATG7, we tested whether ATG7 affects STAT1 binding to the *HIF1A* gene promoter in HUVECs. Chromatin immunoprecipitation (ChIP) assay showed that silencing *ATG7* significantly increased STAT1 binding to the *HIF1A* promotor in both normoxic and hypoxic conditions (Figure 3.6 H and I). Taken together, upregulation of STAT1 mediates the negative regulation of *HIF1A* in ATG7-deficient endothelial cells.

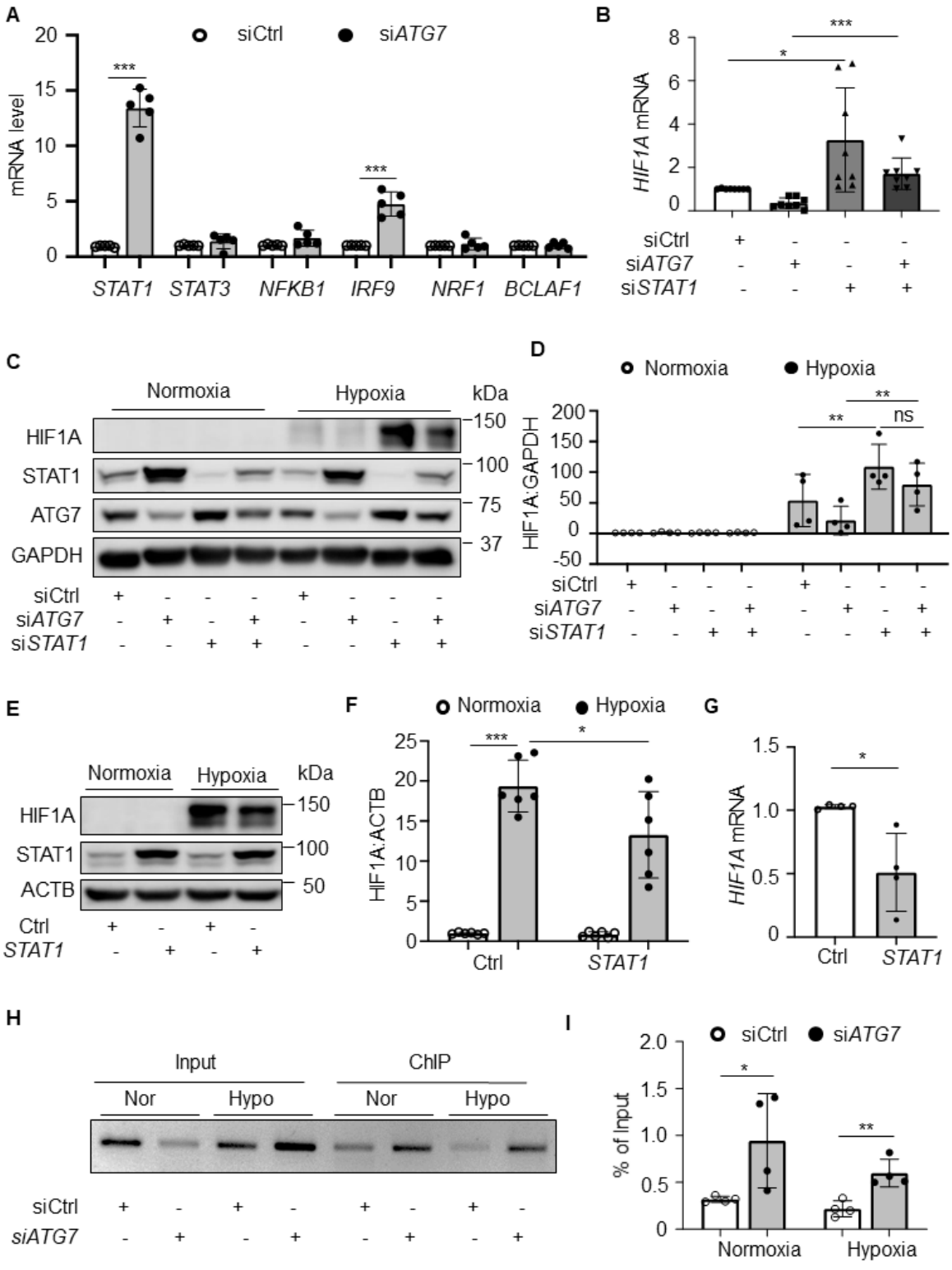

Figure 3.6 Upregulation of STAT1 inhibits HIF1A expression in ATG7-deficient conditions.

(A) Expression of genes related to HIF1A expression, including *STAT1*, *STAT3*, *NFKB1/NFκB*, *IRF9*, *NRF1*, *BCALF1* was determined by RT-PCR in control and ATG7-deficient HUVECs, N = 5, *** $p < 0.001$. (B) HUVECs were transfected with siCtrl, si*ATG7*, *STAT1* siRNA (si*STAT1*), or si*ATG7* and si*STAT1* for 48 h, HIF1A mRNA expression was determined by RT-PCR. N = 8, * $p < 0.05$, *** $p < 0.001$. (C) HUVECs were transfected with siCtrl, siATG7, siSTAT1, or siATG7 and siSTAT1 for 24 h, and then incubated in hypoxic chamber for another 16 h. HIF1A protein level was measured by western blot. (D) Densitometric analysis of the western blots. N = 4, ** $p < 0.01$, ns, not significant. (E) HUVECs were transfected with Flag-control (Ctrl) or Flag-STAT1 (STAT1) plasmid for 24 h, and then incubated in hypoxia chamber for another 16 h. Protein levels of STAT1 and HIF1A were determined by western blot. (F) Quantitative analysis of HIF1A protein levels. N = 6, * $p < 0.05$, *** $p < 0.001$. (G) HUVECs were transfected with *STAT1* or Ctrl plasmid for 24 h, *HIF1A* mRNA was determined by RT-PCR. N = 4, * $p < 0.05$. (H and I) HUVECs were transfected with siCtrl or si*ATG7* for 48 h and followed by hypoxia stimulation for 1 h. ChIP analysis was performed to determine the association of STAT1 and *HIF1A* promoter region. (H) RT-PCR products were analyzed by ethidium bromide-stained gel analysis. (I) RT-PCR quantitative analysis. N = 4, * $p < 0.05$, ** $p < 0.01$.

3.5.4 Loss of ATG7 increases STAT1 expression and inhibits tube formation.

As silencing *STAT1* significantly mitigated the reduction of HIF1A expression in ATG7-deficient condition, we explored the mechanism by which ATG7 modulates STAT1 expression. As demonstrated in Figure 3.7 A and B, deletion of *Atg7* increased SQSTM1/p62 protein level and reduced the conversion of MAP1LC3A/LC3-I to MAP1LC3A/LC3-II in MLECs. Similar results were also found in HUVECs transfected with si*ATG7* (Figure 3.8 A, B, and C). In addition, treating MLECs with chloroquine (CQ) to inhibit lysosomal enzyme activity significantly increased MAP1LC3A/LC3-II:MAP1LC3A /LC3-I level in WT MLECs but the effect was prevented in *atg7* KO MLECs, suggesting that lack of *Atg7* completely blocked the conversion of MAP1LC3A/LC3-I to MAP1LC3A/LC3-II (Figure 3.7 C and D). The deletion of *Atg7* also significantly upregulated *Stat1* mRNA (Figure 3.7 E), and increased STAT1 protein level and phosphorylation of STAT1 at tyrosine 701 (Y701) (p-STAT1) (Figure 3.7 F and G), but did not affect the protein levels of p-STAT6, p-STAT3, and p-STAT5 (Figure 3.7 H and I). Also, silencing *ATG7* in HUVECs upregulated *STAT1* mRNA expression (Figure 3.8 D), and increased STAT1 and p-STAT1 protein levels (Figure 3.8 E, F, G and H), but had no effect on

protein expression of STAT3, p-STAT3, STAT5, p-STAT5, and STAT6 (Figure 3.8 4I). To determine whether the regulatory effect of ATG7 on STAT1 is dependent on its role in regulating autophagy, we silenced *ULK1*, a key initiator of mammalian autophagy (D. Egan et al., 2011), and observed a significant suppression of autophagy, as indicted by increased SQSTM1/p62 and reduced the ratio of MAP1LC3A/LC3-II:MAP1LC3A /LC3-I (Figure 3.7 J and K). However, suppression of autophagy by silencing *ULK1* did not increase protein levels of STAT1 and p-STAT1 (Figure 3.7 L and M). Similarly, inhibition of autophagy by either silencing *SQSTM1/p62* (Figure 3.9 A and B) or administrating CQ had no effect on STAT1 and p-STAT1 expression (Figure 3.9 E and F). Further, inhibition of autophagy by knockout of *atg5* (*atg5*$^{-/-}$) did not upregulate *Stat1* mRNA in *atg5*$^{-/-}$ mouse embryo fibroblasts (MEFs) (Figure 3.9 G). Notably, silencing *Atg7* in *ulk1* KO MLECs significantly upregulated STAT1 and p-STAT1 levels (Figure 3.9 H and I). Likewise, knocking down of *ATG7* in HUVECs-transfected with *ULK1* siRNA increased STAT1 and p-STAT1 protein expression (Figure 3.9 J and K). These results suggest that ATG7 deficiency upregulates STAT1 independently of autophagy activity.

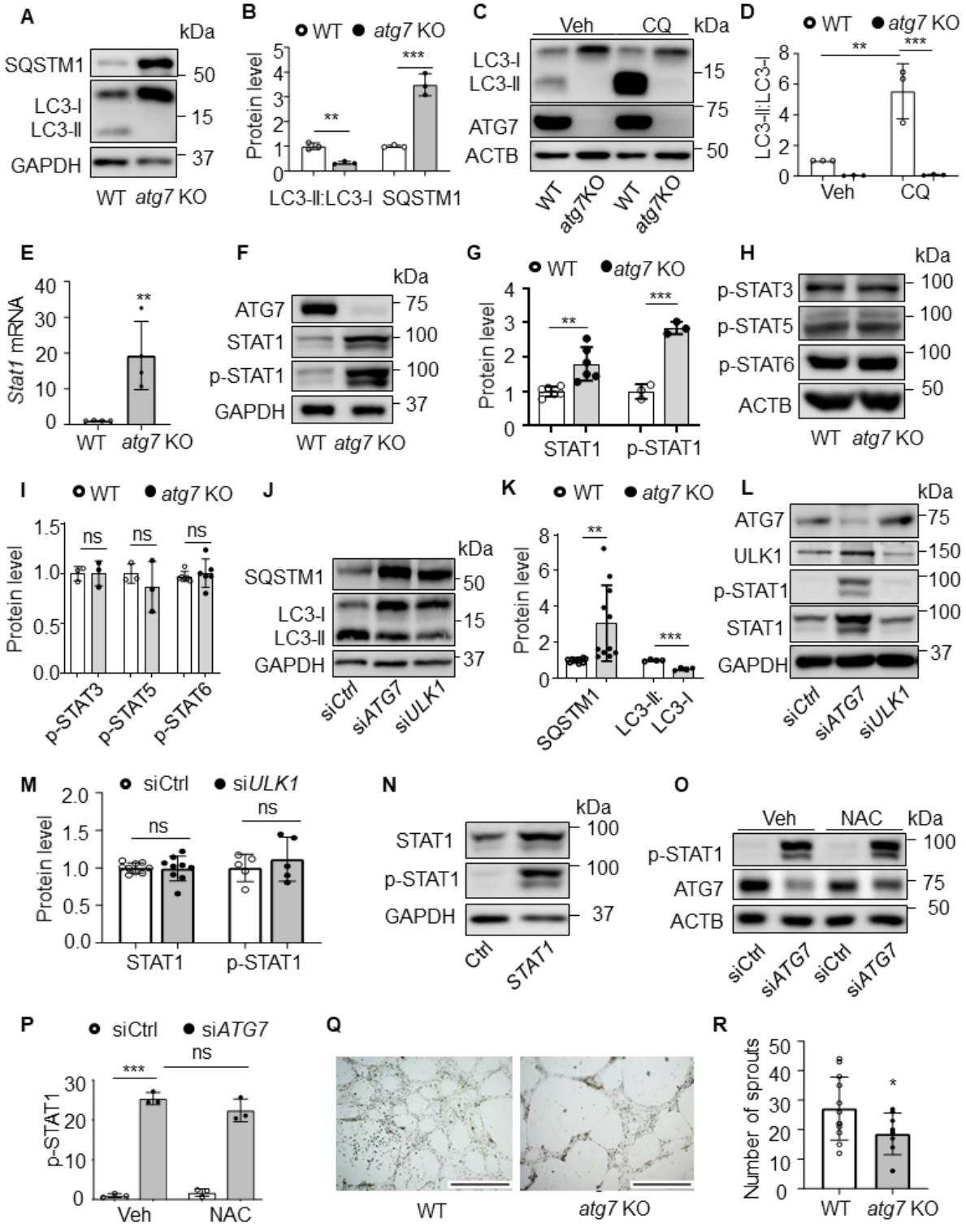

Figure 3.7 Deletion of Atg7 increases STAT1 expression but reduces tube formation

(A) The protein levels of SQSMT1/p62 and MAP1LC3A/LC3-II:MAP1LC3A/LC3-I were determined by western blot in MLECs isolated from WT and *atg7* KO mice. (B) Densitometric analysis of the blots. N = 3, ** $p < 0.01$; *** $p < 0.001$. (C and D) WT and *atg7* KO MLECs were treated with or without chloroquine (CQ, 3 μM) for 24 h, MAP1LC3A/LC3-II:MAP1LC3A/LC3-I protein level was detected by western blot. Densitometric analysis of the blots. N = 3, ** $p < 0.01$, *** $p < 0.001$. (E) *Stat1* mRNA expression was detected by RT-PCR in MLECs isolated from WT and *atg7* KO mice. N = 4, ** $p < 0.01$. (F) STAT1 and phospho-STAT1 (Y701) protein levels were measured by western blot. (G) Quantitative analysis of STAT1 and phosphorylated STAT1 at tyrosine 701 (Y701; p-STAT1) protein expression, N = 3-6, ** $p < 0.01$, *** $p < 0.001$. (H) Western blot analysis of phosphorylated STAT3 at serine 727 (S727; p-STAT3), phosphorylated STAT5 at tyrosine 694 (Y694; p-STAT5), and phosphorylated STAT6 at tyrosine 641 (Y641; p-STAT6) in MLECs from WT and *atg7* KO mice. (I) Densitometric analysis of the blots. (J) HUVECs were transfected with siCtrl, si*ATG7*, or *ULK1* siRNA (si*ULK1*) for 48 h, SQSMT1/p62 and MAP1LC3A/LC3-II:MAP1LC3A/LC3-I protein levels were analyzed by western blot. (K) Quantitative analysis of the blots. N = 4-11, ** $p < 0.01$. (L) HUVECs were transfected with siCtrl, si*ATG7*, or si*ULK1* for 48 h, levels of total STAT1 and p-STAT1 (Y701) were measured by western blot. (M) Quantitative analysis of STAT1 and p-STAT1 (Y701) protein expression. N = 4-9, ns, not significant. (N) HUVECs were transfected with control and STAT1 plasmid for 24 h, protein levels of STAT1 and p-STAT1 (Y701) were detected by western blot. (O and P) HUVECs were transfected with siCtrl or si*ATG7* for 48 h, and the cells were treated with vehicle or N-acetyl-l-cysteine (NAC, 1 mM) for additional 1 h. p-STAT1 (Y701) protein expression was measured by western blot. N = 3, *** $p < 0.001$, ns, not significant. (Q) Tube formation assay was performed in MLECs isolated from WT and *atg7* KO mice. Representative images selected from 4 independent experiments. Scale bar: 1 mm. (R) Quantitative analysis of the number of sprouts. N = 12 fields, * $p < 0.05$.

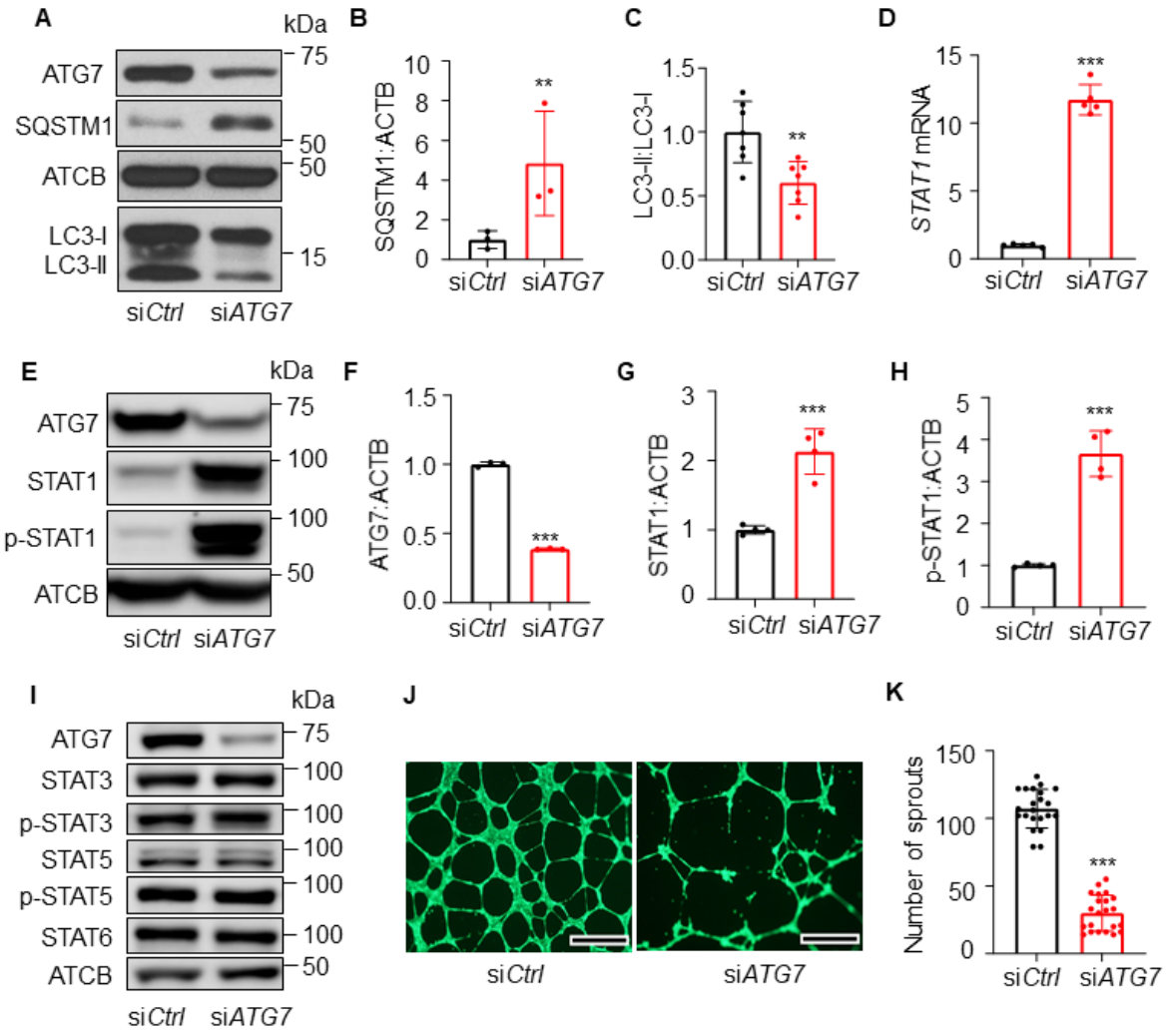

Figure 3.8 . Silencing of Atg7 upregulates STAT1 and inhibits tube formation in HUVECs. (A-C) HUVECs were transfected with siCtrl or siATG7 for 48 h. The protein levels of SQSMT1/p62 and MAP1LC3A/LC3-II:MAP1LC3A /LC3-I were determined by western blot and densitometry. N = 3-7, ** p < 0.01. (D) STAT1 mRNA expression was detected by RT-PCR, N = 5, *** $p < 0.001$. (E-H) ATG7, STAT1, and p-STAT1 (Y701) protein levels were measured by western blot and densitometry. N = 3-4, *** $p < 0.001$. (I) Protein levels of STAT3, p-STAT3 (S727), STAT5, p-STAT5 (Y694), and STAT6 were measured by western blot in HUVECs transfected with siCtrl or siATG7, N = 3. (J) Tube formation assay was performed in HUVECs transfected with siCtrl or siATG7. The representative images were selected from 3 independent experiments. Scale bar: 2 mm. (K) Quantitative analysis of sprout number, N = 22 fields, *** $p < 0.001$.

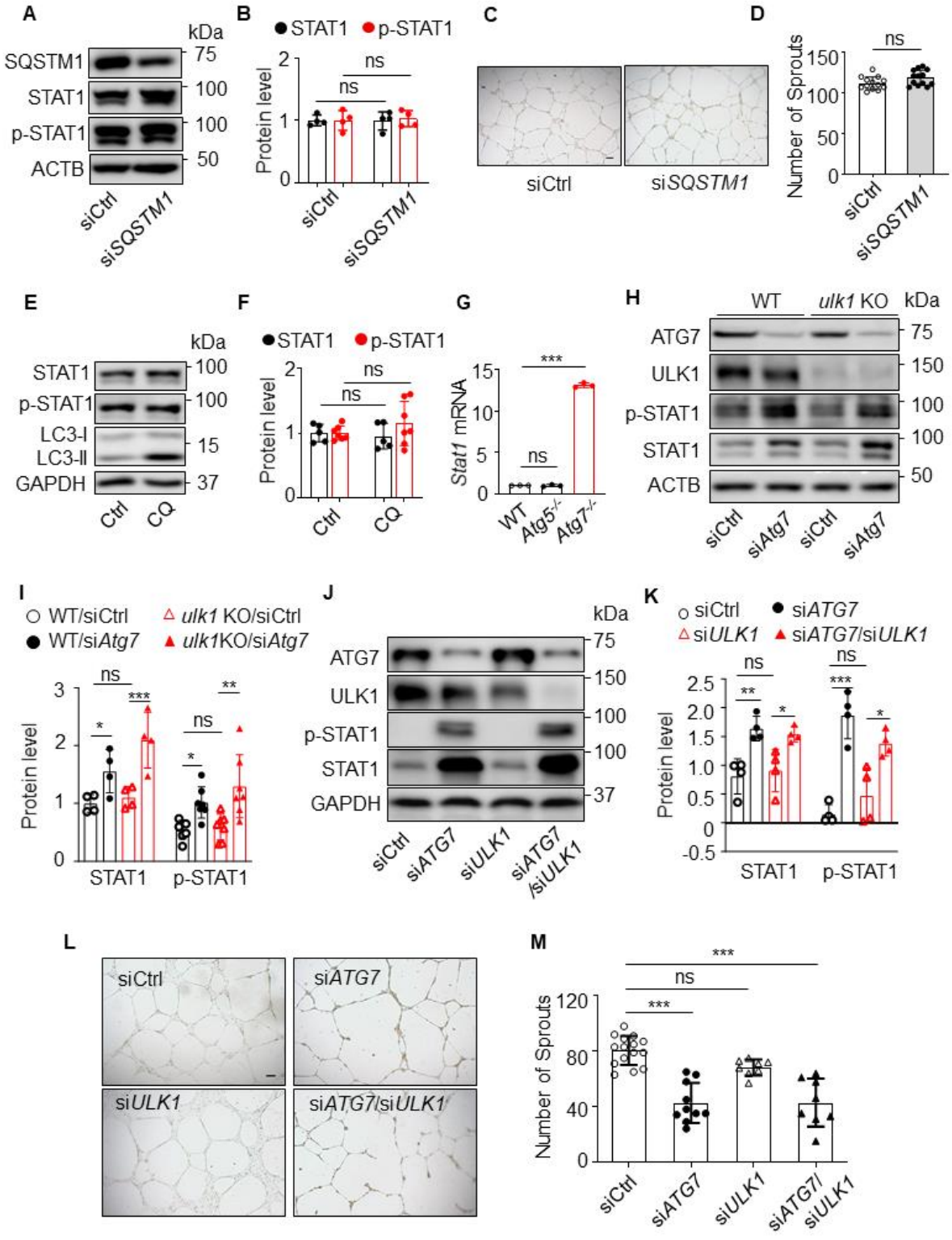

Figure 3.9 Suppression of autophagy activity is not involved in increased STAT1 and reduced tube formation by ATG7 deficiency.

(A) HUVECs were transfected with siCtrl or siSQSTM1 for 48 h, levels of total STAT1 and p-STAT1 (Y701) were measured by western blot. (B) Quantitative analysis of STAT1 and p-STAT1 (Y701) protein expression. N = 4, ns, not significant. (C) Tube formation assay was performed in HUVECs transfected with siCtrl or si*SQSMT1*. The representative results were selected from 3 independent experiments. Scale bar: 200 μm. (D) Quantitative analysis of sprout number, N = 13 views, ns, not significant. (E and F) HUVECs were treated with or without chloroquine (CQ, 10 μM) for 16 h, STAT1 and p-STAT1 (Y701) protein levels were detected by western blot. N = 5-7, ns, not significant. (G) *Stat1* mRNA level was measured by RT-PCR in wild-type (WT), *atg5*-/-, and *atg7*-/- MEFs, N = 3, *** $p < 0.001$, ns, not significant. (H and I) WT and ulk1 KO MLECs were transfected with siCtrl or siAtg7, total STAT1 and p-STAT1 (Y701) levels were measured by western blot. N = 4-7, * $p < 0.05$, ** $p < 0.01$, *** $p < 0.001$, ns, not significant. (J and K) HUVECs were transfected with siCtrl, si*ATG7*, si*ULK1*, or si*ATG7* and si*ULK1* for 48 h, total STAT1 and p-STAT1 (Y701) levels were measured by western blot. N = 4, * $p < 0.05$, ** $p < 0.01$, *** $p < 0.001$, ns, not significant. (L) Tube formation assay was performed in HUVECs transfected with siCtrl, si*ATG7*, si*ULK1*, or si*ATG7* and si*ULK1*. The representative results were selected from 3 independent experiments. Scale bar: 200 μm. (M) Quantitative analysis of sprout number, N = 8-15 views, *** $p < 0.0001$, ns, not significant.

Given that ATG7 deficiency upregulated STAT1 protein expression, accompanied by higher level of phosphorylated STAT1, we reasoned that overexpression of STAT1 could increases phosphorylated STAT1. Indeed, transfection of HUVECs with STAT1 plasmid significantly enhanced STAT1 protein level, concurrent with increased phosphorylation of STAT1 (Figure 3.7 N). Moreover, H_2O_2 and/or derived reactive oxygen species (ROS) directly activate STAT1 in cultured astrocytes (Gorina, Petegnief, Chamorro, & Planas, 2005), glia (Gorina, Sanfeliu, Galito, Messeguer, & Planas, 2007) and in vascular smooth muscle cells (Madamanchi, Li, Patterson, & Runge, 2001), and the absence of autophagy leads to accumulation of ROS (Tal et al., 2009), we further examined whether inhibition of ROS prevents STAT1 phosphorylation in ATG7-deficent condition using N-acetyl-l-cysteine (NAC), a well-known inhibitor of ROS (Figure 3.7 O and P). The result showed that NAC had no significant effect on STAT1 phosphorylation in ATG7-deficient HUVECs.

ATG7 regulates brain angiogenesis via RELA/p65-dependent interleukin 6 production (S. F. Zhuang et al., 2017), suggesting that RELA/p65 could be a link between ATG7 and STAT1, we therefore determined whether RELA/p65 mediates ATG7 deficiency-enhanced STAT1 expression. Silencing *ATG7* did not affect *NFKB1*/*NFκB* mRNA expression (Figure 3.6 A) and failed to increase the binding between RELA/p65 and *HIF1A* promoter (Figure 3.10 A). In addition, silencing *Rela/p65* did not reduce protein levels of STAT1 and p-STAT1 in WT MLECs and could not prevent the enhancement of STAT1 and p-STAT1 protein levels in *atg7* KO MLECs (Figure 3.10 B, C, and D). Taken together, RELA/p65 is not involved in upregulation of STAT1 in ATG7-deficient conditions.

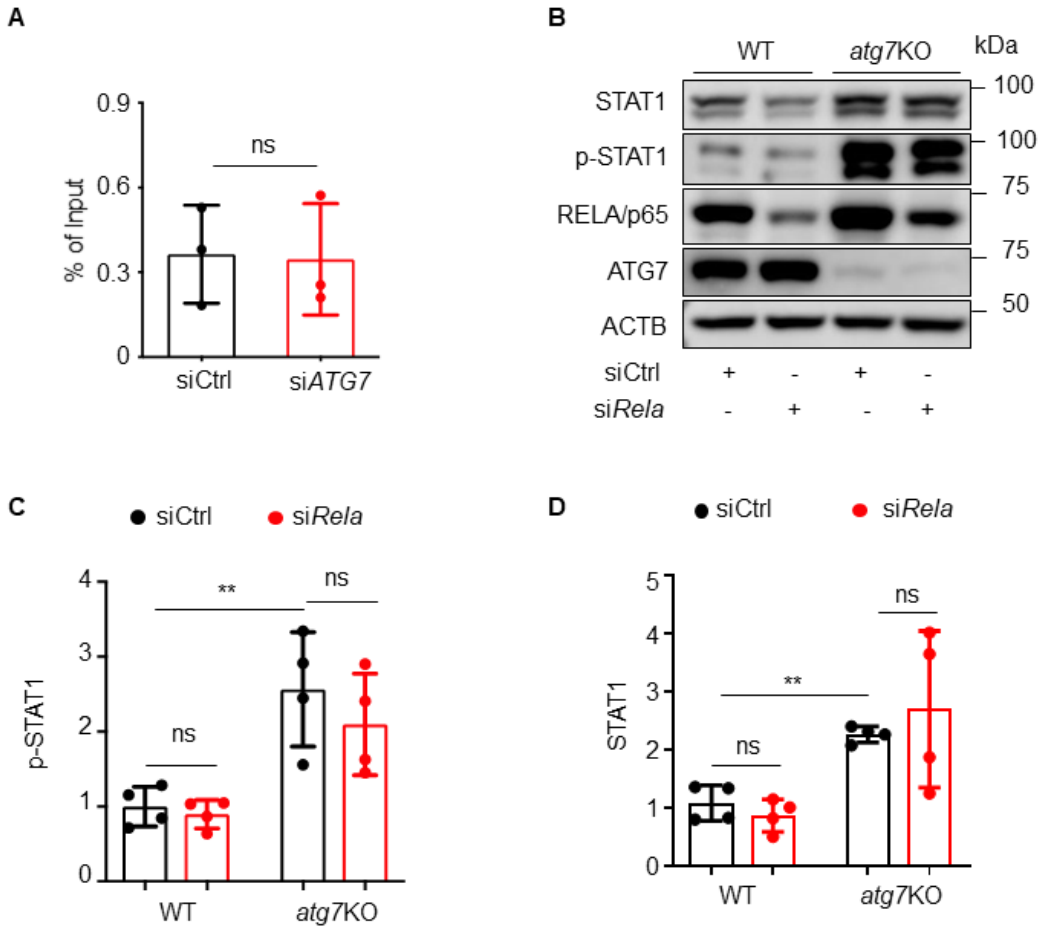

Figure 3.10 Deletion of Atg7 has no effects on NFκB expression.
(A) Chromatin immunoprecipitation (ChIP) assay was performed to analyze the interaction between RELA/p65 and the *HIF1A* promoter. HUVECs were transfected with siCtrl or si*ATG7* for 48 h, and the chromatin was immunoprecipitated with an antibody against RELA/p65. Mouse IgG was used as a negative control. Precipitated DNA or 2% of the chromatin input were analyzed by PCR. (B, C, and D) WT and *atg7* KO MLECs were transfected with siCtrl and si*Rela* for 48 h, levels of STAT1 and p-STAT1 (Y701) were measured by western blot. N = 4, ** $P < 0.01$, ns, not significant.

To verify the inhibitory effect of ATG7 deficiency on angiogenesis *in vitro*, we examined whether *Atg7* deficiency inhibits tube formation in cultured endothelial cells. Indeed, the tube formation was inhibited in *atg7* KO MLECs (Figure 3.7 Q and R) and si*ATG7*-transfected HUVECs (Figure 3.8 J and K), as indicated by reducing the number of sprouts. To determine

whether ATG7 deficiency inhibits angiogenesis independently of autophagy, we examined the effect of autophagy inhibition on tube formation in HUVECs using *SQSMT1/p62* siRNA, and found that silencing *SQSMT1/p62* did not have any effect on tube formation (Figure 3.9 C and D). Also, suppression of autophagy by silencing *ULK1* did not influence tube formation in HUVECs either. However, silencing of *ATG7* inhibited tube formation in HUVECs transfected with either siCtrl or si*ULK1* (Figure 3.9 L and M). These data suggest that ATG7 deficiency inhibits angiogenesis in an autophagy-independent manner.

3.5.5 Overexpression of ATG7 has no effects on STAT1 expression and tube formation.

Next, we determined the effects of *ATG7* overexpression on STAT1 expression. Overexpression of *ATG7* by transfecting a plasmid encoding *MYC-ATG7* (*ATG7*) increased MAP1LC3A/LC3-II:MAP1LC3A/LC3-I ratio and reduced SQSTM1/p62 protein level, indicating autophagy activation (Figure 3.11 A, B, and C). However, overexpression of *ATG7* did not affect STAT1 and p-STAT1 (Y701) protein expression (Figure 3.11 D, E, and F). Moreover, RT-PCR assay demonstrated that *STAT1* mRNA level in the HUVECs transfected with *ATG7* plasmid was comparable with that of the HUVECs transfected with *MYC*-Control plasmid (Ctrl) (Figure 3.11 G). Correspondingly, no obvious differences were observed in tube formation between control and *ATG7*-overexpressed HUVECs, as indicated by the comparable number of sprouts (Figure 3.11 H and I). These data indicate that overexpression of *ATG7* does not affect STAT1 expression although it activates autophagy, supporting that regulatory effect of ATG7 deficiency on STAT1 is independent of autophagic process.

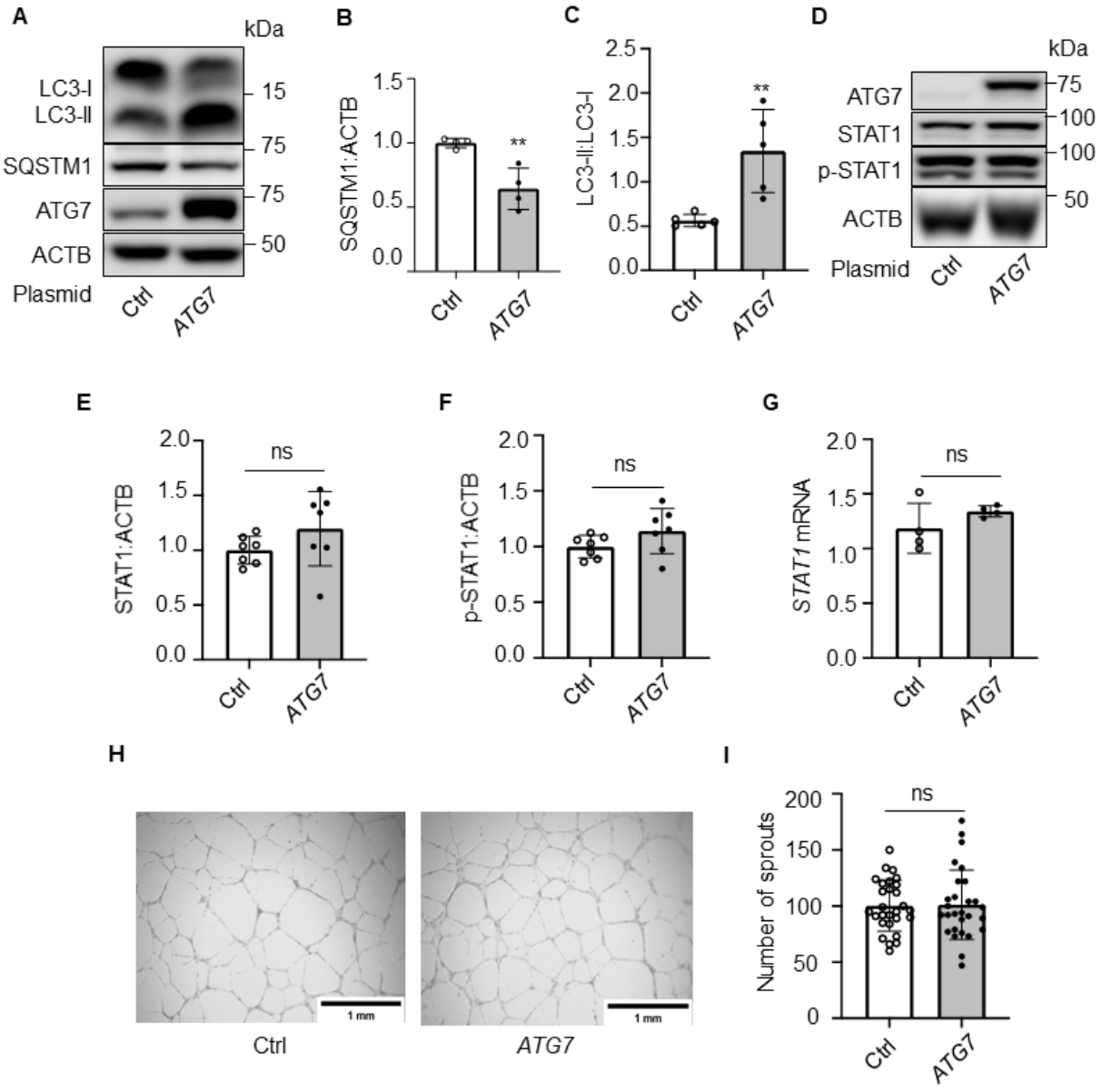

Figure 3.11 Overexpression of ATG7 does not affect STAT1 protein expression and tube formation.

(A) HUVECs were transfected with MYC-control (Ctrl) or *MYC-ATG7* (*ATG7*) plasmid for 24 h. (B and C) SQSMT1/p62 and MAP1LC3A/LC3-II:MAP1LC3A/LC3-I protein expression was measured by western blot. Densitometric analysis of the blots, N = 4-5, ** $P < 0.01$. (D) STAT1 and phospho-STAT1 (Y701) protein levels were analyzed by western blot. (E and F) Densitometric analysis of the blots, N = 7, ns, not significant. (G) *STAT1* mRNA level was determined in by RT-PCR. N = 4, ns, not significant. (H) Tube formation assay was performed 24 h after transfection of Ctrl or *ATG7* plasmid, three independent experiments. (I) Quantitative analysis of sprout number, N = 28 fields, ns, not significant. Scale bar: 1 mm.

3.5.6 Suppression of STAT1 recovers the angiogenic potential in ATG7-deficient cells.

Since *ATG7* deficiency significantly elevated STAT1 expression and inhibited angiogenesis, we tested if inhibition of STAT1 counteracts the inhibitory effects of *ATG7* deficiency on angiogenesis. To this end, we administrated fludarabine, a STAT1 inhibitor (50 μM, 16 h), in siCtrl- and si*ATG7*-treated HUVECs, and determined the phosphorylation of STAT1 by western blot. The result indicated that fludarabine significantly suppressed phosphorylation of STAT1 at tyrosine 701 (Figure 3.12 A and B). Next, we examined the effects of fludarabine on tube formation in HUVECs transfected with siCtrl or si*ATG7*, and found that silencing *ATG7* reduced the number of sprouts, and the reduction in tube formation was attenuated by fludarabine treatment (Figure 3.12 C and D). We further determined whether inhibition of STAT1 attenuates the inhibitory effect of ATG7 deficiency on tube formation by co-transfecting HUVECs with *ATG7* and *STAT1* siRNAs (Figure 3.12 E and F). We observed that the co-transfection of *STAT1* siRNA and *ATG7* siRNA restored tube formation as compared with the transfection of si*ATG7* (Figure 3.12G and H). The results suggest that STAT1 upregulation may mediate the inhibitory effect of ATG7-deficiency on angiogenesis *in vitro*.

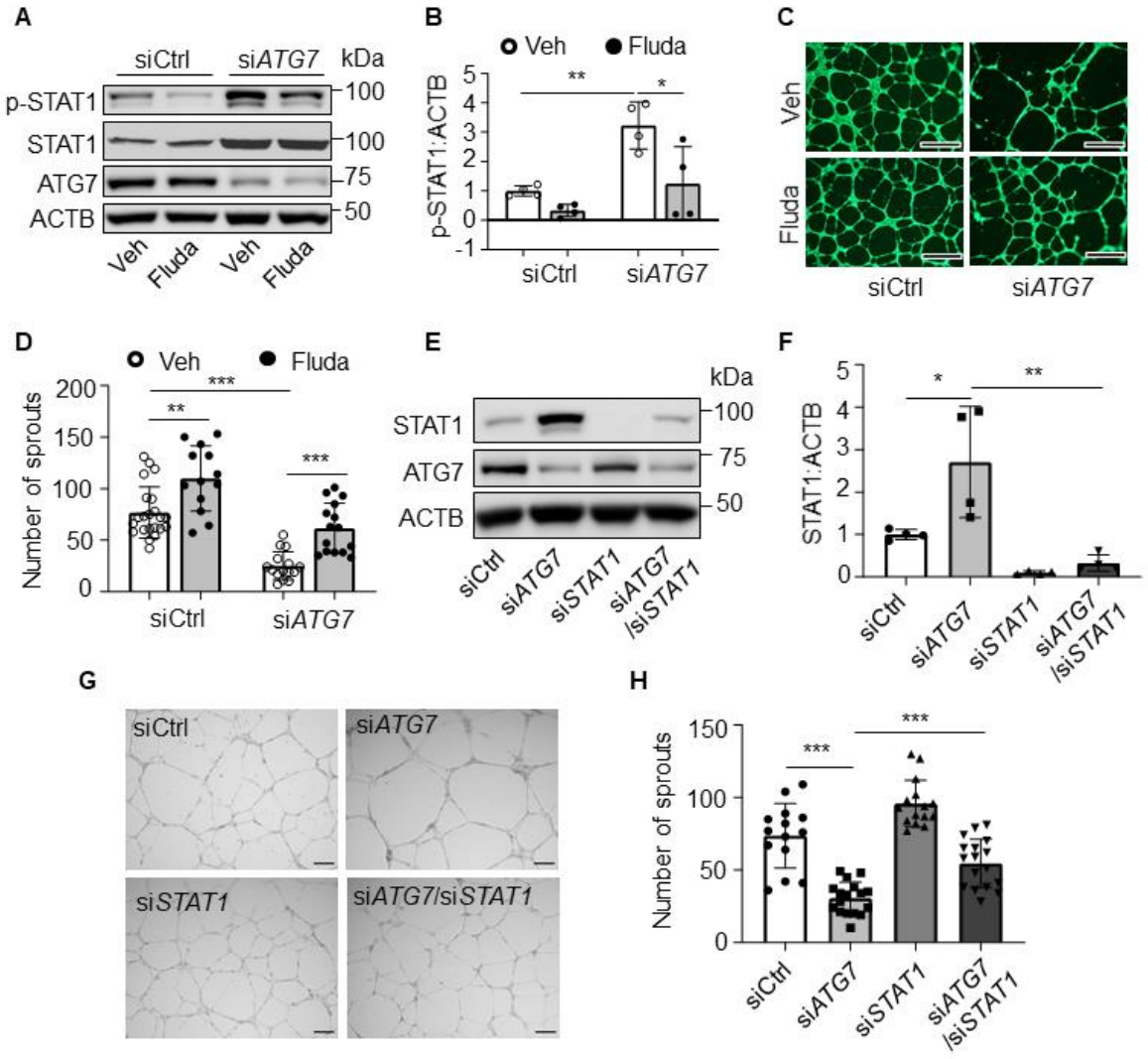

Figure 3.12 Suppression of STAT1 recovers the potential of tube formation in HUVECs. (A-D) HUVECs were transfected with siCtrl or si*ATG7* and treated with STAT1 inhibitor, fludarabine phosphate (Fluda, 50 μM) for 24 h. (A) Total STAT1 and p-STAT1 (Y701) protein levels were measured by western blot. (B) Densitometric analysis of p-STAT1 (Y701), N = 4, * $p < 0.05$, ** $p < 0.01$. (C) Tube formation assay was performed after the treatment. Scale bar: 1 mm. (D) Quantification of the number of sprouts. Three independent experiments. N = 13-22 fields, ** $p < 0.01$, *** $p < 0.001$. (E-H) HUVECs were transfected with siCtrl, si*ATG7*, si*STAT1*, or si*ATG7* and si*STAT1*. (E) Protein levels of ATG7 and STAT1 were determined by western blot. (F) The quantification analysis of the blots. N = 4, * $p < 0.05$, ** $p < 0.01$. (G) Tube formation assay was performed after the treatment. Scale bar: 1 mm. (H) Quantification of the number of sprouts. Three independent experiments. N = 14-16 fields, *** $p < 0.001$.

3.5.7 ATG7 deficiency promotes ZNF148/ZBP-89 nuclear translocation, increasing STAT1 expression.

Given that ZNF148/ZBP-89 (zinc finger protein 148, protein encoded by the human *ZNF148* or mouse *Zfp148* locus) is required for constitutive STAT1 expression (Bai & Merchant, 2003), we determined whether ZNF148/ZBP-89 is involved in ATG7 regulating STAT1 expression by detecting STAT1 expression in HUVECs transfected with control siRNA (siCtrl) or *ZNF148* siRNA (si*ZNF148*). Transfection of *ZNF148* siRNA downregulated *STAT1* mRNA expression, and reduced STAT1 and p-STAT1 protein levels (Figure 3.13 A and B).

To address whether ATG7 interacts with ZNF148/ZBP-89 to regulate *STAT1* expression, we examined the subcellular distribution of ATG7 and ZNF148/ZBP-89 in WT and *atg7* KO MLECs by immunofluorescence staining. In WT MLECs, ATG7 and ZNF148/ZBP-89 were mainly present in the cytosol, in which some ATG7 staining was colocalized with ZNF148/ZBP-89 staining. However, no colocalization of ATG7 and ZNF148/ZBP-89 staining was observed in the nucleus. The cytosol ZNF148/ZBP-89 immunofluorescence intensity was significantly lower in *atg7* KO MLECs, as compared with that of WT MLECs. However, nuclear ZNF148/ZBP-89 immunofluorescence intensity was higher in *atg7* KO MLECs than that in WT MLECs (Figure 3.13 C and D). Consistently, western blot analysis of ZNF148/ZBP-89 expression in subcellular fractions verified that ZNF148/ZBP-89 protein level in cytosol fraction was higher in WT MLECs relative to that of *atg7* KO MLECs, while nuclear ZNF148/ZBP-89 protein level in WT MLECs was lower than that in *atg7* KO MLECs (Figure 3.13 E, F, and G), suggesting that lack of ATG7 promotes ZNF148/ZBP-89 nuclear translocation. Similar result was also observed in HUVECs transfected with siCtrl and si*ATG7* (Figure 3.14 A and B). However, deletion of *Atg7* had no effect on *Zfp148* mRNA expression in MLECs (Figure 3.13 H). We reasoned that *ATG7*-

deficiency reduces the association of ATG7 and ZNF148/ZBP-89, which promotes ZNF148/ZBP-89 nuclear translocation and upregulates STAT1 expression. Thus, we investigated whether ATG7 directly associates with ZNF148/ZBP-89. Immunoprecipitation of ATG7 followed by western blotting of ZNF148/ZBP-89 showed that ATG7 indeed physically associated with ZNF148/ZBP-89 (Figure 3.13 I and J). We further examined the effect of silencing *ZNF148* on *STAT1* mRNA expression in HUVECs transfected with either siCtrl or si*ATG7*. In *ATG7*-deficient HUVECs, silencing *ATG7* significantly increased *STAT1* mRNA expression, and the increase in *STAT1* mRNA was abolished by silencing *ZNF148* (Figure 3.13 K).

By contrast, overexpression of *ATG7* did not alter ZNF148/ZBP-89 nuclear translocation manifested by immunofluorescence staining and western blot analysis of subcellular fractions in HUVECs (Figure 3.14 C, D, E, F, and G). Taken together, these data reveal that lack of *ATG7* reduces its association with ZNF148/ZBP-89, increases ZNF148/ZBP-89 nuclear translocation, and upregulates STAT1 expression.

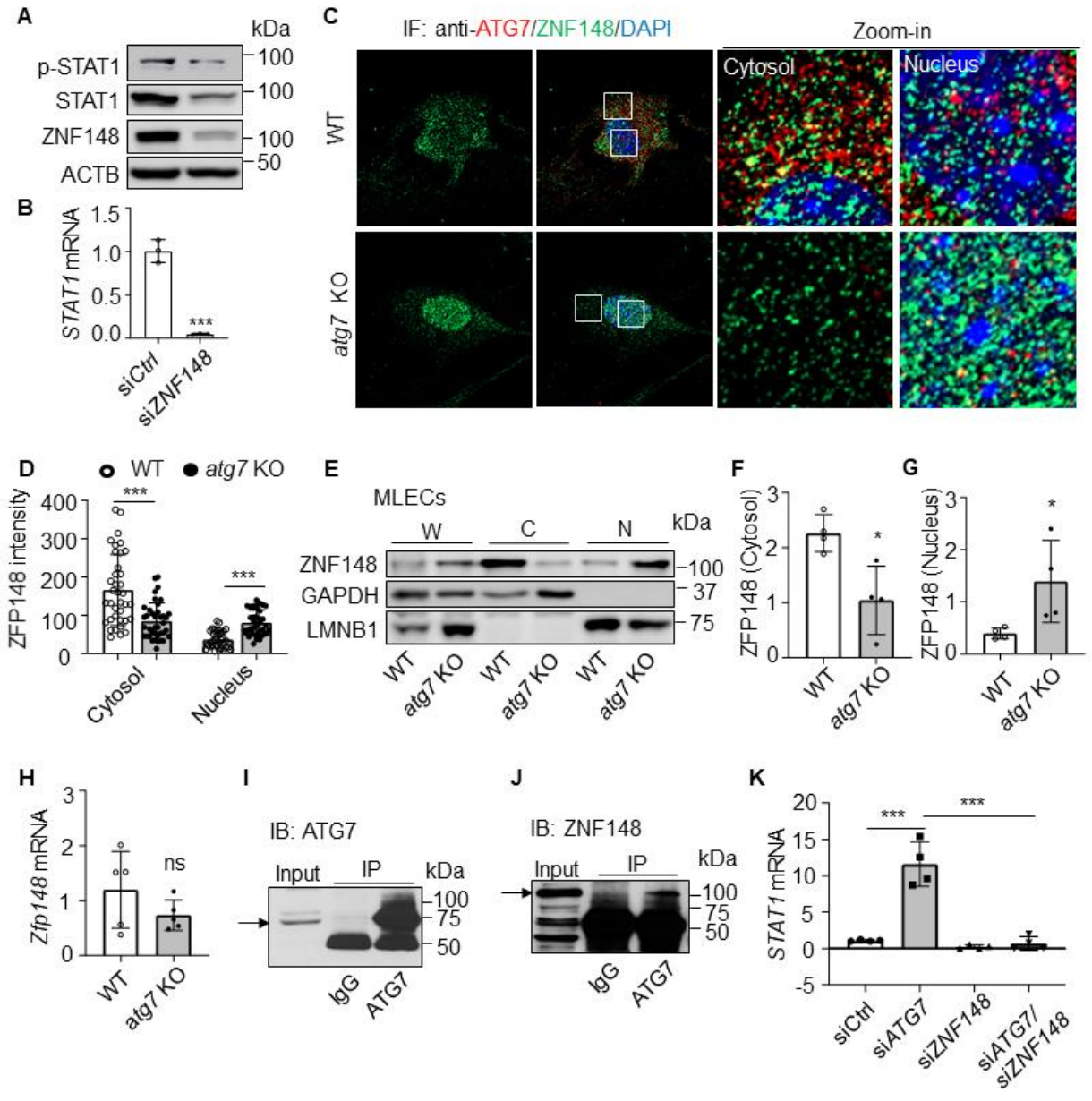

Figure 3.13 Lack of ATG7 increases ZNF148/ZBP-89 nuclear translocation and STAT1 expression

(A) Western blot analysis of STAT1, p-STAT1 (Y701), and ZNF148/ZBP-89 in HUVECs transfected with siCtrl or *ZNF148* siRNA (si*ZNF148*). (B) *STAT1* mRNA level was analyzed by RT-PCR. N = 3, *** p < 0.001. (C and D) Representative images of immunofluorescence staining of ZNF148/ZBP-89 (C). Quantitative analysis of immunofluorescence intensity of ZNF148/ZBP-89. Four independent experiments. N = 37-39 cells, *** $p < 0.001$ (D). (E) ZNF148/ZBP-89 protein expression was measured by western blot in whole cell lysates (W), cytosol (C), and nuclear (N) fractions in MLECs isolated form WT and *atg7* KO mice. (F and G) Quantitative analysis of nuclear ZNF148/ZBP-89 protein levels in cell fractions, N = 4, * $p <$ 0.05. (H) Zfp148 mRNA level was detected by RT-PCT in WT and atg7 KO MLECs. N = 5; ns,

not significant. (I and J) The interaction between ATG7 and ZNF148/ZBP-89 was detected by immunoprecipitation (IP) and western blot (IB). N = 3. (K) HUVECs were transfected with siCtrl, si*ATG7*, si*ZNF148*, or si*ATG7* and si*ZNF148* for 48 h. *STAT1* mRNA level was measured by RT-PCR. N = 4, *** $p < 0.001$.

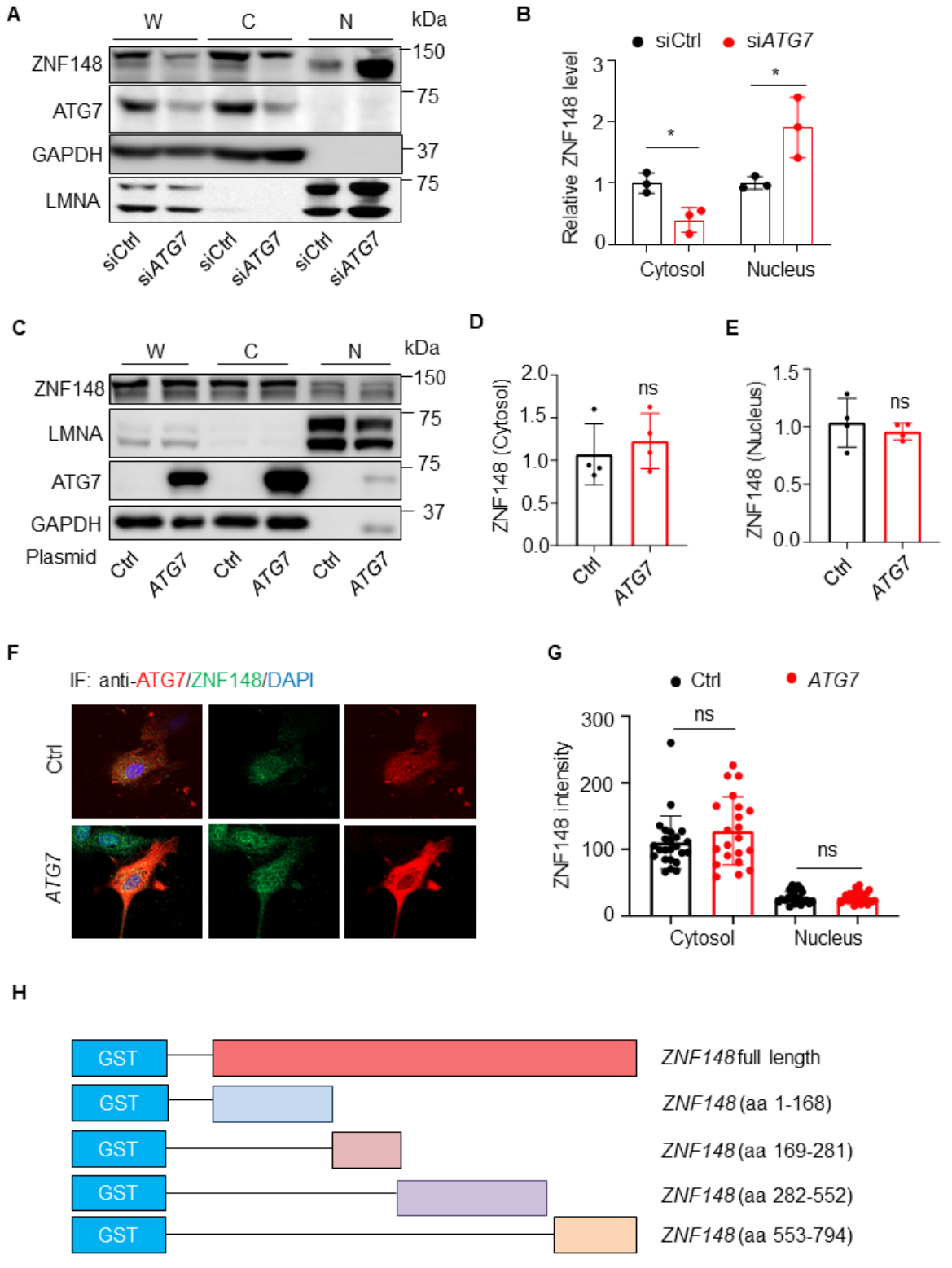

Figure 3.14 Lack of ATG7 increases ZNF148/ZBP-89 nuclear translocation and STAT1 expression

(A) Western blot analysis of STAT1, p-STAT1 (Y701), and ZNF148/ZBP-89 in HUVECs transfected with siCtrl or *ZNF148* siRNA (si*ZNF148*). (B) *STAT1* mRNA level was analyzed by RT-PCR. N = 3, *** $p < 0.001$. (C and D) Representative images of immunofluorescence staining of ZNF148/ZBP-89 (C). Quantitative analysis of immunofluorescence intensity of ZNF148/ZBP-89. Four independent experiments. N = 37-39 cells, *** $p < 0.001$ (D). (E) ZNF148/ZBP-89 protein expression was measured by western blot in whole cell lysates (W), cytosol (C), and nuclear (N) fractions in MLECs isolated form WT and atg7 KO mice. (F and G) Quantitative analysis of nuclear ZNF148/ZBP-89 protein levels in cell fractions, N = 4, * $p < 0.05$. (H) *Zfp148* mRNA level was detected by RT-PCT in WT and atg7 KO MLECs. N = 5; ns, not significant. (I and J) The interaction between ATG7 and ZNF148/ZBP-89 was detected by immunoprecipitation (IP) and western blot (IB). N = 3. (K) HUVECs were transfected with siCtrl, si*ATG7*, si*ZNF148*, or si*ATG7* and si*ZNF148* for 48 h. *STAT1* mRNA level was measured by RT-PCR. N = 4, *** $p < 0.001$.

3.5.8 Identification of binding domain between ATG7 and ZNF148/ZBP-89.

Since ZNF148/ZBP-89 is reported to regulate target genes by interacting with p53 (Bai & Merchant, 2001), SP1 (Sp1 transcription factor), EP300 (E1A binding protein p300) (Merchant, Bai, & Okada, 2003), and STAT3 (Y. Wu, Diab, Zhang, Izmailova, & Zehner, 2004), we determined whether ATG7 interacts with these proteins in HUVECs. The immunoprecipitation and western blot demonstrated that ATG7 did not interact with these proteins in HUVECs (Figure 3.15 A and B), and there was no interaction between ZNF148/ZBP-89 and p53 (Figure 3.15 C). To identify the region of ZNF148/ZBP-89 interacting with ATG7, we generated *ZNF148* truncations fused with GST (Fig. S7H), overexpressed the truncations in human embryonic kidney 293 (HEK293) cells, and co-transfected the cells with *MYC-ATG7* plasmid. *ZNF148* truncations fused with GST were pulled down by glutathione-sepharose beads. The efficiency of overexpressing ZNF148/ZBP-89 fragments and the association of ATG7 and ZNF148/ZBP-89 were determined by blotting GST and ATG7, respectively (Figure 3.15 D and E). The ATG7 protein interacted with full-length ZNF148/ZBP-89 and GST- ZNF148/ZBP-89 (amino acids 169-281), but did not interacted with the N-terminal (amino acids 1-168), C-terminal (amino acids 553-794), and GST- ZNF148/ZBP-89 (amino acids 282-552) (Figure 3.15

D and E). The results indicate that ZNF148/ZBP-89 (amino acids 169-281) is required for ZNF148/ZBP-89 interacting with ATG7.

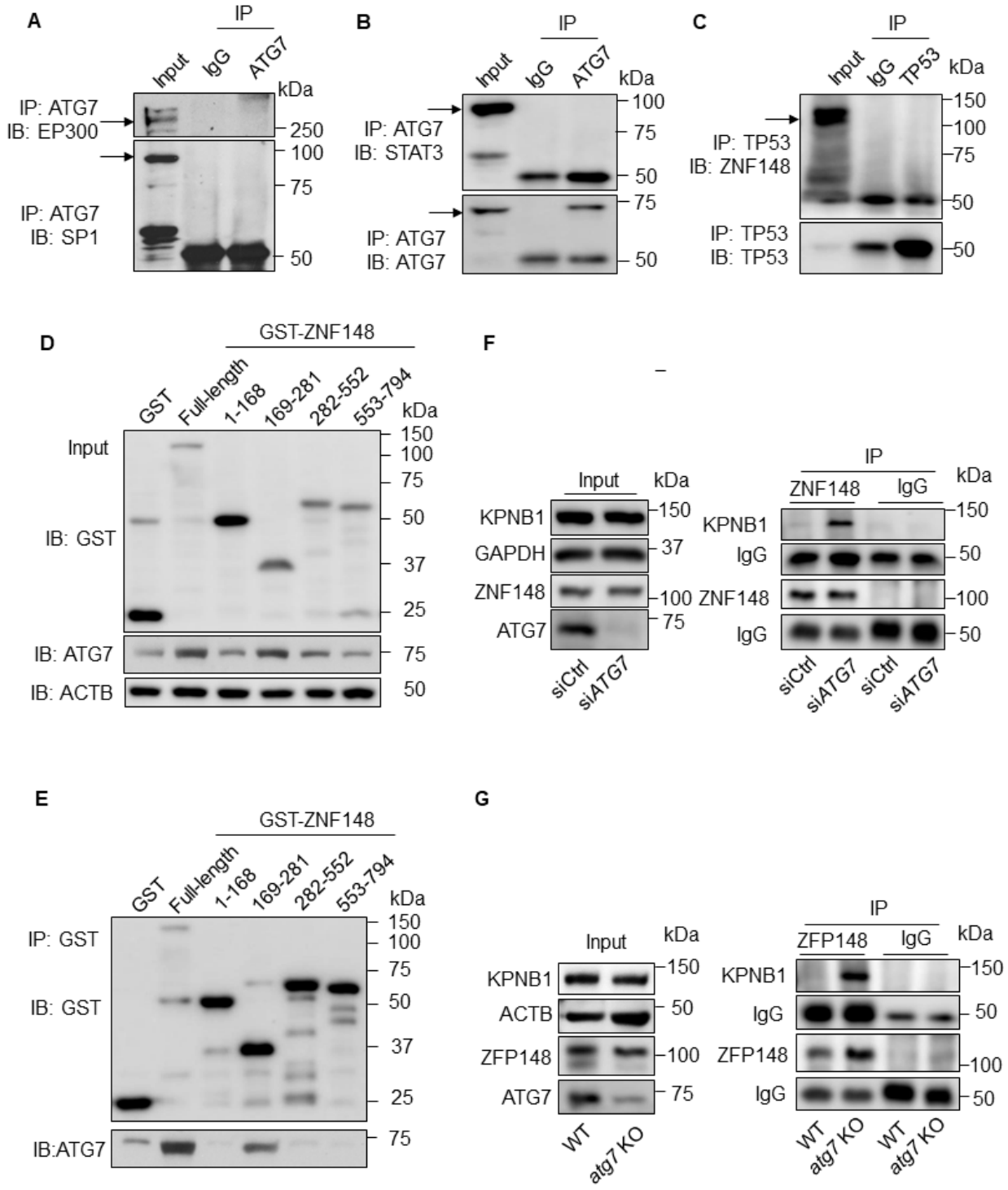

Figure 3.15 Lack of ATG7 increases the binding between ZNF148/ZBP-89 and KPNB1

(A and B) Determine the potential interacting proteins with ATG7 in HUVECs. ATG7 was immunoprecipitated by ATG7 antibody, and EP300, SP1, and STAT3 were determined by western blotting. (C) Cell lysates were prepared from cultured HUVECs, TP53/p53 was immunoprecipitated, and ZNF148/ZBP-89 was detected by western blot. N = 3. (D and E) HEK 293T cells were transfected with *MYC-ATG7* plasmid and *GST*-control (*GST*) or GST fused with *ZNF148/ZBP-89* full length or *ZNF148/ZBP-89* truncations (amino acids 1-168, 169-281, 282-552, 553-794), respectively. Binding region of ZNF148/ZBP-89 on ATG7 was determined by GST immunoprecipitation. N = 4. (F) HEK 293T cells were transfected with siCtrl or siATG7 for 48 h, the interaction of ZNF148/ZBP-89 and KPNB1 was determined by immunoprecipitation and western blot. N = 3. (G) The interaction of ZNF148/ZBP-89 and KPNB1 in MLECs isolated from WT and atg7 KO mice was determined by immunoprecipitation and western blot. N = 3.

3.5.9 ATG7 deficiency enhances the binding between ZNF148/ZBP-89 and KPNB1.

Given that the transport of molecules into and out of the nucleus is mediated by the KPNB1 superfamily (S. J. LEE ET AL., 2003), we determined whether ATG7 deficiency affects the association of ZNF148/ZBP-89 and KPNB1 in HEK293 cells transfected with control siRNA (siCtrl) or *ATG7* siRNA (si*ATG7*). Immunoprecipitation and western blot revealed that there was rarely interaction between ZNF148/ZBP-89 and KPNB1 in HEK293 transfected with control siRNA, but the association of ZNF148/ZBP-89 and KPNB1 was significantly increased in HEK293 cells transfected with *ATG7* siRNA (Figure 3.15 F). Similarly, no association between ZNF148/ZBP-89 and KPNB1 was observed in WT MLECs, whereas the interaction of ZNF148/ZBP-89 and KPNB1 was significantly higher in *atg7* KO MLECs than that in WT MLECs (Figure 3.15 G), suggesting that ATG7 deficiency enhances association between ZNF148/ZBP-89 and KPNB1, which promotes ZNF148/ZBP-89 nuclear translocation.

3.5.10 Inhibition of STAT1 by fludarabine recovers blood perfusion in ischemic limbs of atg7 KO mice.

To verify that upregulation of STAT1 inhibits HIF1A-mediated angiogenesis in *Atg7*-deficient condition *in vivo*, we examined whether administration of fludarabine (100 mg/kg, i.p.,

once every other day) in WT and *atg7* KO mice can improve angiogenesis in mouse hind limb ischemic model. Deletion of *Atg7* led to an increase in p-STAT1 (Y701) protein level in both sham-operated and ischemic groups, the increase in STAT1 phosphorylation was significantly mitigated by fludarabine treatment (**Fig. 9A and B**). At the same time, downregulation of HIF1A in *atg7* KO mice was attenuated by administration of fludarabine **(Fig. 9C and D**). In agreement with the alteration of HIF1A, Laser Doppler Imaging revealed that blood flow restoration in *atg7* KO mice was significantly improved as compared with saline-treated *atg7* KO mice (**Fig. 9E and F**). In addition, reduction in PECAM-1/CD31 staining in ischemic *atg7* KO mice was abolished by administration of fludarabine (**Fig. 9G and H**). To validate these results, we further determined whether silencing of *Stat1* attenuates the inhibitory effect of ATG7 deficiency on angiogenesis by transfecting WT and *atg7* KO aortic rings with control siRNA *or Stat1* siRNA. Lack of *Atg7* reduced sprout number and length in aortic rings. Transfection of *Stat1* siRNA prevented the reduction of sprout number and shortening of the sprout length in *atg7* KO aortic rings (**Fig. S8A, B and C**), confirming that STAT1 upregulation mediates the inhibitory effect of ATG7-deficiency on angiogenesis. Taken together, inhibition of STAT1 restores HIF1A expression and angiogenesis in *Atg7*-deficient conditions.

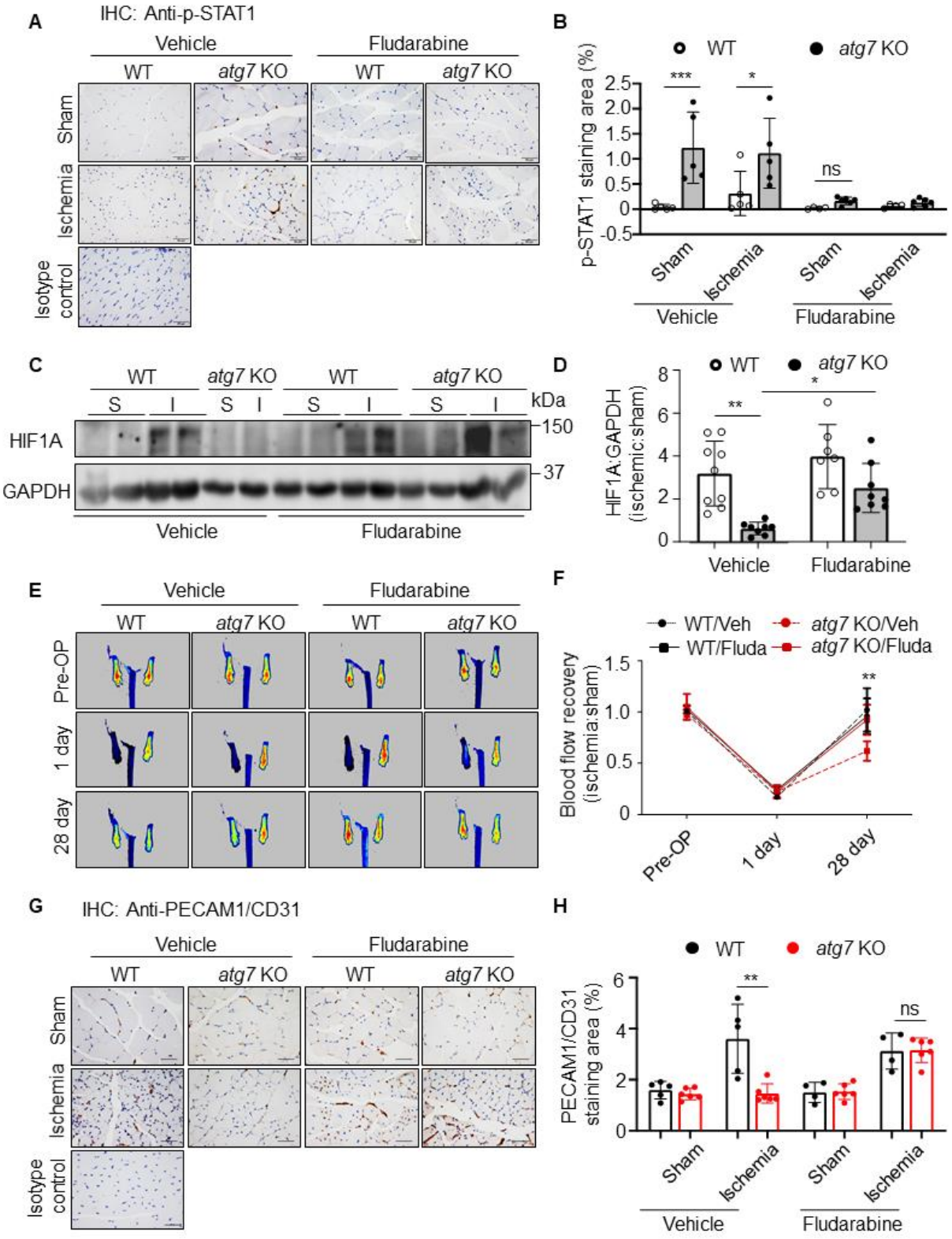

Figure 3.16 Inhibition of STAT1 by fludarabine recovers blood flow in ischemic hind limbs of atg7 KO mice

Femoral artery ligation was performed in 8–10-week-old WT and *atg7* KO mice. Fludarabine phosphate was administrated 1 week post ligation (100 mg/kg, i.p., once every other day). Blood flow was detected by Laser Doppler Imaging at the indicated time points. (A) Immunohistochemical staining of p-STAT1 (Y701) in the gastrocnemius muscular tissue. (B) Quantification of p-STAT1 (Y701) positive staining area. N = 4-6, * $p < 0.05$, *** $p < 0.001$, ns, not significant. (C) Western blot analysis was used to determine HIF1A protein expression in gastrocnemius muscular tissue in WT and *atg7* KO mice. (D) Densitometry analysis quantification of western blot, the ratio of ischemic limb to sham-surgery limb, N = 7-9, * $p < 0.05$, ** $p < 0.01$. S: Sham, I: Ischemia. (E) Representative images showing blood flow reperfusion assessed by Doppler laser ultrasound after ischemic injury. (F) The ratio of ischemic/non-ischemic perfusion, N = 4-7, ** $p < 0.01$. (G) Immunohistochemical staining of PECAM1/CD31 in the gastrocnemius muscular tissue. (H) Quantitative analysis of the ratio of PECAM1/CD31 positive staining area to muscular area, N = 4-6, ** $p < 0.01$; ns, not significant.

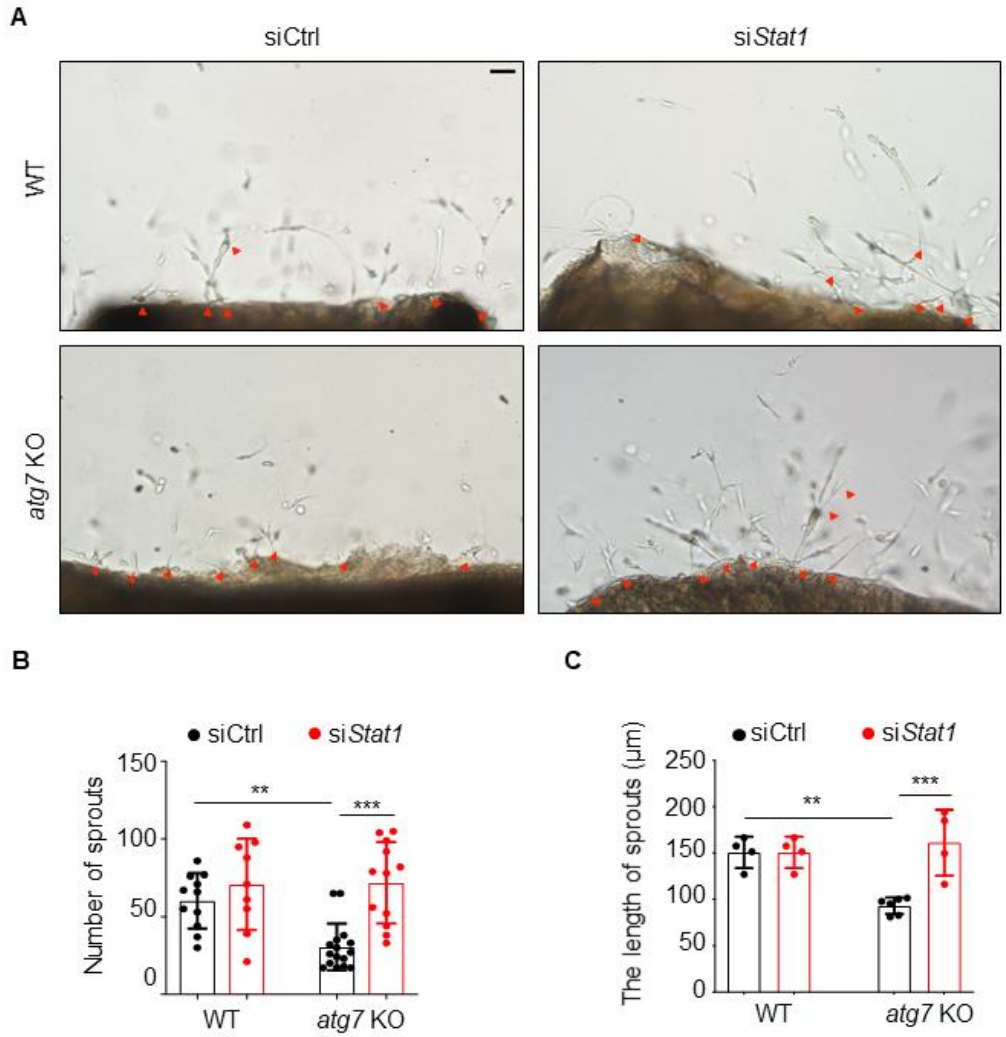

Figure 3.17 Silencing Stat1 recovers vascular sprouts in atg7 KO aortic rings.
(A) Inhibition of STAT1 by silencing *Stat1* restores vascular sprouts in *atg7* KO aortic rings. Representative images of aortic ring assay. Scale bar: 50 μm. (B) Quantification of sprout number. N = 9-16 rings. (C) Quantification of sprout length. N = 4-6 rings. ** $p < 0.01$, *** $p < 0.001$

3.6 Discussion

ATG7 has been demonstrated to be essential for autophagosome biogenesis, but its role in vascular biology remains largely unknown. In the present study, using EC-specific *atg7* KO mice, we found that lack of ATG7 in the cytoplasm disrupted the association between ATG7 and transcription factor ZNF148/ZBP-89 that is required for STAT1 constitutive expression (Bai & Merchant, 2003), increased the binding between ZNF148/ZBP-89 and KPNB1, which promoted ZNF148/ZBP-89 nuclear translocation, and increased STAT1 expression. STAT1 bond to *HIF1A* promotor and suppressed *HIF1A* mRNA expression, thereby preventing ischemia-induced angiogenesis. Our results demonstrate that *ATG7* deficiency is a novel suppressor of ischemia-induced angiogenesis.

Our understanding of the role of autophagy in vascular biology is relatively limited. It seems that this intracellular process acts as a two-edged sword against various cellular insults in ECs. For example, laminar flow promotes autophagic response in ECs, which suppresses oxidant-induced endothelial cell death (Liu et al., 2015). Activation of autophagy protects against senescence and apoptosis in high-glucose-induced endothelial cells (F. Chen et al., 2014). In addition, oxidized LDL-inhibited autophagy mediates endothelial apoptosis (Zheng & Lu, 2020), loss of *Atg7* promotes endothelial-to-mesenchymal transition and up-regulates key genes involved in TGF-β signaling and fibrosis. (Singh et al., 2015). However, autophagy has also been recognized as a cell death pathway in mammalian systems. Therefore, further researches are needed for comprehensively understanding the role of autophagy in endothelial biology and angiogenesis. Previous studies have shown that inhibition of autophagy by 3-methyladenine or silencing *ATG5* suppresses angiogenesis in aortic endothelial cells (Du et al., 2012). Deletion of endothelial *Atg7* results in lower microvessel density in the brain (S. F. Zhuang et al., 2017), but

does not affect the vascular density in skeletal muscle and retina (Torisu et al., 2013). In addition, endothelial *Atg7* deficiency promotes cutaneous wound healing, but does not affect angiogenesis in the injured skin (K. C. Li et al., 2020; H. J. Wang et al., 2018). These data suggest that *Atg7* deficiency may have less impact on angiogenesis in physiological and some pathological conditions. Nevertheless, it is reported that endothelial *Atg7* deletion attenuates ischemia/reperfusion-induced acute cerebral injury and inflammatory response by inhibiting pro-inflammatory cytokines through RELA/p65-dependent transcriptional regulation (K. C. Li et al., 2020; H. J. Wang et al., 2018). Although decreased microvessel density in *atg7*$^{-/-}$ mouse brain is associated with reducing interleukin 6 production through inhibiting RELA/p65 nuclear translocation (S. F. Zhuang et al., 2017), it is not clear if RELA/p65 mediates ATG7 deficiency-enhanced STAT1 expression and whether ATG7 regulating RELA/p65 nuclear translocation is dependent or independent of autophagy. Our study provided compelling evidence demonstrating that *Atg7* deficiency significantly inhibited ischemia-induced angiogenesis by activating STAT1-inhibited HIF1A expression that initiated angiogenesis by sensing environmental oxygen concentration and promoting growth factor transcription: 1) *Atg7* deficiency delayed blood perfusion recovery and impaired ischemia-induced angiogenesis in hind limb ischemic model. 2) Deletion of *Atg7* promoted STAT1 expression and negatively regulated tube formation. 3) Lack of *Atg7* upregulated STAT1 that inhibited HIF1A expression. 4) Silencing *STAT1* recovered the tube formation in cultured *Atg7*-deficient ECs. 5) Consistent with the observation that fludarabine attenuates cerebral ischemic injury by reducing cell apoptosis (Q. Xu et al., 2015), inhibition of STAT1 by fludarabine prevented *Atg7*-ablation-inhibited HIF1A expression, and promoted blood perfusion recovery and angiogenesis in hind limb ischemic model. Our results demonstrate that RELA/p65 is not involved in ATG7 deficiency-upregulated STAT1, and

uncovers three previously undescribed regulatory mechanisms linked to inhibition of ischemic angiogenesis in ATG7-deficient conditions—that is, STAT1 is a transcriptional inhibitor of HIF1A, loss of *ATG7* reduces HIF1A expression by upregulating STAT1, and ATG7 regulates STAT1 protein expression in an autophagy-independent manner: lack of ATG7 in the cytoplasm disrupts the association between ATG7 and transcription factor ZNF148/ZBP-89, increases the binding between ZNF148/ZBP-89 and KPNB1, which promotes ZNF148/ZBP-89 nuclear translocation, and increases STAT1 expression. Together, these findings establish a previously undescribed mechanism that lack of ATG7 inhibits angiogenesis by suppression of HIF1A expression through upregulation of STAT1 independently of autophagy under ischemic conditions.

HIF1A is not only regulated at the protein level by post-translational modifications and degradation, but also regulated at transcriptional level by transcription factors (Galban & Gorospe, 2009; Gerber & Pober, 2008; Koyasu et al., 2018; Park et al., 2017; Rius et al., 2008; Wen et al., 2019). By screening six reported HIF1A transcription factors, we found that the most significantly increased gene was *STAT1* in *ATG7*-deficient cells. Currently, the precise role of STAT1 in regulating HIF1A expression remains controversial in the literature. For example, in human aortic valve interstitial cells, the combination of IFNG/IFN-γ (interferon gamma) and lipopolysaccharide (LPS) promotes HIF1A induction, and silencing *Stat1* inhibits HIF1A protein induction (Parra-Izquierdo et al., 2019), indicating that STAT1 is the upstream signaling required for *HIF1A* expression. By contrast, in human glioblastoma cell lines, IFNG/IFN-γ suppresses the HIF1-dependent gene transcription and silencing *Stat1* abolishes the inhibitory effect of IFNG/IFN-γ on hypoxia-induced reporter gene activity (Hiroi, Mori, Sakaeda, Shimada, & Ohmori, 2009), suggesting that IFNG/IFN-γ-activated STAT1 functions as a negative

transcriptional regulator of HIF1A. Our study showed that silencing *Stat1* mitigated *Atg7* deficiency-inhibited HIF1A expression at both mRNA and protein levels, and silencing *ATG7* significantly increased STAT1 binding to the *HIF1A* promotor and inhibited *HIF1A* transcription, indicating that loss of *ATG7* reduces HIF1A expression by upregulating STAT1.

Another finding of this study is that ATG7 regulated STAT1 expression in an autophagy-independent manner. We found that *ATG7* deficiency enhanced *Stat1* mRNA and protein expression, concurrent with autophagy suppression. However, suppression of autophagy by silencing *ULK1*, knock down of *SQSMT1*, or administration of CQ failed to increase STAT1 expression. Moreover, silencing *Atg7* in *Ulk1*-deficient ECs, in which autophagic flux was inhibited, significantly upregulated STAT1 level. Overexpression of *ATG7* to promote autophagy had no obvious impact on STAT1 expression, indicating that inactivation of autophagy does not upregulate STAT1 expression, and ATG7 deficiency enhances STAT1 expression in autophagy-defective cells. Similar to our finding, *Atg5* or *Atg7* depletion is reported to increase total and phosphorylated STAT1 by downregulating ATF3 (activating transcription factor 3) (E. Kong, Kim, & Kim, 2020). On the contrary, another group reports that STAT1 expression is lower in *atg5* KO MEFs and the *Atg5* deficiency inhibits IFNG/IFN-γ-induced STAT1 phosphorylation, suggesting that IFNG/IFN-γ autophagy-dependently induces STAT1 activation (Chang et al., 2010). Moreover, the regulatory effects of ATG7 on STAT1 may vary in diverse cell types. For example, in murine alveolar macrophage cell line, *ATG7* deficiency impairs STAT1 activation as *P. aeruginosa* stimulation, but does not affect STAT1 protein expression (X. Li, Ye, Zhou, Huang, & Wu, 2015). In Michigan Cancer Foundation-7 (MCF7) cells, *ATG7* deficiency upregulates STAT1 protein expression (Ambjorn et al., 2013) (Schwartz-Roberts et al., 2015). However, these reports do not investigate the mechanisms by which ATG7 regulates

STAT1 expression. To bridge this gap, our study reveals a new mechanism by which *ATG7* deficiency upregulates STAT1 expression at transcriptional level via an autophagy independent pathway.

Interestingly, we observed that loss of ATG7 reduced angiogenesis *in vivo*, and inhibited tube formation in cultured ECs. However, overexpression of *ATG7* had no significant impact on the tube formation. This may be explained by the facts that STAT1 is a transcription factor that suppresses HIF1A expression, and the interaction of ZNF148/ZBP-89 with ATG7 and KPNB1 regulates the nuclear translocation of ZNF148/ZBP-89. Our study showed that ZNF148/ZBP-89 contained a binding region of ATG7, which was required for ATG7 physically associating with ZNF148/ZBP-89. Under basal conditions, there was rarely association between ZNF148/ZBP-89 and KPNB1, but the interaction of ZNF148/ZBP-89 and KPNB1 was significantly increased in ATG7-deficient conditions. In MLECs, both ATG7 and ZNF148/ZBP-89 was present in the cytoplasm, and the association of ATG7 and ZNF148/ZBP-89 was observed in the cytoplasm but not in the nucleus. In *atg7* KO MLECs, cytosolic ZNF148/ZBP-89 was significantly reduced, while nuclear ZNF148/ZBP-89 was dramatically increased, which was concurrent with the upregulation of STAT1. By contrast, overexpression of *ATG7* did not alter ZNF148/ZBP-89 nuclear translocation and STAT1 expression. These data suggest that under basic conditions, most ZNF148/ZBP-89 is anchored in the cytoplasm due to its binding to ATG7, which dissociates ZNF148/ZBP-89 from KPNB1, thus only small amount of ZNF148/ZBP-89 is able to enter the nucleus to maintain basic STAT1 expression. Although overexpression of ATG7 increases ATG7 expression, it does not significantly increase the association of ZNF148/ZBP-89 and ATG7, thus failing to reduce the nuclear translocation of ZNF148/ZBP-89 and STAT1 expression. However, under *ATG7*-deficient conditions, lack of *ATG7* disrupts the association of

ATG7 and ZNF148/ZBP-89. ZNF148/ZBP-89 is released from the ATG7-ZNF148/ZBP-89 complex and binds to KPNB1 that transports ZNF148/ZBP-89 from the cytoplasm to the nucleus, where ZNF148/ZBP-89 binds to *STAT1* gene promoter and upregulates STAT1 expression, leading to inhibition of HIF1A expression and angiogenesis.

Our findings may lead to improvements for the clinical cares of patients with tumor or ischemic cardiovascular diseases. Since angiogenesis has been characterized as an essential process for tumor cell proliferation and viability, our results that deletion of ATG7 can suppress angiogenesis suggest that inactivation of ATG7 is sufficient to inhibit tumor angiogenesis and suggest new clinical strategies to block tumor growth. Additionally, we found that inhibition of STAT1 by genetic or pharmacological means prevents inhibitory effects of ATG7 deficiency on ischemia-induced angiogenesis. This finding suggests that STAT1 inhibition may be a potential therapeutic target for the treatment of ischemic cardiovascular diseases.

In conclusion, *Atg7* deficiency impairs angiogenesis and delays blood flow reperfusion under ischemic conditions. Lack of *Atg7* upregulates STAT1 that transcriptionally inhibits HIF1A expression, thus impairing post-ischemic angiogenesis. Our studies uncover a new molecular mechanism for the negative effect of *Atg7* deficiency on angiogenesis and demonstrate that lack of ATG7 inhibits angiogenesis by suppression of HIF1A expression through upregulation of STAT1 independently of autophagy under ischemic conditions. Our findings may suggest new therapeutic strategies for cancer and cardiovascular disorders.

3.7 Materials and Methods

3.7.1 Reagents

Antibodies and reagents were purchased from the indicated companies. ATG7 (Cell Signaling Technology 8558), APG7 (B-9; Santa Cruz Biotechnology, sc-376212), MAP1LC3A/B (Cell Signaling Technology, 4108), EP300 (Cell Signaling Technology, 54062S), SQSTM1/p62 (Abcam, 56416), STAT1 (Cell Signaling Technology, 9172), p-STAT1 (Y701; Cell Signaling Technology, 9167), STAT3 (Cell Signaling Technology, 9139), p-STAT3 (S727; Cell Signaling Technology, 9136), STAT5 (Cell Signaling Technology, 9363), p-STAT5 (Y694) (Cell Signaling Technology, 9359), STAT6 (Cell Signaling Technology, 5397), p-STAT6 (Y641) (Cell Signaling Technology, 9361), HIF1A (Cell Signaling Technology, 36169), HIF1A (Santa Cruz Biotechnology, sc-13515), HIF2A (Cell Signaling Technology, 7096), ULK1 (Cell Signaling Technology, 8054), PECAM1/CD31 (Cell Signaling Technology, 77699), ZNF148/ZBP-89 (Santa Cruz Biotechnology, sc-137171), ZNF148/ZBP-89 (GeneTex, GTX104894) ACTB/β-actin (Santa Cruz Biotechnology, sc-47778), GAPDH (Santa Cruz Biotechnology, sc-32233), TUBA/α-Tubulin (Cell Signaling Technology, 3873), LMNA/lamin A/C (Cell Signaling Technology, 4777), LMNB1/lamin b1 (Cell Signaling Technology, 12586). SP1 (Santa Cruz Biotechnology, sc-59TRITC), TP53/p53 (Cell Signaling Technology, 2527S), GST (Cell Signaling Technology, 2624S), KPNB1/Importin β (proteintech, 10077-1-AP), SQSTM1 (proteintech, 18420-1-AP), NFκB RELA/p65 (Cell Signaling Technology, 4764S), mouse secondary antibody (Cell Signaling Technology, 7076), rabbit secondary antibody (Cell Signaling Technology, 7074), donkey anti-mouse IgG conjugated to Alexa Fluor 488 green (ThermoFisher Scientific, 21202), donkey anti-rabbit IgG conjugated to Alexa Fluor 488 green (ThermoFisher Scientific, 21206), goat anti-mouse IgG conjugated to Alexa Fluor 555 red

(ThermoFisher Scientific, 21422), goat anti-rabbit IgG conjugated to Alexa Fluor 555 red (ThermoFisher Scientific, 21428). EnVision® + Dual Link System-HRP (DAB+) (Dako Cytomation, 3468). *ATG7* siRNA (Cell Signaling Technology, 6604), *ATG7* siRNA (Thermo Fisher Scientific, 135754), *STAT1* siRNA (Cell Signaling Technology, 6331), *STAT1* siRNA (Thermo Fisher Scientific, VHS40871), *Stat1* siRNA (Thermo Fisher Scientific, 151007), *ZNF148/ZBP-89* siRNA (Santa Cruz Biotechnology, sc-38639), *SQSTM1* siRNA (human) (Santa Cruz Biotechnology, sc-29679), *Nfκb Rela/p65* siRNA (mouse; Santa Cruz Biotechnology, sc-29411), *Atg7* siRNA (Santa Cruz Biotechnology, sc-41448). *ULK1* siRNA (Santa Cruz Biotechnology, sc-44182) for *ex vivo* transfection. The siRNA delivery reagent Lipofectamine RNAiMAX (ThermoFisher Scientific, 13778-150), Lipofectamine® 2000 (ThermoFisher Scientific, 11668-019). Matrigel (Corning, 356237), fludarabine phosphate (Sigma-Aldrich, 1272204), chloroquine diphosphate salt (Sigma-Aldrich, C-6628), Pierce™ ECL Western Blotting Substrate (ThermoFisher Scientific, 32106). Stat1 alpha Flag pRc/CMV was a gift from Jim Darnell (Addgene, 8691); pCAG-HIF1 alpha was a gift from Connie Cepko (Addgene, 21101); *ATG7* plasmid was obtained as a gift from Dr. Zhixue Liu (Georgia State University), *ZNF148* plasmid (GenScript, OHu09001).

3.7.2 Mouse model of hind limb ischemia

Wild-type (WT, *C57BL/6J*, stock number 000664), *Ulk1*$^{flox/flox}$ (Stock number 017916), and vascular endothelial *Cdh5* (cadherin 5)-Cre mice (006137) were obtained from the Jackson Laboratory. *Atg7*$^{flox/flox}$ mice were purchased from RIKEN BioResource Research Center (RBRC02759). We generated *atg7*-EC-specific knockout mice (*atg7* KO, *Atg7*$^{flox/flox}$/*Cdh*5-Cre^{+}) by mating female *Atg7*$^{flox/flox}$ mice with male *Cdh5*-Cre mice to generate heterozygous mice (*atg7*/f/wt:Cre/wt mice). Next, we assigned heterozygous breeding pairs to obtain homozygous

mice. We PCR genotyped offspring using DNA from tail-snip biopsies. The mouse genotypes were determined using following primers: *Atg7* forward primer: TGGCTGCTACTTCTGCAATGATGT, reverse primer: CAGGACAGAGACCATCAGCTCCAC. Cdh5 transgene forward: AGGCAGCTCACAAAGGAACAAT; transgene reverse: TCGTTGCAT CGACCGGTAA; internal positive control forward, CTAGGCCACAGAATTGAAAGATCT; internal positive control reverse, GTAGGTGGAAATTCTAGCATCATCC. We selected two groups of mice for this study: *(a)* EC *atg7* KO (*atg7* KO) mice with genotype $Atg7^{flox/flox}$/*Cdh5*-Cre^{+} and *(b)* littermate control mice (WT) with genotype $Atg7^{flox/flox}$/*Cdh5*-Cre^{-}. We used 8 to 10-week-old male mice for the experiment. Mice were housed in temperature-controlled cages under a 12-h light-dark cycle and given free access to water and normal chow.

Mouse hind limb ischemia was induced as described previously (Niiyama, Huang, Rollins, & Cooke, 2009) . Briefly, the left femoral artery was exposed under a dissection microscope. The left common iliac and femoral arteries were ligated with 6-0 sutures. A sham procedure, in which the arteries were isolated but not ligated, was performed on the contralateral leg (Q. Lu et al., 2018). Blood flow was measured by Laser Doppler Imaging (Moor Instruments, Devon, UK). Ischemic and non-ischemic limb perfusion was measured before and directly after surgery, and then at 7, 14, 21, and 28 days after surgery. Image analysis software (PimSoft; Moor Instruments, Devon, UK) was used to calculate the limb mean flux units, and the final blood flow values were expressed as the ratio of ischemic to non-ischemic hind limb perfusion.

To examine the effect of STAT1-specific inhibitor, fludarabine phosphate, on *Atg7*-deficiency- induced inhibition of angiogenesis, one-week post-surgery we treated *atg7* KO and WT mice with fludarabine phosphate (100 mg/kg, i.p.) or vehicle once every other day as described previously (He, Li, Viollet, Zou, & Xie, 2015). After treatment, blood flow of hind limbs was measured by Laser Doppler Imaging. The animal protocol was approved by the Institutional Animal Care and Use Committee at Georgia State University. All experiment were carried out in compliance with IACUC.

3.7.3 Cell culture

HUVECs were obtained from the American Type Culture Collection (PCS-100–013) and grown in EBM medium (Lonza Bioscience, CC-3121), which was supplemented with endothelial cell growth supplement (Lonza Bioscience, CC-4133) and 5% fetal bovine serum (Sigma-Aldrich, 12303) in total. All culture media were supplemented with penicillin (100 Units/ml) and streptomycin (100 μg/ml; ThermoFisher Scientific, 15140-122). HUVECs were used between passages four to six. For pharmacological inhibition of STAT1, HUVECs were treated with fludarabine phosphate (50 nM) for 16 h.

3.7.4 Mouse lung endothelial cells isolation

Mouse lung endothelial cells (MLECs) were isolated as previously described (Sobczak, Dargatz, & Chrzanowska-Wodnicka, 2010). Mouse lung was excised and cut minced finely. Tissue was digested by type II collagenase (Worthington Biochemical, LS004177) at 37°C for 45 min, and followed by aspirating the tissue into a 20 ml syringe with 14 g cannula to get single cell suspension. Pulmonary endothelial cells were purified by anti-PECAM1/CD31 antibody

(BD Biosciences, 553369) conjugated magnetic beads (ThermoFisher Scientific, 11041) and anti-ICAM2 antibody (BD Biosciences, 553325) conjugated magnetic beads, sequentially. MLECs were grown and maintained in EBM medium (Lonza Bioscience, CC-3121) supplemented with endothelial cell growth supplement (Lonza Bioscience, CC-4133) and 20% fetal bovine serum (Sigma-Aldrich, 12303). MLECs were used between passage two to four. Cultured cells were incubated under standard cell culture conditions (37°C, 20% O_2, 5% CO_2). To observe the effect of hypoxia, the cells were cultured under the condition of 37°C, 1% O_2, 5% CO_2, 94% N_2.

3.7.5 Aortic Ring assay

The procedure was performed as previous described (Baker et al., 2011). Briefly, WT and *atg7* KO mice were euthanized at 3 months of age. The aortas were isolated, the fat tissue was cleaned, and aortas were cut into 0.5 mm aortic rings. WT and *atg7* KO aortic rings were subjected to transfection of control siRNA or *Stat1* siRNA overnight. Then aortic rings were embedded into Matrigel (Corning, 356230) and cultured in 2.5% FBS Opti-MEM containing VEGF (vascular endothelial growth factor) (30 ng/ml; ThermoFisher Scientific, PHC9394). Images were taken 6 days after implantation.

3.7.6 Retina staining

Retinas were isolated from WT and *atg7* KO mice on postnatal day 8. Endothelial cells were stained with isolectin GS-IB4 (1:100; ThermoFisher Scientific, I21413) and pericytes were co-stained by either NG2 (1:100; Millipore Sigma, AB5320) or DES/desmin (1:200; Cell Signaling Technology, 5332S).

3.7.7 Wound healing assay

HUVECs were transfected with control siRNA or *ATG7* siRNA for 48 h and the cells were scratched with 200 µl tips, and Images were taken at indicated time points (0 and 6 h) using an inverted microscope. The images were analyzed with the ImageJ.

3.7.8 Spheroid sprouting angiogenesis assay

The spheroid sprouting angiogenesis assay was performed following established protocol (Tetzlaff & Fischer, 2018). Briefly, methyl cellulose stock solution was prepared by dissolving methyl cellulose (6 g; Sigma-Aldrich, 9004-67-5) in EBM basal medium (500 ml) (Lonza, CC-3121). HUVECs (the number of cells, 2000) were suspend in 1 ml 20% methyl cellulose, 5% FBS EBM (with EGM supplements (Lonza, CC-3124) 25 µl drops of cell suspension were pipetted on a 15-cm Petri dish using an 8-channel pipette and kept upside-down in the cell culture incubator (37°C, 5% CO_2) for 24 h. The spheroids were collected, spun down, and re-suspend in 0.5 ml methyl cellulose (containing 20% FBS). The same amount of collagen (2 mg/ml; ThermoFisher Scientific, A1048301) was added to the solution of spheroids, and the mixed solution was transferred into 24-well plate and kept in cell culture incubator for 30 min to allow the *collagen* gel to *polymerize*. Finally, 200 µl cell culture medium was added to the mix solution and cultured for another 24 h in cell culture incubator (37°C, 5% CO_2). The spheroids were fixed by 10% formalin and pictures were taken by inverted microscope.

3.7.9 Constructs of truncations of ZNF148

Truncations of *ZNF148* were generated by PCR using the corresponding primers. *ZNF148* (1-168 bp): Forward 5'-GTGTCGACCATGAACATTGACGACAAACTGGAAG-3', Reverse 5'-ATGCGGCCGCTTAAGGGGTTTTCAAACCAAGTGATC-3', ZNF148 (169-281): Forward 5'- GTGTCGACCATGAAATCTCACGTTTGTGAGCACTG-3', Reverse 5'-ATGCGGCCGCTTAGTCATGATTTTCATGGCACATACG-3', ZNF148 (282-552): Forward 5'- GTGTCGACCATGAAAAAACTAAATAGATGTGCCATCAAAG-3', Reverse 5'-ATGCGGCCGCTTAAGCTTTGTGGGAATAATGATCC-3', ZNF148 (553-794): Forward 5'-GTGTCGACCATGAATGGACAGCATGAGATATCCTTC-3', Reverse 5'-ATGCGGCCGCTTAGCCAAAAGTCTGGCCAG-3'. The fragments of *ZNF148* were constructed into PRK5-GST plasmid with Sal-I and Not-I restriction enzyme. All the constructs were confirmed by DNA sequencing.

3.7.10 Plasmid and siRNA transfection

To overexpress *ATG7, STAT1*, or *HIF1A*, HUVECs were transfected with *ATG7* plasmid (*MYC-ATG7*), STAT1 plasmid (*Flag-STAT1*), *HIF1A* plasmid (*MYC-HIF1A*), or empty plasmid (Ctrl) in OPTI-MEM reduced-serum media (ThermoFisher Scientific, 31985) by using Lipofectamine 2000 (ThermoFisher Scientific, 11668019) for 24 h. To silence *ATG7, STAT1*, *ULK1* or *ZNF148/Zfp148/ZBP-89*, HUVECs or MLECs were transfected with *Atg7* siRNA, *Stat1* siRNA, *ZNF148/Zfp148/ZBP-89* siRNA, or control siRNA in OPTI-MEM reduced-serum media using Lipofectamine RNAiMax transfection reagent (ThermoFisher Scientific, 13778150) for 48 h. The transfection efficiencies of the siRNAs and plasmids were determined by western blot analysis of target protein expression.

3.7.11 Immunohistochemistry and immunofluorescence staining

Skeletal muscle was isolated, fixed in 4% paraformaldehyde, embedded in paraffin, and cut into 4 μm sections. The sections were deparaffinized, rehydrated, and heated in citrate buffer to unmask the antigens. Muscular sections were incubated with primary antibodies against PECAM-1/CD31, p-STAT1 (Y701), or HIF1A overnight at 4°C, respectively. After rinsing in PBS (Millipore Sigma, D5652-50L) 3 times, sections were incubated with a horseradish peroxidase-labeled polymer detection system (DAKO EnvisionCDual link, K4061) and stained with DAB chromogen (DAKO, K3468).

HUVECs or MLECs were fixed with -20°C methanol (Fisher Scientific, 67-56-1) and permeabilized using 0.2% Triton X-100 (Sigma-Aldrich, T8787). Cells were blocked by goat serum (Fisher Scientific, HK112-9K) for 30 min and incubated with corresponding primary antibody at 4°C, overnight. The cells were washed with 0.5% Tween-20 (Sigma-Aldrich, P1379) in PBS 3 times, then incubated with fluorescent secondary antibody for 1 h at room temperature, and mounted with DAPI (Sigma-Aldrich, D9564). Images were recorded using an Olympus fluorescence microscope (Olympus BX53, Tokyo, Japan) and quantified using Image-Pro Plus 6.0 (Media Cybernetics, Rockville, MD).

3.7.12 Immunoprecipitation and western blot analysis

Proteins were extracted from skeletal muscles, HUVECs, and MLECs using RIPA lysis buffer (Santa Cruz Biotechnology, sc-24948A). Protein content was determined using the bicinchoninic acid protein (BCA) assay reagent (ThermoFisher Scientific, 23223, 23224). For

immunoprecipitation, proteins (500 μg for each sample) were incubated with anti-ATG7 antibody or Rabbit IgG overnight at 4°C. Protein A sepharose beads (Sigma Aldrich, GE 17-0780-01) were added and rotated at 4°C for 3 h. The sepharose beads were washed 5 times with lysis buffer and subjected to western blot analysis. For western blot analysis, 30 mg of protein were resolved by SDS-PAGE, transferred to nitrocellulose membranes (Bio-Rad Laboratories, 1620112), and probed with specific antibodies. The signals were visualized using the ECL (ThermoFisher Scientific, 32106) detection system. The intensity of individual bands was measured by Image J and the background was subtracted from the calculated area.

To determine the location of ATG7 binding domain on *ZNF148,* HEK 293T cell were transfected with glutathione S-transferase (GST)-tagged *ZNF148* truncations or GST-control plasmid, and co-transfected with *MYC-ATG7* plasmid. Cell lysates were obtained 24 h after transfection. GST was pulled down by glutathione-sepharose beads (Sigma-Aldrich, GE17-0756-01), and the overexpression efficacy and the interaction of ZNF148/ZBP-89 and ATG7 were determined by blotting GST and ATG7 antibody, respectively.

3.7.13 RNA Extraction and quantitative Real-Time (qRT)-PCR analysis

Total mRNA was extracted from cultured cells with Trizol reagent (ThermoFisher Scientific, 15596018). For reverse transcription, 1 μg of the total mRNA was converted to first strand complementary DNA in a 20 μL reaction volume using a cDNA synthesis Kit (Bio-Rad Laboratories, 1708891). PCR primers used for amplification of genes were as follows:

Stat1 (mouse): forward 5'-GCTGCCTATGATGTCTCGTTT -3', reverse 5'-TGCTTTTCCGTATGTTGTGCT-3'; *STAT1* (human): forward 5'-

AGGAAAAGCAAGCGTAATCTTCA-3’; reverse 5’-TATTCCCCGACTGAGCCTGAT-3’; *GAPDH* (human): forward 5’-CATCAATGGAAATCCCAT-3’; reverse 5’-TTCTCCATGGTGGTGAAGAC-3’; *HIF1A* (human): forward 5’-TCCAAGAAGCCCTAACGTGT-3’; reverse 5’-TTTCGCTTTCTCTGAGCATTCTG-3’; *NEAT1* (human): forward 5’-GTTCCGTGCTTCCTCTTCTG-3’; reverse 5’-GTGTCCTCCGACTTTACCAG-3’; *IRF9* (human): forward 5’-GCCCTACAAGGTGTATCAGTTG-3’; reverse 5’-TGCTGTCGCTTTGATGGTACT-3’; *BCLAF1* (human): forward 5’-CCGCGATTCGGCGTGTCAGG-3’; reverse 5’-GACCCATTTCTTTTCTCCTTGGTT-3’; *NRF1* (human): forward 5’-AGGAACACGGAGTGACCCAA-3’; 5’-TATGCTCGGTGTAAGTAGCCA-3’; *Hif1a* (mouse): forward 5’-CCTGCACTGAATCAAGAGGTTGC-3’; reverse 5’-CCATCAGAAGGACTTGCTGGCT-3’; *Zfp148* (mouse): forward 5’-GAGATTTCCTTCAGCGTTTAC-3’; reverse 5’-TTTGGAAGGGTCTGGTTGTC-3’; β-actin (mouse): forward 5’-GGCTGTATTCCCCTCCATCG-3’; reverse 5’-CCAGTTGGTAACAATGCCATGT-3’. All samples were run in duplicate and underwent initial denaturation at 95°C for 5 min, followed by 40 rounds of amplification (95°C for 30 s, 60°C for 30 s) using iQ™ SYBR® Green Supermix (Bio-Rad Laboratories, 1708884) and the CFX96™ Real-Time System (Bio-Rad Laboratories). All data were analyzed using the $2^{-\Delta\Delta CT}$ method and normalized with *GADPH* or *Actb* as described previously (Mu, Zhang, Tian, Xie, & Zou, 2020).

3.7.14 Chromatin immunoprecipitation (ChIP) assays

The ChIP assay were performed using SimpleChIP® Enzymatic Chromatin IP Kit (Cell Signaling Technology, 9003s) according to the manufacture’s instruction. 4×10^6 HUVECs were

used for each immunoprecipitation. Protein was crossed-linked to DNA by addition of 1% of formaldehyde, and the cross-linking process was terminated by glycine. Chromatin was sonicated to 100 to 500 bp fragments. To determine the interaction between STAT1 and *HIF1A* promoter, the DNA fragments were immunoprecipitated with antibodies against STAT1 (dilution 1:50) or normal rabbit IgG (Cell Signaling Technology, 2729) overnight at 4°C. All DNA samples were purified, and PCR was conducted to measure the relative amount of interaction between STAT1 and *HIF1A* promoter. The following primers were used for the amplification: forward: 5'-CACATCTGAGCAACGAGACCAAAGG-3', reverse: 5'-GCGCTGCTGAGAAGGGATTTC-3'. The enrichment of *HIF1A* gene DNA fragments was normalized to the input of total genomic DNA for each sample. To determine the interaction between RELA/p65 and *HIF1A* promoter, the DNA fragments were immunoprecipitated with antibodies against RELA/p65 (dilution 1:50; Cell Signaling Technology, 6956S) or normal mouse IgG (Vector Laboratories, I-2000) overnight at 4°C. All DNA samples were purified, and PCR was conducted to measure the relative amount of interaction between RELA/p65 and *HIF1A* promoter. The following primers were used for the amplification: forward: 5'-GAGTTCCCCTGTGCTCCGTG-3', reverse: 5'-TTCTCCTCGGCCTCAGTGCT-3'. The enrichment of *HIF1A* gene DNA fragments was normalized to the input of total genomic DNA for each sample.

3.7.15 Cytosol and nuclear fractionation

HUVECs or MLECs were washed with ice-cold PBS (pH7.4) twice and collected into 1.5 ml micro-centrifuge tube. The cells were lysed by adding 600 µl RIPA containing protease cocktail. 200 ul of the lysate was collected as "whole cell lysate". The remained 400-µl lysates

were centrifuged for 10 s at the maximum speed of Eppendorf (Sigma Aldrich, Eppendorf Centrifuge 5418 R). 200 µl of the supernatant was collected as “cytosolic fraction”. The pellet was resuspended by 1 ml RIPA buffer and centrifuged for 10 s at the maximum speed of the Eppendorf. The pellet resuspended by adding 200 µl RIPA buffer and used as “nuclear fraction”.

3.7.16 Tube formation assay

The experiment was performed as manufacture’s instruction (Corning, 356237). HUVECs were used less than passage 5. Passage 2 of MLECs were used in this experiment. Twenty-four-well culture plates were coated with Matrigel (280 µl/ well) according to the manufacturer’s instructions. HUVECs were transfected with siRNA or plasmid for 24 h, and then seeded on coated plates at 5×10^4 cells/well in EBM containing 10% FBS and incubated at 37°C for another 16 h under normoxic or hypoxic conditions. Tube formation was observed using an inverted fluorescence microscope (Olympus IX73, Tokyo, Japan). Images were captured with a video graphic system (CellSens Software, Tokyo, Japan). The degree of tube formation was quantified by measuring the number of sprouts in three randomly chosen low-power fields from each well using the NIH Image Program. Each experiment was repeated at least three times.

3.7.17 Statistical analysis

Data were expressed as mean ± standard deviation (SD). One- or two-way ANOVA was used to determine the differences among three or more groups, followed by Bonferroni post-hoc analysis using GraphPad Prism 9 software (GraphPad Software, Inc., La Jolla, CA).

Comparisons between 2 groups of values were assessed using the Student's t test. $P < 0.05$ was considered statistically significant.

4 RESULT 2: AUTOPHAGY INHIBITION AGGREGATES T1D-INDUCED ENDOTHELIAL DYSFUNCTION

ULK1 deficiency worsen STZ-induced endothelial dysfunction by two pipelines—elevating ROS production and inhibiting eNOS phosphorylation

Hongmin Yao, Xiaoxu Zheng, Jian Li, Qilong Wang, Gloria Andrea Torres Rivera, Ming-Hui Zou and Zhonglin Xie

4.1 Abstract

ULK1 is a serine/threonine kinase and involved in the initiation of autophagy, which maintains intracellular metabolic needs by digesting intracellular materials. However, whether and how autophagy is involved in hyperglycemia-induced endothelial dysfunction are still not fully understood. Here, we generated endothelial-specific *Ulk1* knockout (*ulk1* KO) mice, treated the mice with streptozotocin (STZ) to induce type 1 diabetic animal model, and analyzed endothelial function, reactive oxygen species (ROS) production, and eNOS phosphorylation. We found that STZ-induced type 1 diabetes inhibited autophagic flux and reduced protein levels of autophagy gene related protein, including ULK1, ATG7, ATG5, and Beclin1, which was accompanied by overproduction of ROS, inactivation of eNOS, and impairment of acetylcholine-induced relaxation of isolated mouse aortas. *Ulk1* deletion in endothelial cells (ECs) exacerbated endothelium-dependent vessel relaxation, intensified ROS production, and worsened eNOS inactivation in STZ-treated mouse aorta. In addition, we determined that the overproduced ROS was predominantly derived from mitochondria but not NOX (Nicotinamideadenine-dinucleotide phosphate (NADPH) oxidase) system. Importantly, eNOS phosphorylation at Ser1177 was reduced in *ULK1*-deficient conditions. Therefore, defective autophagy is an important event in

diabetes-induced endothelial dysfunction. Activation of autophagy and overexpression of ULK1 may be potential strategies to prevent endothelial dysfunction in diabetes.

4.2 Introduction

Diabetes mellitus is a metabolic disease characterized by hyperglycemia resulting from defects in insulin secretion or action. Diabetes is basically divided into two types, type 1 diabetes is dependent on external insulin, and type 2 diabetes is characterized by insulin resistance. The chronic hyperglycemia of diabetes is associated with endothelial dysfunction, an early event of cardiovascular diseases. Type 1 diabetic patients exhibit abnormal glucose metabolism, ROS overproduction, and enhanced AGEs (advanced glycation end products) products (Katsarou et al., 2017). The endothelium is a single layer of endothelial cells (ECs) lining the entire vascular system (Kruger-Genge et al., 2019). . Glucose enters the cells through GLUT-1 (Glucose transporter 1), and predominantly regulated by extracellular glucose levels. Thus, endothelial cells are more susceptible to hyperglycemia-induced damage than other cell types (Knapp, Tu, & Wu, 2019).

Autophagy is a highly conserved intracellular catabolic process for degradation of long-lasting protein, protein aggregation, malfunctioned organisms, and even pathogen (He & Klionsky, 2009). It is maintained in a certain level in nutrition sufficient condition, but it is highly activated in nutrition deprivation (Cuervo & Macian, 2012). Many reports indicate that autophagy is impaired in hyperglycemia conditions (Niu et al., 2019; Xie et al., 2011), the role of autophagy, however, in hyperglycemia-induced endothelial dysfunction remains elusive. In particularly, whether high glucose inhibits or promotes autophagy is debatable, and how autophagy affects endothelial function is still unclear.

ULK1 (unc-51-like kinase 1), the initiator of classic autophagy, is a serine/threonine protein kinase and usually forms a large complex with ATG13 and FIP200, ATG101, which serves

as a platform to recruit other autophagic molecules to initiate autophagy. mTORC1 (mammalian target of rapamycin complex 1) phosphorylates ULK1 and ATG13, leading to inhibition of the ULK1 complex; while the complex can be activated by stress conditions by disassociating mTORC1 from the complex (Jung et al., 2009). For example, in glucose starvation condition, ULK1 is phosphorylated by AMPK at Ser 317 and Ser 777, which prevents mTORC1-phosphorylating ULK1 at Ser 757 (Kim et al., 2011). ULK1 also targets ATG4B, ATG9, ATG14L, Beclin 1, and subunit of the PI3K complex to facilitate autophagy occurrence (Nakatogawa, 2020). Besides the autophagy-related functions, ULK1 also regulates glycolysis since several essential glycolytic enzymes are the substrates of ULK1 (T. Y. Li et al., 2016). However, if ULK1 is involved in the development of endothelial dysfunction in diabetes is unknown. In the present study, we aim to determine the role of ULK1 and autophagy in hyperglycemia-induced endothelial dysfunction.

4.3 Results

4.3.1 Hyperglycemia reduces ATG protein expression and inhibits autophagy activity

To understand the relationship between autophagy activity and endothelial dysfunction in diabetic conditions, we treated C57BL/6J mice with streptozotocin (STZ) to induce type 1 diabetes, and determined the effect of hyperglycemia on autophagy by analyzing ATG protein expression in STZ-treated mouse aortas. The homogenized aortic samples were prepared and the expression of SQSTM-1/p62, ATG7, ATG5, Beclin 1, ULK1, and the ratio of LC3-II to LC3-I was determined by western blot. The results indicated that hyperglycemia reduced the expression of ATG proteins, including ATG7, Beclin1, and ULK1. Concomitantly, autophagy flux was suppressed, as evidenced by reduced conversion of LC3-I to LC3-II and increased SQSTM-1/p62 protein levels. (Figure 4.1 A and B). We also verified the effect of hyperglycemia on

autophagy in cultured human umbilical vein endothelial cells (HUVECs) and found that high glucose significantly increased SQSTM1 protein levels and reduced the lipidated form of LC3 (LC3-II) (Figure 4.1 C and D). Blocking autophagy using chloroquine (CQ) increased both LC3-II and SQSTM-1/p62 levels at both control and HG conditions (Figure 4.1 E, F and G). Consistent with the in vivo finding that hyperglycemia inhibits ULK1 protein expression in aortic tissues, high glucose also reduced ULK1 protein expression in cultured HUVECs (Figure 4.1 H and I). The data suggested that hyperglycemia reduces ULK1 expression and inhibits autophagy in ECs. High glucose inactivates AMPK but has no effect on TFEB nuclear translocation.

4.3.2 High glucose inactivates AMPK but has no effect on TFEB nuclear translocation

The activated transcription factor EB (TFEB) enters into the nucleus to regulate the expression of genes involved in different steps of the autophagy process (Bala & Szabo, 2018; Napolitano & Ballabio, 2016). We therefore examined the effects of high glucose on TFEB protein expression, and observed similar TFEB protein expression in HUVECs treated with either normal glucose or high glucose (Figure 4.2 A). Because nuclear translocation is required for TFEB inducing the expressions of targeted genes, we determined the subcellular distribution of TFEB in HG condition by detecting TFEB protein levels in subcellular fractions. The TEFB protein levels in cytosol and cellular fractions are comparable between the cells treated with either normal glucose or high glucose (Figure 4.2 B). Previous studies show that diabetes inhibits AMP-activated protein kinase (AMPK) activity, a central regulator of metabolism and autophagy (Towler & Hardie, 2007). We determined the effect of high glucose on AMPK activity by measuring the phosphorylation of AMPK at Thr172. Compared with normal glucose treatment,

high glucose significantly reduced AMPK phosphorylation (Figure 4.2 C and D), suggesting that HG inhibits AMPK signaling pathway but had not effect on TFEB signaling pathway in endothelial cells.Inhibition of autophagy by endothelial-specific ulk1 knockout worsens diabetes-induced endothelial dysfunction.

4.3.3 Inhibition of autophagy by endothelial-specific ulk1 knockout worsens diabetes-induced endothelial dysfunction

To establish the role of autophagy in the development of diabetes-induced endothelial dysfunction, we generated endothelial-specific *ulk1* deleted mice by mating *ulk1*$^{flox/flox}$ mice with *Chd5*^{Cre} mice to generate *ulk1*$^{flox/flox}$ Cdh5^{+} (*ulk1* KO) mice and *ulk1*$^{flox/flox}$ Chd5^{-} (WT) mice. The *ulk1*$^{flox/flox}$ *Chd5*$^{-}$ littermate was used as wild-type (WT) control (Figure 4.3 A). Analysis of *Ulk1* expression by real-time PCR indicated that *Ulk1* mRNA level was abolished in *ulk1* KO mouse lung endothelial cells (MLECs) (Figure 4.3 B). Western blot analysis showed that the protein expression of ULK1 was barely detected in MLECs of *ulk1* KO mice. In contrast, ULK1 expression in aortic smooth muscle cells (SMCs) was not affected (Figure 4.3 C). Moreover, immunohistochemistry staining of ULK1 in WT and *ulk1* KO mouse aortas showed that positive staining of ULK1 was observed in WT but not *ulk1* KO mouse endothelium (Figure 4.3 D), indicating that *Ulk1* was successfully deleted in EC cells in *ulk1* KO mice. As ULK1 is the essential for autophagy initiation, we further assessed the autophagic changes in *Ulk1*-deficient MLECs. Treating MLECs with chloroquine (CQ) to inhibited lysosomal enzyme activity significantly increased LC3-II and SQSTM1 levels in both WT and *ulk1* KO MLECs, suggesting that deletion of *Ulk1* prevents autophagy process (Figure 4.3 E).

We then determined the effect of autophagy suppression on endothelial function by treating WT and *ulk1* KO mice with STZ to induce type 1 diabetes. The fasting blood glucose

assay indicated that STZ treatment significantly enhanced blood glucose in both WT and *ulk1* KO mice, but deletion of *Ulk1* did not affected blood glucose in either vehicle- or STZ-treated mice *(*Figure 4.4*).* Immunohistochemistry staining of ULK1 showed that the positive staining of ULK1 in vehicle-treated WT aortas was stronger than that in vehicle-treated *ulk1* KO, STZ-treated WT, and STZ-treated *ulk1* KO mice (Figure 4.3 F).

Next, we tested whether autophagy contributes to endothelial dysfunction in diabetic mice. Compared with control aortic rings, aortic rings from STZ-treated mice exhibited impaired endothelial-dependent relaxation induced by acetylcholine (Ach). However, endothelium-dependent vasorelaxation induced by Ach was not impaired in *ulk1* KO mouse aortas (Figure 4.3 G). The impairment of Ach-induced endothelium-dependent relaxation in aortic rings from *ulk1* KO was more server than that in aortic rings from STZ-treated WT mice (Figure 4.3 G), indicating that suppression of autophagy contributes to endothelial dysfunction in diabetic mice. However, suppression of autophagy by *Ulk1* deletion had no effect on endothelium-independent vasorelaxation induced by SNP (Figure 4.3H). The above results manifest that deletion of *Ulk1* to inhibit autophagy aggravates STZ-induced endothelial dysfunction.

4.3.4 Autophagy deficiency intensifies hyperglycemia-induced ROS overproduction

Reactive oxygen species (ROS) overproduction is one of the main causes of hyperglycemia- induced endothelial dysfunction, as ROS accumulation correlates with eNOS uncoupling and decrease the bioavailability of nitric oxide (NO) (Montezano & Touyz, 2012) . We next detect ROS generation in aortas isolated from WT and *ulk1* KO mice treated with either STZ or vehicle by Dihydroethidium (DHE) staining. The result depicted that in WT mice, STZ stimulation promoted ROS formation relative to vehicle injection. Deletion of ULK1 exacerbated ROS generation in STZ-treated *ulk1* KO mice although ROS production did not significantly

increase in vehicle-treated *ulk1* KO mice (**Figure 4.5 A and B**). Mitochondria are the major contributor to ROS production in diabetes (J. Chen, Stimpson, Fernandez-Bueno, & Mathews, 2018; Kaludercic & Di Lisa, 2020). The absence of autophagy impairs mitochondrial functions, leading to ROS overproduction (Roca-Agujetas et al., 2019; Thomas & Gustafsson, 2013). We further examined the effect of defective autophagy on mitochondrial ROS production in diabetic conditions. HUVECs transfected with *ULK1* siRNA or control siRNA were treated with HG or osmotic control (OC) for 48 h, and the cells were stained with MitoSox. The result showed that compared to OC, silencing *ULK1* significantly elevated MitoSox fluorescent intensity in control cells. HG treatment tended to increase MitoSox fluorescence intensity in the cells transfected with siCtrl, and induced more MitoSox fluorescence intensity in si*ULK1*-treated cells (**Figure 4.5 C and D**). The results suggest that inhibition of autophagy by silencing *ULK1* augments HG-induced mitochondrial ROS production.

4.3.5 High glucose does not influence that NADPH oxidases (NOXs) expression

Given that NADPH oxidases (NOXs) are one of the major sources of cellular ROS (Bedard & Krause, 2007), we also tested if high glucose induced NOXs expression or enhanced their activity. We found that hyperglycemia had no effects on NOX2 protein and mRNA expression in STZ-treated mouse aortas. In addition, high glucose concentrations did not affect the expression of NOX2 and NOX4 in high glucose-treated HUVECs (**Figure 4.6 A-D**). We next tested whether or not components of NADPH oxidase are affected by high glucoses by western blotting for p22, p47, and p67 phox in HUVECs. Exposing HUVECs to high glucose for 24 did not change the expression of p22 phox, p47 phox, and p67 phox (Figure 5E-G), suggesting that NADPH may not be involved in HG-induced ROS overproduction in endothelial cells.

4.3.6 ULK1 deficiency inhibits eNOS phosphorylation

As we found that diabetes inhibited autophagy, associated with decrease in protein level of ULK1, a serine/threonine-specific protein kinase, and impairment of eNOS-related vessel relaxation, we therefore investigated whether the decrease in ULK1 expression participates in the reduction of eNOS phosphorylation at Ser1177 (p-eNOS). To this end, we measured the protein levels of total and phosphorylated eNOS in HUVECs transfected with *ULK1* siRNA or control siRNA. The results indicated that silencing *ULK1* significantly inhibited phosphorylation of eNOS at S1177, but had no obvious impact on total eNOS protein expression (**Figure 4.7 A, B and C**). In addition, immunofluorescence (IF) staining of p-eNOS in aortas isolated from WT and *ulk1* KO mice treated with either STZ or vehicle showed that STZ-treated mice expressed lower p-eNOS protein expression in endothelium relative to vehicle-treated mice. *Ulk1* deletion decreased p-eNOS expression and exacerbated HG-reduced p-eNOS protein level (**Figure 4.7 D** and **E**).

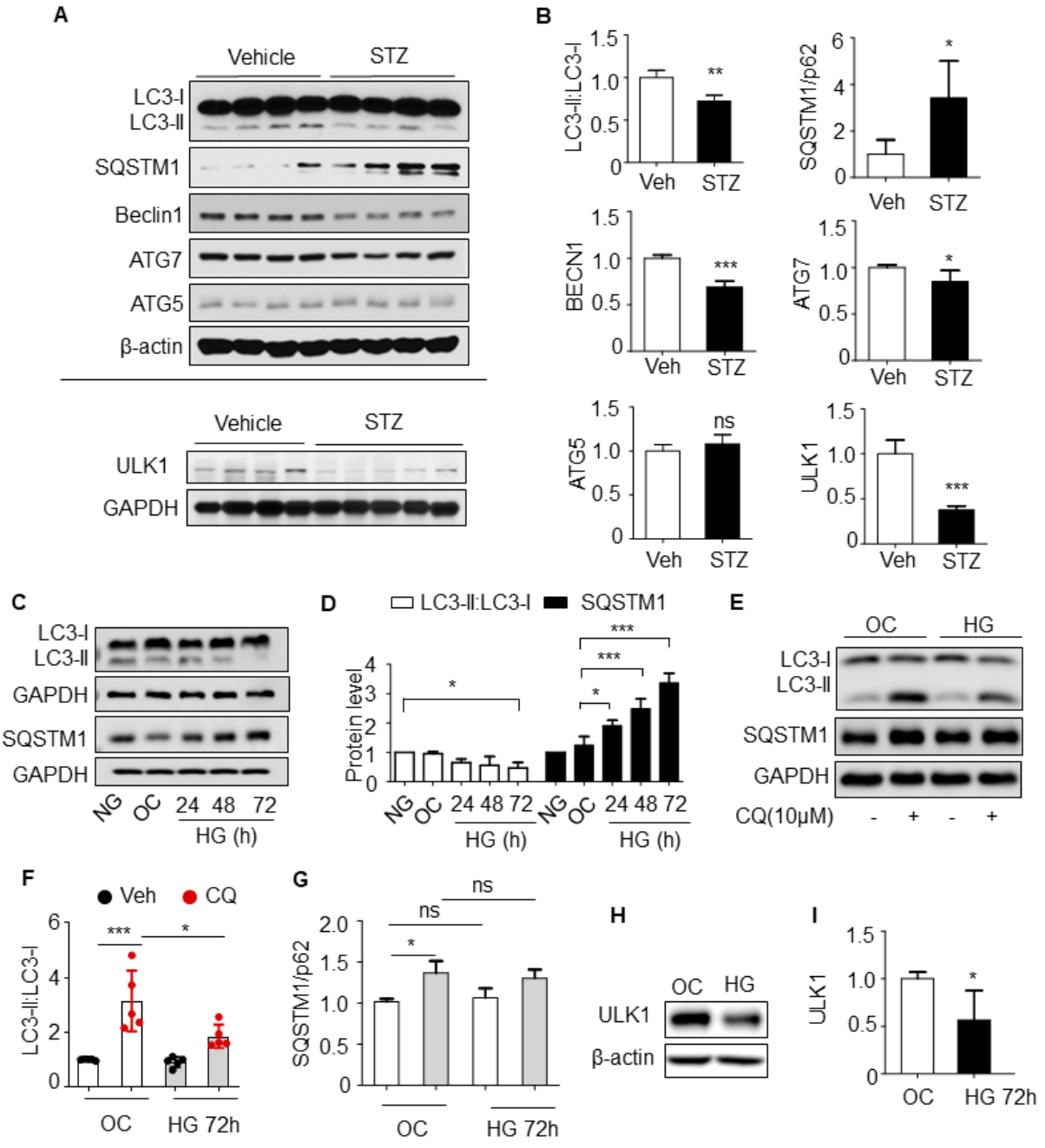

Figure 4.1 Hyperglycemia inhibits autophagic flux in ECs
(**A-C**) Wild-type (WT; C57BL/6J) mice were treated with STZ or vehicle at 2 to 3 months of age, and aortic tissues were collected after diabetes induction for 6 months. (**A**) Protein levels of ATG7, ATG5, ULK1, Beclin1, SQSTM1 and LC3-I/LC3-II were analyzed in mouse aortic homogenates. (**B**) Densitometric analysis of western blots in panel A. (**C**) HUVECs were treated with normal glucose (NG; 5 mM), osmotic control (OC; 5 mM glucose + 25 mM mannitol), or high glucose (HG; 30 mM) for indicated time. LC3-I/LC3-II and SQSTM1/p62 protein levels were measured by western blot. (**D**) Densitometric analysis of SQSTM1/p62 protein levels and the ratio of LC3-II:LC3-I. * $P < 0.05$, *** $P < 0.001$, N = 3-4. (**E** and **F**) HUVECs were treated

osmotic control or high glucose for 72 h, and the cells were treated with CQ (10μM) or vehicle for 16 h before collecting the samples. LC3-I:LC3-II ratio and SQSTM1/p62 protein levels were measured by western blot (E). (**F** and **G**) Densitometric analysis of SQSTM1/p62 protein levels and the ratio of LC3-II:LC3-I. * $P < 0.05$, *** $P < 0.001$, ns, not significant, N = 3-5. (**H**) HUVECs were treated with high glucose for 72h, ULK1 protein expression was determined by western blot. (**I**) Densitometric analysis of ULK1 protein levels. * $P < 0.05$, N = 5.

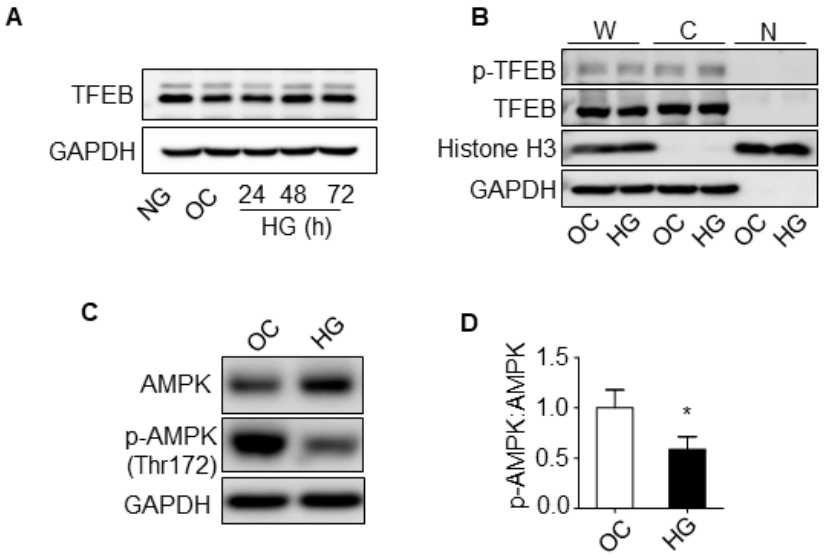

Figure 4.2 High glucose inactivates AMPK but has no effect on TFEB nuclear translocation (**A**) HUVECs were treated with NG, OC, or HG for indicated time, and TFEB expression was measured by western blot. (**B**) HUVECs were treated with OC or HG for 24 h. Cytosol (C) and nuclear (N) fractions were prepared, and TFEB protein levels in the fractions were measured by western blot. (**C**) WT MLECs were treated with OC or HG for 72 h, AMPK and p-AMPK protein levels were measured by western blot. (**D**) Densitometry analysis of p-AMPK protein level. * $p < 0.05$.

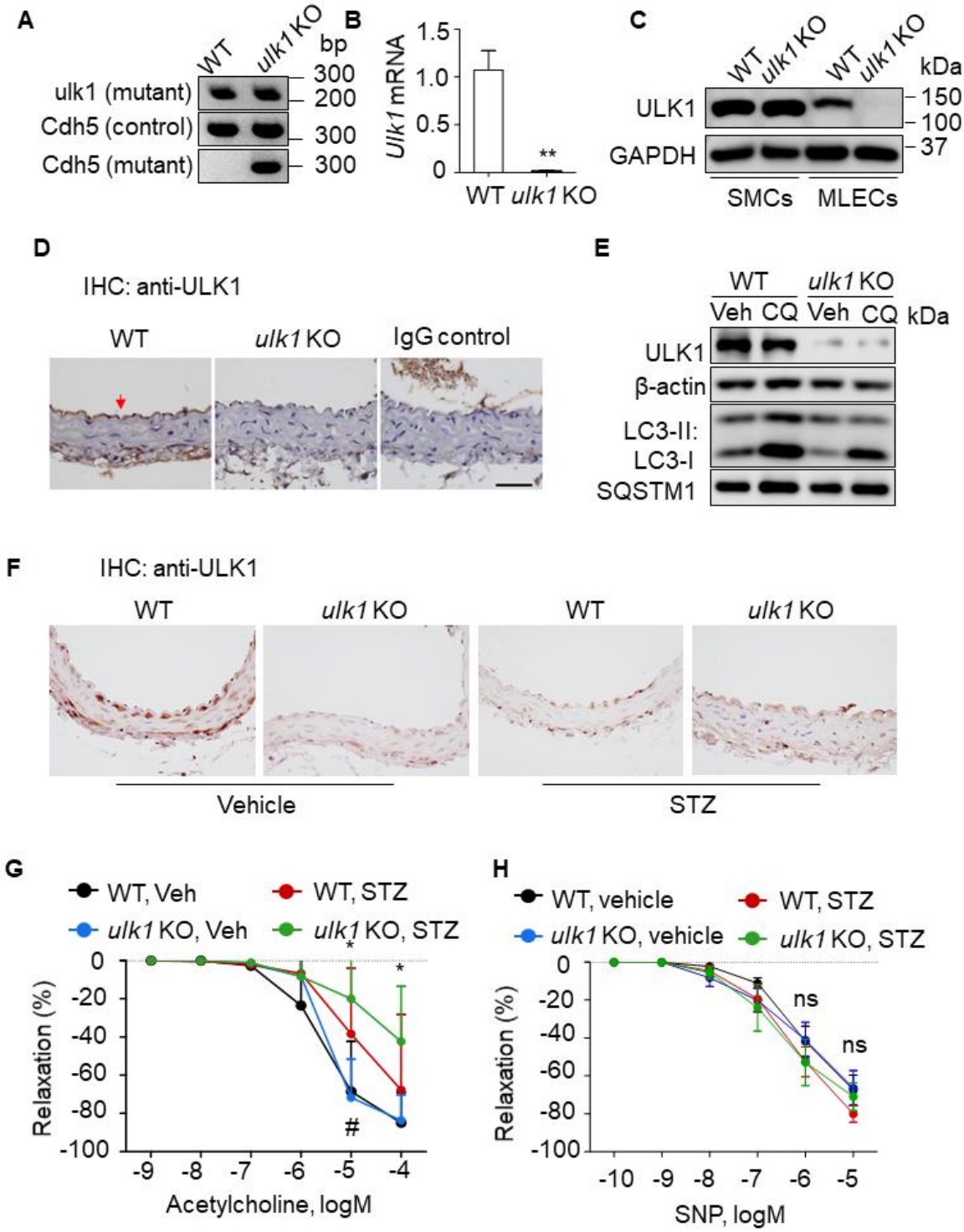

Figure 4.3 Endothelial-specific ulk1 knockout worsens diabetes-induced endothelial dysfunction (**A**) Genotyping of *Ulk1*$^{flox/flox}$ *Cdh5*$^{+}$ (*ulk1* KO) and *Ulk1*$^{flox/flox}$ *Cdh5*$^{-}$ (wild-type; WT) mice. (**B**) *Ulk1* mRNA level was detected by PCR in mouse lung endothelial cells (MLECs) isolated from WT and *ulk1* KO mice. (**C**) Western blot analysis of ULK1 protein expression in vascular smooth muscle cells (VSMCs) and MLECs isolated from WT and *ulk1* KO mice. (**D**) Immunohistochemical staining of ULK1 was performed in mouse aortas collected from WT and

ulk1 KO mice. Scale bar: 50 μm. (**E)** MLECs obtained from WT or *ulk1* KO mice were treated with vehicle (Veh) or chloroquine (CQ; 3 μM) for 16 h. Protein levels of ULK1, SQSTM1, and LC3-I:LC3-II ratio were detected by western blot. (**F**) Aortas were stained with ULK1 antibody in WT and *ulk1* KO mice treated with STZ or vehicle (Veh). (**G-H**) *Ulk1* deficiency exacerbates STZ-induced endothelial dysfunction. WT and *ulk1* KO mice were treated with either vehicle or STZ for 6 months. (**G**) Endothelium-dependent vasodilator responses were measured in the presence of acetylcholine (Ach, 10^{-9} to 10^{-4} M). (**H**) Endothelium-independent vasodilator responses were measured in the presence of sodium nitroprusside (SNP, 10^{-10} to 10^{-5} M) (**H**) N= 4-7. * $P < 0.05$, WT+Veh vs. ulk1 KO+ STZ; # $P < 0.05$, ulk1 KO+Veh vs. ulk1 KO+ STZ.

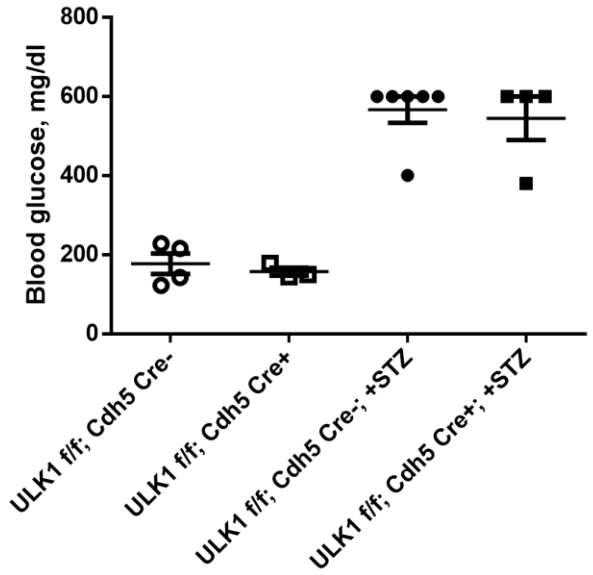

Figure 4.4 Blood glucose level
Fasting blood glucose determination in WT+Veh, *ulk1* KO+Veh, WT+STZ and *ulk1* KO +STZ mice after STZ or Vehicle treatment for 6 months. N = 3-6.

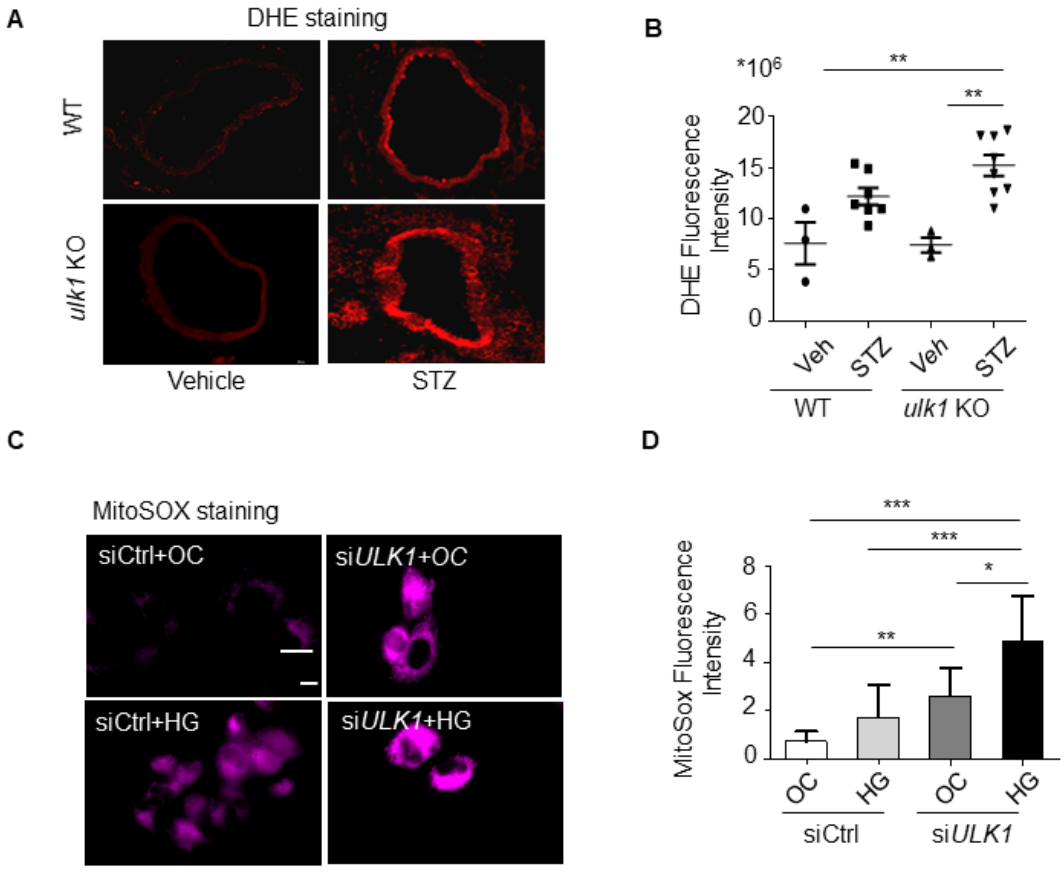

Figure 4.5 Ulk1 deficiency enhances ROS formation in diabetic conditions.
(**A**) DHE staining was performed in aortic tissues isolated from WT and *ulk1* KO mice treated with vehicle or STZ for 6 months. (**B**) Quantitative analysis of DHE fluorescence intensity. N = 3-8, ** $P < 0.01$. (**C**) Mitochondrial ROS production was determined by MitoSOX staining. Scale bar: 1 mm (**D**) Quantitative analysis of MitoSox fluorescence intensity. N = 3-4, * $P < 0.05$, ** $P < 0.01$, *** $P < 0.001$.

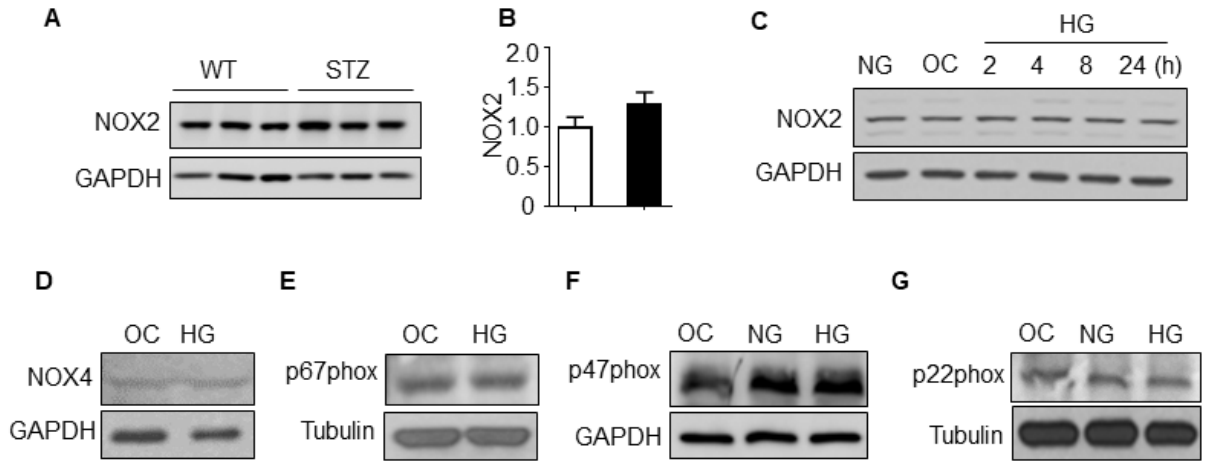

Figure 4.6 High glucose has no effect on NOXs expression.
(A and B) C57BL/6J mice were treated with vehicle (Veh) or STZ for 6 month, NOX2 protein level in aortas was determined by western blot and densitometry. (C) HUVECs were treated with NG, OC, or HG for indicated time, and NOX2 expression was measured by western blot. (D and E) HUVECs were treated with NG, OC, or HG for 24 h, protein levels of NOX4 (D) and p67phox (E) were measured by western blot. (F and G) HUVECs were treated with NG, OC, or HG for 24 h, protein levels of p47phox (F) and p22phox (G) were measured by western blot.

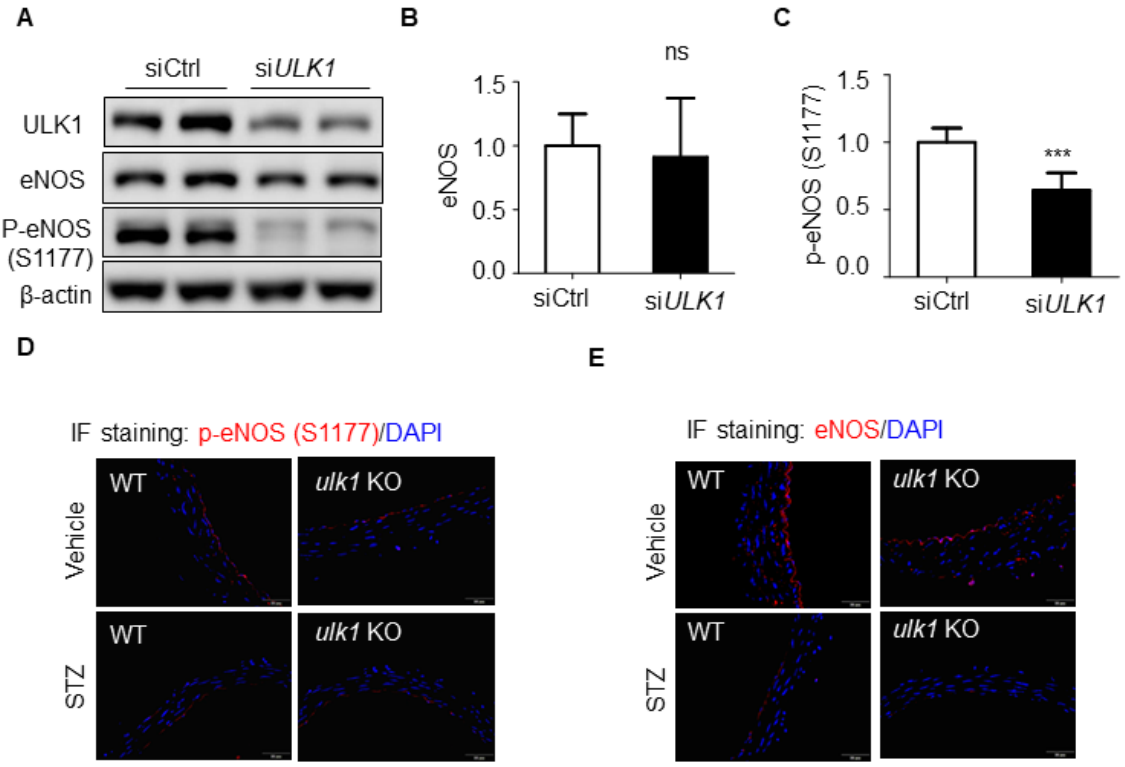

Figure 4.7 ULK1 deficiency inhibits eNOS phosphorylation.
(**A**) HUVECs were transfected with ULK1 siRNA or control siRNA for 48 h, protein levels of ULK1, eNOS, p-eNOS were measured by western blot. (**B** and **C**) Densitometry analysis of A. N = 8-9, ns: not significant， *** $P < 0.0001$. (**D**) Aortas were stained with p-eNOS antibody in WT and *ulk1* KO mice treated with STZ or vehicle (Veh). (**E**) Aortas were stained with eNOS antibody in WT and *ulk1* KO mice treated with STZ or vehicle (Veh).

4.4 Discussion

In the current study, we found that hyperglycemia impaired endothelium-dependent vasorelaxation, which accompanied by reduced autophagy-related protein levels and inhibited autophagic flux. Inhibition of autophagy by deletion of ULK1 worsened hyperglycemia-induced endothelial dysfunction. Mechanistically, the hyperglycemia-induced ROS-overproduction impaired endothelial function, diabetes-reduced ULK1 expression inhibited eNOS phosphorylation. In addition, suppression of autophagy by knocking out ULK1 aggravated ROS

overproduction, and induced a further decrease in eNOS phosphorylation, thereby exacerbating endothelial dysfunction.

Both activation and inhibition of autophagy by hyperglycemia have been reported by different research groups (Niu et al., 2019; Ruart et al., 2019). The controversial results prompted us to determine the effects of hyperglycemia on endothelial autophagy activity. In this study, we determined a wide spectrum of autophagic related proteins in endothelial cells and found that most of them were decreased, the transformation of LC3-II from LC3-I was significantly inhibited, and SQSTM1 protein was accumulated in diabetic conditions. These results convinced us that autophagy was inhibited by HG stimulation. Another important evidence that HG inhibited AMPK phosphorylation at thr172, which inhibited autophagy signaling and suppressed autophagy activity. Since nuclear translocation of TFEB is required for the expression of genes involved in different steps of the autophagy process, we examined if HG affect TEFB protein expression and nuclear translocation. It seems that HG did not affect TFEB expression and subcellular distribution. Our results suggest that HG suppresses autophagy activity via inhibition of AMPK but not TFEB signaling. To understanding the role of deficient autophagy in hyperglycemia-induced endothelial dysfunction, we deleted endothelial *Ulk1* gene to inhibit autophagy and induced diabetes in these mice. Although endothelium-dependent vasorelaxation induced by Ach was not impaired in *ulk1* KO mouse aortas. STZ-induced endothelial dysfunction was more server in STZ-treated *ulk1* KO than STZ-treated WT mice, supporting that defective autophagy is an important event in diabetes-induced endothelial dysfunction.

It is well known that diabetes-induced ROS overproduction is one of the main causes of hyperglycemia-induced endothelial dysfunction. Using DHE staining of aortas, we demonstrated that suppression of autophagy by deletion of ULK1 exacerbated hyperglycemia-induced ROS

generation in STZ-induced diabetic mice. Consistently with that mitochondria are the major source of ROS production, and absence of autophagy cannot efficiently remove dysfunctional mitochondria, leading to ROS overproduction, MitoSox staining showed that HG induced more mitochondrial ROS production in *ULK1*-deficient HUVECs. Notably, HG did not affect the expression of components of NADPH oxidase, including NOX2, NOX4, p22, p47, and p67phox. Our study indicates that autophagy deficiency aggravates diabetes-induced mitochondrial ROS overproduction.

ULK1 is a serine/threonine protein kinase. In addition to its autophagy-related functions, ULK1 also regulates glycolysis by directly phosphorylates several essential glycolytic enzymes (T. Y. Li et al., 2016). In the amino acid/ serum starvation conditions, ULK1/2 phosphorylates and potentiates hexokinase (HK) activity leading to increase in glucose uptake, meanwhile, dampens phosphofructokinase 1 (PFK1), enolase 1(ENO1), and swerves glycolysis to pentose phosphate pathway (PPP) pathway, which also generates reductant, NAPDH, to sustain intracellular homeostasis (T. Y. Li et al., 2016). We provided new evidence suggesting ULK1 may directly phosphorylate eNOS, as silencing ULK1 reduced phosphorylation of eNOS at Ser1172 without affecting eNOS protein expression, deletion of endothelial ULK1 reduced eNOS phosphorylation in ulk1 KO endothelium and induced a further reduction in diabetic *ulk1* KO mice. Thus, further investigations are warranted to characterize the mechanism by which ULK1 influences eNOS activity.

In summary, hyperglycemia inhibits both autophagy activity and eNOS phosphorylation, accompanied by ROS overproduction, which leads to reduction in NO bioavailability and impairment of endothelial dependent vasorelaxation. Importantly, these effects are augments in EC-specific *ulk1* KO mice. Therefore, defective autophagy in an important event in diabetes-

induced endothelial dysfunction. Activation of autophagy and overexpression of ULK1 may be potential strategies to prevent endothelial dysfunction in diabetes.

4.5 Method and Materials

4.5.1 Ulk1 KO mice

Ulk1$^{flox/flox}$ mice in a C57BL/6J background and *Cre*$^{Cdh5+}$ mice were purchased from The Jackson Laboratory (Bar Harbor, ME). The endothelial cell-specific *ulk1* knockout (*ulk1*$^{f/f}$*Cdh5*$^{+}$*; ulk1 KO)*) mice were generated by crossing female *Ulk1*$^{f/f}$*Cdh*$^{5+/-}$ with male *Ulk1*$^{f/f}$*Cdh*$^{5+/-}$ mice. Littermate *Ulk1*$^{f/f}$*Cdh*$^{5-}$ mice were used as wild-type (WT) control. The offspring was genotype by PCR using the primers listed in Table 4.1. All mice were C57BL/6J background, maintained on a 12:12-h light-dark cycle at 25 °C, and given free access to water and food.

Table 4.1 Genotyping primer

Target gene	Primer sequence
Cdh5 Trans FW	AGGCAGCTCACAAAGGAACAAT
Cdh5 Trans RV	TCGTTGCAT CGACCGGTAA
Cdh5 ctrl FW	CTAGGCCACAGAATTGAAAGATCT
Cdh5 ctrl RV	GTAGGTGGAAATTCTAGCATCATCC
Ulk1 WT FW	CAGTTAGGTTCACTGCAGACTTG
Ulk1 WT RV	TTTATCCGTCTTCTGCTATTGG
Ulk1 Mutant FW	CTTGGGTGGAGAGGCTATTC
Ulk1 Mutant RV	AGGTGAGATGACAGGAGATC

4.5.2 Streptozocin (STZ)-induced type 1 diabetic mouse model

Streptozocin (STZ; Sigma Aldrich, S0130-1g) was used to induce diabetic mouse model as previously described (Furman, 2015). The WT and *ulk1* KO mice were received intraperitoneal injections of STZat a dose of 50 mg/kg body weight (BW) for 5 constitutive days. Blood glucose level was measured from a tail-vein blood sample using a One Touch Basic blood glucose monitoring system 28 days after STZ stimulation. Development of diabetes was defined

by blood glucose more than 300 mg/dL 7 days after the first injection of STZ. The animal protocol in this study was approved by the Institutional Animal Care and Use Committee at Georgia State University.

4.5.3 Assays of endothelium-dependent and endothelium-independent vasorelaxation

Vessel bioactivity was assessed by organ chamber as described previously. Thoracic aortic rings (3-4 mm) were prepared and mounted in 5 ml organ baths containing Kreb's solution (118.3 mM NaCl, 4.7 mM KCl, 1.2 mM $MgSO_4$, 1.2 mM KH_2PO_4, 2.5 mM $CaCl_2$, 25 mM $NaHCO_3$, 0.026 mM EDTA, and 11 mM glucose). The organ bath was bubbled with 95% O_2 and 5% CO_2 gases and was maintained at 37°C. Aortic rings were equilibrated in organ bath for 15 min under a tension of 5 mN. Contractile responses of aortic rings were evoked using 30 nM U46619 to obtain reproducible responses. At the plateau of contraction, acetylcholine (1×10^{-8} to 1×10^{-4} mol/L) or SNP (1×10^{-10} to 1×10^{-6} mol/L) was sequentially added according to concentration gradient to the organ bath to induce endothelium-dependent or -independent relaxation, correspondingly. The aortas were rinsed by Kreb's solution for 10 min in each time of reagent change.

4.5.4 Cell culture

HUVECs were obtained from the American Type Culture Collection (PCS-100-010) and grown in EBM medium (Lonza Bioscience, CC-3121), which was supplemented with endothelial cell growth supplement and 5% fetal bovine serum. All culture media were supplemented with penicillin (100 Units/ml) and streptomycin (100 μg/ml). HUVECs were used between passage four to six. Cultured cells were incubated under standard cell culture conditions (37 °C, 20% O_2, 5% CO_2).

Mouse lung endothelial cells (MLECs) were isolated as previously described (Sobczak et al., 2010). Mouse lung was excised and minced with scissors. Tissue was digested by type II collagenase (Worthington Biochemical, LS004177) at 37 °C for 45 min, and followed by aspirating the tissue into a 20 ml syringe with 14 g cannula to get single cell suspension. Lung endothelial cells were purified by anti-PECAM1/CD31 antibody conjugated magnetic beads and anti-ICAM2 antibody conjugated magnetic beads, sequentially. MLECs were grown and maintained in EBM medium (Lonza Bioscience, CC-3121) supplemented with endothelial cell growth supplement (Lonza Bioscience, CC-4133) and 20% fetal bovine serum (Sigma-Aldrich, 12303). MLECs were used between passage two to four. Cultured cells were incubated under standard cell culture conditions (37 °C, 20% O_2, 5% CO_2).

Aortic smooth muscle cell isolation: the mice at 8 to 10 weeks of age were sacrificed, thoracic aortas were dissected, and the adventitia were removed. The vessels were incised longitudinally, and the endothelial cells were gently scraped off. The aortas were then minced into square with side length of 1-2 mm. The aorta pieces were attached to a 60-mm Patri dish coated with FBS for 1 h and then SMCs culture medium, DMEM/F12 (Corning, 10-092-CV) media containing 10% FBS and 1% P/S was added to the attached aorta pieces carefully. After sub-culturing for 3 passages, the cultured cells were verified to be VSMCs by immunostaining with anti-smooth muscle α-actin antibody, followed by counterstaining with Hoechst (Thermo Fisher Scientific, 62249)

4.5.5 Mouse aortic homogenates preparation

Aortas were isolated from WT and *ulk1* KO mice, treated with STZ or vehicle, perivascular connective tissue was cleaned, and cut into small pieces. Aortic tissues were homogenized in RIPA lysis buffer (Santa Cruz Biotechnology, sc-24948A). The protein-rich

supernatant was obtained by centrifugation (12,000×g, 20 min, 4 °C). Protein concentration was determined by bicinchoninic acid protein (BCA) assay kit (Thermo Fisher Scientific, 23225).

4.5.6 Western blot analysis

Proteins were extracted from aortas or cells by using RIPA lysis buffer (Santa Cruz Biotechnology, sc-24948A). Protein content was determined using the BCA assay reagent,30 μg of protein were resolved by SDS-PAGE, transferred to nitrocellulose membranes (Bio-Rad Laboratories, 1620112), and probed with specific antibodies. The signals were visualized using the ECL (ThermoFisher Scientific, 32106) detection system. The intensity of individual bands was measured by ImageJ.

4.5.7 Assessment of ROS production in vivo

Fresh aorta was immersed in tissue freezing medium (O.C.T compound; VWR, 25608-930), snap frozen in liquid nitrogen. Frozen sections (8 □m) was incubated in PBS containing 5 □M dihydroethidium (DHE) in a light-protected humidified chamber at 37°C for 30 min. Sections were then observed under an Olympus BX-51 fluorescence microscope using the same imaging settings in each experimental condition. Superoxide production was evaluated by fluorescence intensity at Ex 470 and Em 580 nm.

4.5.8 Detection of mitochondrial ROS production in HUVECs

HUVECs were subjected to corresponding treatment and then incubated with 0.5 μM MitoSox (Thermo Fisher Scientific, M36008) for 30 min. Cells were washed with sterilized PBS solution (Millipore Sigma, D5652-50L) 3 times, and changed to normal culture medium. The pictures were taken by inverted fluorescence microscope (Olympus IX73, Tokyo, Japan).

4.5.9 SiRNA transfection

HUVECs were transfected with *ULK1* siRNA, or control siRNA in OPTI-MEM reduced-

serum media using Lipofectamine RNAiMax transfection reagent (ThermoFisher Scientific, 13778150) for 48 h. The transfection efficiency of the siRNAs was determined by western blot analysis of target protein expression.

4.5.10 Immunohistochemistry and immunofluorescence staining

Aorta was isolated, fixed in 4% paraformaldehyde, embedded in paraffin, and cut into 4-μm sections. The sections were deparaffinized, rehydrated, and heated in citrate buffer to unmask the antigens. Aortic sections were incubated with primary antibodies against ULK1 overnight at 4 °C. After rinsing with PBS 3 times, sections were incubated with a horseradish peroxidase-labeled polymer detection system (DAKO EnvisionCDual link, K4061) and stained with DAB chromogen (DAKO, K3468).

Immunofluorescence staining was performed as previously described. Freshly dissected mouse aortic tissues were embedded in Tissue-Tek OCT Compound and frozen in -80 °C. The aortic segments were cut into 8μM. The section was immersed in -20 °C acetone for 15 min and washed with PBS 3 times, and the sections were incubated with corresponding primary antibody at 4°C, overnight. Then incubated with fluorescent secondary antibody for 1 h at room temperature, and mounted with DAPI (Sigma-Aldrich, D9564). Images were recorded using an Olympus fluorescence microscope (Olympus BX53, Tokyo, Japan) and quantified using Image-Pro Plus 6.0 (Media Cybernetics, Rockville, MD).

4.5.11 Data analysis

Data were expressed as mean ± standard deviation (SD). One- or two-way ANOVA was used to determine the differences among three or more groups, followed by Bonferroni's post-hoc analysis using GraphPad Prism 9 software (GraphPad Software, Inc., La Jolla, CA).

The Student's t test was used to compare the means between two groups. $P < 0.05$ was considered statistically significant.

5 DISCUSSION

Our findings, for the first time, revealed that lack of ATG7 inhibited ischemia-induced angiogenesis by suppression of HIF1A expression, identified STAT1 as a suppressor of *HIF1A* expression by binding to *HIF1A* promoter to inhibit *HIF1A* transcription, thereby preventing angiogenesis, and demonstrated that ATG7 regulated STAT1 expression in an autophagy-independent manner, instead ATG7 associated with ZNF148/ZBP-89, the constitutive transcriptional factor of STAT1, to prevent its nuclear translocation. In the absence of ATG7, ZNF148/ZBP-89 was released from the ATG7-ZNF148/ZBP-89 complex and associated with KPNB1, which transported ZNF148/ZBP-89 into the nucleus, where it bond to the *STAT1* gene promoter, upregulating *STAT1* expression. We propose that normalizing ATG7 to potentiate angiogenesis may prevent ischemic heart disease and peripheral artery disease, while inhibiting ATG7 may have therapeutic effect on tumorigenesis and metastasis.

We also showed hyperglycemia or high glucose treatment inhibited autophagic activity in ECs. Inhibition of endothelial autophagy by deletion of *ULK1* exacerbated endothelial dysfunction by reducing NO production and enhancing ROS production. In addition, eNOS phosphorylation was significant inhibited in ULK1-deficient conditions. We also determined that mitochondria was the prominent sources of ROS.

5.1 Defective angiogenesis and angiogenesis therapy: from the view of autophagy

Uncontrolled angiogenesis is essential for the progression of tumor and retinopathies, while inadequate angiogenesis is critical for the development of cardiovascular disease. The precise role of autophagy in angiogenesis under various conditions may be opposite. Autophagy occurring at basal levels recycles cellular nutrients during stress conditions and promotes cell

survival. Disruption of this process prevents cell survival in diverse organisms (Allen & Baehrecke, 2020; Das, Shravage, & Baehrecke, 2012). However, autophagy also promotes cell death in some circumstances. Inhibition of autophagy by administration of either 3-MA or *ATG5* siRNA prevents angiogenesis in aortic ECs, whereas derivate of natural product magnolol (Ery5), a potent autophagy activator, also functions as an anti-angiogenesis factor; additionally, gold nanoparticles inhibit retinal angiogenesis by activating autophagy (Shen et al., 2018). The elevated autophagy causes type-II programmed cell death and tumor vasculature shrink (Kumar et al., 2013). Thus, inhibition of autophagy has potential therapeutic effects on cancer in combined with anti-angiogenesis reagents. However, a recent study shows that inhibition of autophagy by either genetic deletion of ATG5 or chloroquine treatment has different effects on tumor growth and angiogenesis (Du et al., 2012; Schaaf et al., 2019). It seems that different approaches to modulate autophagy might generate distinct effects on angiogenesis. Thus, caution will be required when interpreting the results from studies that report the association between manipulation of autophagy activity and angiogenesis.

Temporal function of autophagy in regulating angiogenesis should also be considered because there might be a biphasic response in autophagy dysregulation in some pathological conditions. Recently, a study assessing the effects of autophagy activation on cardiac function in mouse model of anthracycline-induced cardiotoxicity (AIC) demonstrates that ATG7-based autophagy activation improves cardiac function in late stage but has detrimental effect in the earlier stage of AIC (Y. Wang et al., 2021). Furthermore, during the tumor development, in the earlier stages, autophagy promotes tumorigenesis by serving as a facilitator of nutrient recycling and remobilization, but in the later stages, autophagy functions as tumor suppressor by removing

damaged organelle and limiting cell growth (Kardideh, Samimi, Norooznezhad, Kiani, & Mansouri, 2019).

In the present study, we found that in normoxic conditions, loss of *Atg7* downregulates HIF1A expression, thereby inhibiting cell migration and preventing angiogenesis although it has no effect on HIF2A expression. However, deficiency of autophagy related factor, beclin 1, enhances hypoxia-induced angiogenesis by increase HIF2A and erythropoietin expression. Moreover, in basal condition, deficiency of beclin 1 has no significant impact on cell migration and proliferation (S. J. Lee, Kim, Jin, Choi, & Ryter, 2011), which are different from our findings. It might be due to these two autophagic proteins regulate HIFs expression through different signaling pathways. Several Studies have shown that autophagy can promote angiogenesis, for example, autophagy is activated during the recovery of heat-denatured endothelial cells, which is required for angiogenesis. However, ATG7 deficiency promotes wounded skin healing but has no significant impact on angiogenesis, this result suggests that ATG7 possesses autophagy- independent functions, in addition to regulation of autophagosome formation (K. C. Li et al., 2020). Notably, we found that *atg7* overexpression did not promote angiogenesis nor HIF1A expression, concurrently, there were no significant changes in STAT1 protein expression and phosphorylation. It seems that overexpress ATG7 may be potential strategy to restore angiogenesis to normal level in ATG7-deficient diseases without inducing excessive vessel formation (Baselli et al., 2022; Collier, Guissart, et al., 2021; Collier, Olahova, McWilliams, & Taylor, 2021).

Our study demonstrates that ATG7 deficiency-induced STAT1 expression suppresses HIF1A expression, but we cannot exclude that it may also activate other signaling pathways, such as immune response, as STAT1 is a key transcription factor in IFNγ signaling, which is

involved in multiple immune system functions. Thus, our findings suggest a link between autophagic proteins and immune response, and the deficiency of ATG7 in some pathological conditions may provoke immune response.

ECs in tumor site are exposed to a pro-angiogenesis environment that contains high levels of VEGF, nutrient deficiency, and hypoxia. This environment promotes ECs to release matrix metalloproteinases that enhance angiogenesis by degradation of the vascular basement membrane and remodeling of extracellular matrix. Most transcriptional responses to oxygen deficiency in tumor site are mediated by HIFs (hypoxia inducible factors) that control the expression of numerous angiogenic, metabolic, and cell cycle genes (Ke & Costa, 2006; Pugh & Ratcliffe, 2003). Thus, upregulation of HIF-1 appears to be an essential mechanism-mediated resistance to anti-angiogenic therapy (H. Xu et al., 2015). HIF1A can promote the generation of angiogenic factors to escape the anti-angiogenesis treatment by specifically targeting VEGF (Blagosklonny, 2004). HIF1A not only leads to tumor cells resistant to radiation and chemotherapy, but also increases the chances of tumor cells invasion and metastasis and contributes to poor prognosis (Ebos et al., 2009; Paez-Ribes et al., 2009).

Generally, autophagy is considered as protective mechanism under hypoxic conditions and has a high correlation with chemotherapy resistance, for example, genetic or pharmacological inhibition of autophagy sensitizes anti-angiogenic therapy in glioblastoma xenografts (Hu et al., 2012). Thus, the efficacy of inhibition of ATG7 in preventing anti-angiogenesis therapy resistance is worth further investigation.

Our results also suggest that overexpression of ATG7 may have prospective therapeutic utilization in ischemic diseases, as our results show that enhancing ATG7 expression has no significant impact on STAT1 expression and does not induce extra HIF1A expression, which can

prevent the over neovascularization as reported in HIF1A gene treatment in ischemic disease. Nevertheless, the effect of overexpression ATG7 on angiogenesis in ATG7-deficit condition warrants further investigation.

5.2 Prevention of diabetes-induced endothelial dysfunction: from the view of autophagy

NO bioavailability has high correlation with endothelial function, while ROS overproduction induces eNOS uncoupling, leading to reduction in NO bioavailability, and has detrimental effects on endothelial homeostasis. Autophagy is a major process in maintaining cellular homeostasis, and is necessary to maintain redox homeostasis. However, the exact mechanism by which autophagy regulates endothelial function in diabetic conditions remains elusive. It has been reported that autophagy facilitates removal of damaged mitochondria and reduces ROS production (W. Wu et al., 2015). The activation of autophagy by curcumin in ECs protects endothelial cells from the oxidative damage (Han et al., 2012). Glycolytic inhibitor or H_2O_2 induces ROS production, which in turn activates autophagic pathway to protect against those stress stimuli and increase EC viability (Q. Wang, Liang, Shirwany, & Zou, 2011). However, the effects of autophagy regulating NO bioavailability seems controversial. Impairment of autophagy by silencing Atg3 in endothelial cells inhibits shear-stress-induced increases in eNOS phosphorylation and nitric oxide bioavailability. Whereas in the HUVEC cultured in the medium without serum, the inhibition of autophagy by chloroquine restores NO production, reduces superoxide generation, and promotes EC proliferation (Bharath et al., 2014; Pestana, Oishi, Salistre-Araujo, & Rodrigues, 2015). Our study shows that diabetes reduces the expression of ATG proteins, including ULK1, a serine/threonine-specific protein kinase, and demonstrates that ULK1 deficiency inhibits eNOS phosphorylation at Ser1177 to prevent its

activation in diabetic conditions. However, further study is needs to determine whether ULK1 directly phosphorylates eNOS and enhances NO bioavailability.

To date, our understanding about the role of autophagy in vascular biology is relatively limited. This catabolic intracellular process seems to be involved in both protecting and injuring ECs in response to various stimuli. For example, laminar shear stress promotes autophagy in ECs by activating Sirt1 and FoxO1, which induces autophagic genes expression to prevent oxidant-induced endothelial damage (Liu et al., 2015). The elevated autophagy also suppresses high glucose-induced senescence and apoptosis in ECs (F. Chen et al., 2014). Conversely, uncontrolled activation of endothelial autophagy promotes the development of CVD. We find that high glucose undermines autophagy and impairs endothelial function and overexpression ULK1 prevents NO deficiency in response to hyperglycemia and oxidative stress. Taken together, modulating autophagy represents an attractive therapeutic target for treating CVD.

6 REFERENCES

Alderton, W. K., Cooper, C. E., & Knowles, R. G. (2001). Nitric oxide synthases: structure, function and inhibition. *Biochem J, 357*(Pt 3), 593-615. doi:10.1042/0264-6021:3570593

Allen, E. A., & Baehrecke, E. H. (2020). Autophagy in animal development. *Cell Death Differ, 27*(3), 903-918. doi:10.1038/s41418-020-0497-0

Almourani, R., Chinnakotla, B., Patel, R., Kurukulasuriya, L. R., & Sowers, J. (2019). Diabetes and Cardiovascular Disease: an Update. *Curr Diab Rep, 19*(12), 161. doi:10.1007/s11892-019-1239-x

Alp, N. J., & Channon, K. M. (2004). Regulation of endothelial nitric oxide synthase by tetrahydrobiopterin in vascular disease. *Arterioscler Thromb Vasc Biol, 24*(3), 413-420. doi:10.1161/01.ATV.0000110785.96039.f6

Ambjorn, M., Ejlerskov, P., Liu, Y., Lees, M., Jaattela, M., & Issazadeh-Navikas, S. (2013). IFNB1/interferon-beta-induced autophagy in MCF-7 breast cancer cells counteracts its proapoptotic function. *Autophagy, 9*(3), 287-302. doi:10.4161/auto.22831

Antonucci, L., Fagman, J. B., Kim, J. Y., Todoric, J., Gukovsky, I., Mackey, M., . . . Karin, M. (2015). Basal autophagy maintains pancreatic acinar cell homeostasis and protein synthesis and prevents ER stress. *Proc Natl Acad Sci U S A, 112*(45), E6166-6174. doi:10.1073/pnas.1519384112

Arany, Z., Foo, S. Y., Ma, Y., Ruas, J. L., Bommi-Reddy, A., Girnun, G., . . . Spiegelman, B. M. (2008). HIF-independent regulation of VEGF and angiogenesis by the transcriptional coactivator PGC-1alpha. *Nature, 451*(7181), 1008-1012. doi:10.1038/nature06613

Avraamides, C. J., Garmy-Susini, B., & Varner, J. A. (2008). Integrins in angiogenesis and lymphangiogenesis. *Nat Rev Cancer, 8*(8), 604-617. doi:10.1038/nrc2353

Bai, L., & Merchant, J. L. (2001). ZBP-89 promotes growth arrest through stabilization of p53. *Mol Cell Biol, 21*(14), 4670-4683. doi:10.1128/MCB.21.14.4670-4683.2001

Bai, L., & Merchant, J. L. (2003). Transcription factor ZBP-89 is required for STAT1 constitutive expression. *Nucleic Acids Res, 31*(24), 7264-7270. doi:10.1093/nar/gkg929

Baker, M., Robinson, S. D., Lechertier, T., Barber, P. R., Tavora, B., D'Amico, G., . . . Hodivala-Dilke, K. (2011). Use of the mouse aortic ring assay to study angiogenesis. *Nat Protoc, 7*(1), 89-104. doi:10.1038/nprot.2011.435

Bala, S., & Szabo, G. (2018). TFEB, a master regulator of lysosome biogenesis and autophagy, is a new player in alcoholic liver disease. *Dig Med Res, 1*. doi:10.21037/dmr.2018.09.03

Bartoszewska, S., Kochan, K., Piotrowski, A., Kamysz, W., Ochocka, R. J., Collawn, J. F., & Bartoszewski, R. (2015). The hypoxia-inducible miR-429 regulates hypoxia-inducible factor-1alpha expression in human endothelial cells through a negative feedback loop. *FASEB J, 29*(4), 1467-1479. doi:10.1096/fj.14-267054

Baselli, G. A., Jamialahmadi, O., Pelusi, S., Ciociola, E., Malvestiti, F., Saracino, M., . . . Investigators, E. S. (2022). Rare ATG7 genetic variants predispose patients to severe fatty liver disease. *J Hepatol, 77*(3), 596-606. doi:10.1016/j.jhep.2022.03.031

Bedard, K., & Krause, K. H. (2007). The NOX family of ROS-generating NADPH oxidases: physiology and pathophysiology. *Physiol Rev, 87*(1), 245-313. doi:10.1152/physrev.00044.2005

Benjamin, E. J., Blaha, M. J., Chiuve, S. E., Cushman, M., Das, S. R., Deo, R., . . . Stroke Statistics, S. (2017). Heart Disease and Stroke Statistics-2017 Update: A Report From the

American Heart Association. *Circulation, 135*(10), e146-e603. doi:10.1161/CIR.0000000000000485

Bharath, L. P., Cho, J. M., Park, S. K., Ruan, T., Li, Y., Mueller, R., . . . Symons, J. D. (2017). Endothelial Cell Autophagy Maintains Shear Stress-Induced Nitric Oxide Generation via Glycolysis-Dependent Purinergic Signaling to Endothelial Nitric Oxide Synthase. *Arterioscler Thromb Vasc Biol, 37*(9), 1646-1656. doi:10.1161/ATVBAHA.117.309510

Bharath, L. P., Mueller, R., Li, Y., Ruan, T., Kunz, D., Goodrich, R., . . . Symons, J. D. (2014). Impairment of autophagy in endothelial cells prevents shear-stress-induced increases in nitric oxide bioavailability. *Can J Physiol Pharmacol, 92*(7), 605-612. doi:10.1139/cjpp-2014-0017

Blagosklonny, M. V. (2004). Antiangiogenic therapy and tumor progression. *Cancer Cell, 5*(1), 13-17. doi:10.1016/s1535-6108(03)00336-2

Burri, P. H., Hlushchuk, R., & Djonov, V. (2004). Intussusceptive angiogenesis: its emergence, its characteristics, and its significance. *Dev Dyn, 231*(3), 474-488. doi:10.1002/dvdy.20184

Cadwell, K., & Debnath, J. (2018). Beyond self-eating: The control of nonautophagic functions and signaling pathways by autophagy-related proteins. *J Cell Biol, 217*(3), 813-822. doi:10.1083/jcb.201706157

Cai, S., Khoo, J., Mussa, S., Alp, N. J., & Channon, K. M. (2005). Endothelial nitric oxide synthase dysfunction in diabetic mice: importance of tetrahydrobiopterin in eNOS dimerisation. *Diabetologia, 48*(9), 1933-1940. doi:10.1007/s00125-005-1857-5

Cao, Y., & Cao, R. (1999). Angiogenesis inhibited by drinking tea. *Nature, 398*(6726), 381. doi:10.1038/18793

Carmeliet, P., & Jain, R. K. (2011). Molecular mechanisms and clinical applications of angiogenesis. *Nature, 473*(7347), 298-307. doi:10.1038/nature10144

Chamboredon, S., Ciais, D., Desroches-Castan, A., Savi, P., Bono, F., Feige, J. J., & Cherradi, N. (2011). Hypoxia-inducible factor-1alpha mRNA: a new target for destabilization by tristetraprolin in endothelial cells. *Mol Biol Cell, 22*(18), 3366-3378. doi:10.1091/mbc.E10-07-0617

Chang, Y. P., Tsai, C. C., Huang, W. C., Wang, C. Y., Chen, C. L., Lin, Y. S., . . . Lin, C. F. (2010). Autophagy facilitates IFN-gamma-induced Jak2-STAT1 activation and cellular inflammation. *J Biol Chem, 285*(37), 28715-28722. doi:10.1074/jbc.M110.133355

Cheang, W. S., Wong, W. T., Tian, X. Y., Yang, Q., Lee, H. K., He, G. W., . . . Huang, Y. (2011). Endothelial nitric oxide synthase enhancer reduces oxidative stress and restores endothelial function in db/db mice. *Cardiovasc Res, 92*(2), 267-275. doi:10.1093/cvr/cvr233

Chen, F., Chen, B., Xiao, F. Q., Wu, Y. T., Wang, R. H., Sun, Z. W., . . . Hu, S. J. (2014). Autophagy protects against senescence and apoptosis via the RAS-mitochondria in high-glucose-induced endothelial cells. *Cell Physiol Biochem, 33*(4), 1058-1074. doi:10.1159/000358676

Chen, J., Stimpson, S. E., Fernandez-Bueno, G. A., & Mathews, C. E. (2018). Mitochondrial Reactive Oxygen Species and Type 1 Diabetes. *Antioxid Redox Signal, 29*(14), 1361-1372. doi:10.1089/ars.2017.7346

Chen, L., & Hao, G. (2020). The role of angiotensin-converting enzyme 2 in coronaviruses/influenza viruses and cardiovascular disease. *Cardiovasc Res, 116*(12), 1932-1936. doi:10.1093/cvr/cvaa093

Cheng, Y., Ren, X., Hait, W. N., & Yang, J. M. (2013). Therapeutic targeting of autophagy in disease: biology and pharmacology. *Pharmacol Rev, 65*(4), 1162-1197. doi:10.1124/pr.112.007120

Cheung, B. M., & Li, C. (2012). Diabetes and hypertension: is there a common metabolic pathway? *Curr Atheroscler Rep, 14*(2), 160-166. doi:10.1007/s11883-012-0227-2

Cho, C. F., Chen, P. K., Chang, P. C., Wu, H. L., & Shi, G. Y. (2013). Human plasminogen kringle 1-5 inhibits angiogenesis and induces thrombomodulin degradation in a protein kinase A-dependent manner. *J Mol Cell Cardiol, 63*, 79-88. doi:10.1016/j.yjmcc.2013.07.009

Ciafre, S. A., Niola, F., Giorda, E., Farace, M. G., & Caporossi, D. (2007). CoCl(2)-simulated hypoxia in skeletal muscle cell lines: Role of free radicals in gene up-regulation and induction of apoptosis. *Free Radic Res, 41*(4), 391-401. doi:10.1080/10715760601096799

Collier, J. J., Guissart, C., Olahova, M., Sasorith, S., Piron-Prunier, F., Suomi, F., . . . Taylor, R. W. (2021). Developmental Consequences of Defective ATG7-Mediated Autophagy in Humans. *N Engl J Med, 384*(25), 2406-2417. doi:10.1056/NEJMoa1915722

Collier, J. J., Olahova, M., McWilliams, T. G., & Taylor, R. W. (2021). ATG7 safeguards human neural integrity. *Autophagy, 17*(9), 2651-2653. doi:10.1080/15548627.2021.1953267

Cuervo, A. M., & Macian, F. (2012). Autophagy, nutrition and immunology. *Mol Aspects Med, 33*(1), 2-13. doi:10.1016/j.mam.2011.09.001

Dai, M., Cui, P., Yu, M., Han, J., Li, H., & Xiu, R. (2008). Melatonin modulates the expression of VEGF and HIF-1 alpha induced by CoCl2 in cultured cancer cells. *J Pineal Res, 44*(2), 121-126. doi:10.1111/j.1600-079X.2007.00498.x

Daiber, A., Xia, N., Steven, S., Oelze, M., Hanf, A., Kroller-Schon, S., . . . Li, H. (2019). New Therapeutic Implications of Endothelial Nitric Oxide Synthase (eNOS) Function/Dysfunction in Cardiovascular Disease. *Int J Mol Sci, 20*(1). doi:10.3390/ijms20010187

Das, G., Shravage, B. V., & Baehrecke, E. H. (2012). Regulation and function of autophagy during cell survival and cell death. *Cold Spring Harb Perspect Biol, 4*(6). doi:10.1101/cshperspect.a008813

De Bock, K., Georgiadou, M., Schoors, S., Kuchnio, A., Wong, B. W., Cantelmo, A. R., . . . Carmeliet, P. (2013). Role of PFKFB3-driven glycolysis in vessel sprouting. *Cell, 154*(3), 651-663. doi:10.1016/j.cell.2013.06.037

De Vriese, A. S., Verbeuren, T. J., Van de Voorde, J., Lameire, N. H., & Vanhoutte, P. M. (2000). Endothelial dysfunction in diabetes. *Br J Pharmacol, 130*(5), 963-974. doi:10.1038/sj.bjp.0703393

Deanfield, J. E., Halcox, J. P., & Rabelink, T. J. (2007). Endothelial function and dysfunction: testing and clinical relevance. *Circulation, 115*(10), 1285-1295. doi:10.1161/CIRCULATIONAHA.106.652859

Denton, D., Nicolson, S., & Kumar, S. (2012). Cell death by autophagy: facts and apparent artefacts. *Cell Death Differ, 19*(1), 87-95. doi:10.1038/cdd.2011.146

Dimmeler, S., & Zeiher, A. M. (2000). Endothelial cell apoptosis in angiogenesis and vessel regression. *Circ Res, 87*(6), 434-439. doi:10.1161/01.res.87.6.434

Dong, Y., Chen, H., Gao, J., Liu, Y., Li, J., & Wang, J. (2019). Molecular machinery and interplay of apoptosis and autophagy in coronary heart disease. *J Mol Cell Cardiol, 136*, 27-41. doi:10.1016/j.yjmcc.2019.09.001

Drummond, G. R., & Sobey, C. G. (2014). Endothelial NADPH oxidases: which NOX to target in vascular disease? *Trends Endocrinol Metab, 25*(9), 452-463. doi:10.1016/j.tem.2014.06.012

Du, J., Teng, R. J., Guan, T., Eis, A., Kaul, S., Konduri, G. G., & Shi, Y. (2012). Role of autophagy in angiogenesis in aortic endothelial cells. *Am J Physiol Cell Physiol, 302*(2), C383-391. doi:10.1152/ajpcell.00164.2011

Dumitrescu, C., Biondi, R., Xia, Y., Cardounel, A. J., Druhan, L. J., Ambrosio, G., & Zweier, J. L. (2007). Myocardial ischemia results in tetrahydrobiopterin (BH4) oxidation with impaired endothelial function ameliorated by BH4. *Proc Natl Acad Sci U S A, 104*(38), 15081-15086. doi:10.1073/pnas.0702986104

Ebos, J. M., Lee, C. R., Cruz-Munoz, W., Bjarnason, G. A., Christensen, J. G., & Kerbel, R. S. (2009). Accelerated metastasis after short-term treatment with a potent inhibitor of tumor angiogenesis. *Cancer Cell, 15*(3), 232-239. doi:10.1016/j.ccr.2009.01.021

Egan, D., Kim, J., Shaw, R. J., & Guan, K. L. (2011). The autophagy initiating kinase ULK1 is regulated via opposing phosphorylation by AMPK and mTOR. *Autophagy, 7*(6), 643-644. doi:10.4161/auto.7.6.15123

Egan, D. F., Shackelford, D. B., Mihaylova, M. M., Gelino, S., Kohnz, R. A., Mair, W., . . . Shaw, R. J. (2011). Phosphorylation of ULK1 (hATG1) by AMP-activated protein kinase connects energy sensing to mitophagy. *Science, 331*(6016), 456-461. doi:10.1126/science.1196371

Elshabrawy, H. A., Chen, Z., Volin, M. V., Ravella, S., Virupannavar, S., & Shahrara, S. (2015). The pathogenic role of angiogenesis in rheumatoid arthritis. *Angiogenesis, 18*(4), 433-448. doi:10.1007/s10456-015-9477-2

Ferrara, N., Hillan, K. J., Gerber, H. P., & Novotny, W. (2004). Discovery and development of bevacizumab, an anti-VEGF antibody for treating cancer. *Nat Rev Drug Discov, 3*(5), 391-400. doi:10.1038/nrd1381

Fetterman, J. L., Holbrook, M., Flint, N., Feng, B., Breton-Romero, R., Linder, E. A., . . . Vita, J. A. (2016). Restoration of autophagy in endothelial cells from patients with diabetes mellitus improves nitric oxide signaling. *Atherosclerosis, 247*, 207-217. doi:10.1016/j.atherosclerosis.2016.01.043

Folkman, J. (1995). Angiogenesis in cancer, vascular, rheumatoid and other disease. *Nat Med, 1*(1), 27-31. doi:10.1038/nm0195-27

Furman, B. L. (2015). Streptozotocin-Induced Diabetic Models in Mice and Rats. *Curr Protoc Pharmacol, 70*, 5 47 41-45 47 20. doi:10.1002/0471141755.ph0547s70

Galban, S., & Gorospe, M. (2009). Factors interacting with HIF-1alpha mRNA: novel therapeutic targets. *Curr Pharm Des, 15*(33), 3853-3860. doi:10.2174/138161209789649376

Galie, P. A., Nguyen, D. H., Choi, C. K., Cohen, D. M., Janmey, P. A., & Chen, C. S. (2014). Fluid shear stress threshold regulates angiogenic sprouting. *Proc Natl Acad Sci U S A, 111*(22), 7968-7973. doi:10.1073/pnas.1310842111

Galluzzi, L., & Green, D. R. (2019). Autophagy-Independent Functions of the Autophagy Machinery. *Cell, 177*(7), 1682-1699. doi:10.1016/j.cell.2019.05.026

Gerber, S. A., & Pober, J. S. (2008). IFN-alpha induces transcription of hypoxia-inducible factor-1alpha to inhibit proliferation of human endothelial cells. *J Immunol, 181*(2), 1052-1062. doi:10.4049/jimmunol.181.2.1052

Glick, D., Barth, S., & Macleod, K. F. (2010). Autophagy: cellular and molecular mechanisms. *J Pathol, 221*(1), 3-12. doi:10.1002/path.2697

Goodwin, J. M., Dowdle, W. E., DeJesus, R., Wang, Z., Bergman, P., Kobylarz, M., . . . Murphy, L. O. (2017). Autophagy-Independent Lysosomal Targeting Regulated by ULK1/2-FIP200 and ATG9. *Cell Rep, 20*(10), 2341-2356. doi:10.1016/j.celrep.2017.08.034

Gorina, R., Petegnief, V., Chamorro, A., & Planas, A. M. (2005). AG490 prevents cell death after exposure of rat astrocytes to hydrogen peroxide or proinflammatory cytokines: involvement of the Jak2/STAT pathway. *J Neurochem, 92*(3), 505-518. doi:10.1111/j.1471-4159.2004.02878.x

Gorina, R., Sanfeliu, C., Galito, A., Messeguer, A., & Planas, A. M. (2007). Exposure of glia to pro-oxidant agents revealed selective Stat1 activation by H2O2 and Jak2-independent antioxidant features of the Jak2 inhibitor AG490. *Glia, 55*(13), 1313-1324. doi:10.1002/glia.20542

Gorski, T., & De Bock, K. (2019). Metabolic regulation of exercise-induced angiogenesis. *Vasc Biol, 1*(1), H1-H8. doi:10.1530/VB-19-0008

Grover-Paez, F., & Zavalza-Gomez, A. B. (2009). Endothelial dysfunction and cardiovascular risk factors. *Diabetes Res Clin Pract, 84*(1), 1-10. doi:10.1016/j.diabres.2008.12.013

Guo, F., Li, X., Peng, J., Tang, Y., Yang, Q., Liu, L., . . . Wang, G. X. (2014). Autophagy regulates vascular endothelial cell eNOS and ET-1 expression induced by laminar shear stress in an ex vivo perfused system. *Ann Biomed Eng, 42*(9), 1978-1988. doi:10.1007/s10439-014-1033-5

Haffner, S. M. (2006). Relationship of metabolic risk factors and development of cardiovascular disease and diabetes. *Obesity (Silver Spring), 14 Suppl 3*, 121S-127S. doi:10.1038/oby.2006.291

Hamacher-Brady, A., Brady, N. R., Logue, S. E., Sayen, M. R., Jinno, M., Kirshenbaum, L. A., . . . Gustafsson, A. B. (2007). Response to myocardial ischemia/reperfusion injury involves Bnip3 and autophagy. *Cell Death Differ, 14*(1), 146-157. doi:10.1038/sj.cdd.4401936

Han, J., Hou, W., Goldstein, L. A., Stolz, D. B., Watkins, S. C., & Rabinowich, H. (2014). A Complex between Atg7 and Caspase-9: A NOVEL MECHANISM OF CROSS-REGULATION BETWEEN AUTOPHAGY AND APOPTOSIS. *J Biol Chem, 289*(10), 6485-6497. doi:10.1074/jbc.M113.536854

Han, J., Pan, X. Y., Xu, Y., Xiao, Y., An, Y., Tie, L., . . . Li, X. J. (2012). Curcumin induces autophagy to protect vascular endothelial cell survival from oxidative stress damage. *Autophagy, 8*(5), 812-825. doi:10.4161/auto.19471

Hanahan, D., & Folkman, J. (1996). Patterns and emerging mechanisms of the angiogenic switch during tumorigenesis. *Cell, 86*(3), 353-364. doi:10.1016/s0092-8674(00)80108-7

Hanna, A., & Frangogiannis, N. G. (2019). The Role of the TGF-beta Superfamily in Myocardial Infarction. *Front Cardiovasc Med, 6*, 140. doi:10.3389/fcvm.2019.00140

Hartnett, M. E. (2014). Vascular endothelial growth factor antagonist therapy for retinopathy of prematurity. *Clin Perinatol, 41*(4), 925-943. doi:10.1016/j.clp.2014.08.011

He, C., & Klionsky, D. J. (2009). Regulation mechanisms and signaling pathways of autophagy. *Annu Rev Genet, 43*, 67-93. doi:10.1146/annurev-genet-102808-114910

He, C., Li, H., Viollet, B., Zou, M. H., & Xie, Z. (2015). AMPK Suppresses Vascular Inflammation In Vivo by Inhibiting Signal Transducer and Activator of Transcription-1. *Diabetes, 64*(12), 4285-4297. doi:10.2337/db15-0107

Heinitz, S., Gebhardt, C., Piaggi, P., Kruger, J., Heyne, H., Weiner, J., . . . Tonjes, A. (2019). Atg7 Knockdown Reduces Chemerin Secretion in Murine Adipocytes. *J Clin Endocrinol Metab, 104*(11), 5715-5728. doi:10.1210/jc.2018-01980

Heiss, C., Rodriguez-Mateos, A., & Kelm, M. (2015). Central role of eNOS in the maintenance of endothelial homeostasis. *Antioxid Redox Signal, 22*(14), 1230-1242. doi:10.1089/ars.2014.6158

Heiss, E. H., & Dirsch, V. M. (2014). Regulation of eNOS enzyme activity by posttranslational modification. *Curr Pharm Des, 20*(22), 3503-3513. doi:10.2174/13816128113196660745

Hiroi, M., Mori, K., Sakaeda, Y., Shimada, J., & Ohmori, Y. (2009). STAT1 represses hypoxia-inducible factor-1-mediated transcription. *Biochem Biophys Res Commun, 387*(4), 806-810. doi:10.1016/j.bbrc.2009.07.138

Hirota, K., & Semenza, G. L. (2006). Regulation of angiogenesis by hypoxia-inducible factor 1. *Crit Rev Oncol Hematol, 59*(1), 15-26. doi:10.1016/j.critrevonc.2005.12.003

Hoffmann, A., Gloe, T., & Pohl, U. (2001). Hypoxia-induced upregulation of eNOS gene expression is redox-sensitive: a comparison between hypoxia and inhibitors of cell metabolism. *J Cell Physiol, 188*(1), 33-44. doi:10.1002/jcp.1092

Hu, Y. L., DeLay, M., Jahangiri, A., Molinaro, A. M., Rose, S. D., Carbonell, W. S., & Aghi, M. K. (2012). Hypoxia-induced autophagy promotes tumor cell survival and adaptation to antiangiogenic treatment in glioblastoma. *Cancer Res, 72*(7), 1773-1783. doi:10.1158/0008-5472.CAN-11-3831

Inampudi, C., Akintoye, E., Ando, T., & Briasoulis, A. (2018). Angiogenesis in peripheral arterial disease. *Curr Opin Pharmacol, 39*, 60-67. doi:10.1016/j.coph.2018.02.011

Jankowski, J., Floege, J., Fliser, D., Bohm, M., & Marx, N. (2021). Cardiovascular Disease in Chronic Kidney Disease: Pathophysiological Insights and Therapeutic Options. *Circulation, 143*(11), 1157-1172. doi:10.1161/CIRCULATIONAHA.120.050686

Jiao, B., Liu, S., Tan, X., Lu, P., Wang, D., & Xu, H. (2021). Class-3 semaphorins: Potent multifunctional modulators for angiogenesis-associated diseases. *Biomed Pharmacother, 137*, 111329. doi:10.1016/j.biopha.2021.111329

Jiao, W., Ji, J., Li, F., Guo, J., Zheng, Y., Li, S., & Xu, W. (2019). Activation of the NotchNox4reactive oxygen species signaling pathway induces cell death in high glucosetreated human retinal endothelial cells. *Mol Med Rep, 19*(1), 667-677. doi:10.3892/mmr.2018.9637

Jiffry, J., Thavornwatanayong, T., Rao, D., Fogel, E. J., Saytoo, D., Nahata, R., . . . Maitra, R. (2021). Oncolytic Reovirus (pelareorep) Induces Autophagy in KRAS-mutated Colorectal Cancer. *Clin Cancer Res, 27*(3), 865-876. doi:10.1158/1078-0432.CCR-20-2385

Joshi, A., Iyengar, R., Joo, J. H., Li-Harms, X. J., Wright, C., Marino, R., . . . Kundu, M. (2016). Nuclear ULK1 promotes cell death in response to oxidative stress through PARP1. *Cell Death Differ, 23*(2), 216-230. doi:10.1038/cdd.2015.88

Jung, C. H., Jun, C. B., Ro, S. H., Kim, Y. M., Otto, N. M., Cao, J., . . . Kim, D. H. (2009). ULK-Atg13-FIP200 complexes mediate mTOR signaling to the autophagy machinery. *Mol Biol Cell, 20*(7), 1992-2003. doi:10.1091/mbc.E08-12-1249

Kaludercic, N., & Di Lisa, F. (2020). Mitochondrial ROS Formation in the Pathogenesis of Diabetic Cardiomyopathy. *Front Cardiovasc Med, 7*, 12. doi:10.3389/fcvm.2020.00012

Kang, T. Y., Bocci, F., Jolly, M. K., Levine, H., Onuchic, J. N., & Levchenko, A. (2019). Pericytes enable effective angiogenesis in the presence of proinflammatory signals. *Proc Natl Acad Sci U S A, 116*(47), 23551-23561. doi:10.1073/pnas.1913373116

Kardideh, B., Samimi, Z., Norooznezhad, F., Kiani, S., & Mansouri, K. (2019). Autophagy, cancer and angiogenesis: where is the link? *Cell Biosci, 9*, 65. doi:10.1186/s13578-019-0327-6

Katsarou, A., Gudbjornsdottir, S., Rawshani, A., Dabelea, D., Bonifacio, E., Anderson, B. J., . . . Lernmark, A. (2017). Type 1 diabetes mellitus. *Nat Rev Dis Primers, 3*, 17016. doi:10.1038/nrdp.2017.16

Ke, Q., & Costa, M. (2006). Hypoxia-inducible factor-1 (HIF-1). *Mol Pharmacol, 70*(5), 1469-1480. doi:10.1124/mol.106.027029

Kim, J., Kundu, M., Viollet, B., & Guan, K. L. (2011). AMPK and mTOR regulate autophagy through direct phosphorylation of Ulk1. *Nat Cell Biol, 13*(2), 132-141. doi:10.1038/ncb2152

Knapp, M., Tu, X., & Wu, R. (2019). Vascular endothelial dysfunction, a major mediator in diabetic cardiomyopathy. *Acta Pharmacol Sin, 40*(1), 1-8. doi:10.1038/s41401-018-0042-6

Komatsu, M., Waguri, S., Ueno, T., Iwata, J., Murata, S., Tanida, I., . . . Chiba, T. (2005). Impairment of starvation-induced and constitutive autophagy in Atg7-deficient mice. *J Cell Biol, 169*(3), 425-434. doi:10.1083/jcb.200412022

Kong, E., Kim, H. D., & Kim, J. (2020). Deleting key autophagy elongation proteins induces acquirement of tumor-associated phenotypes via ISG15. *Cell Death Differ, 27*(8), 2517-2530. doi:10.1038/s41418-020-0519-y

Kong, X., Qu, X., Li, B., Wang, Z., Chao, Y., Jiang, X., . . . Chen, S. L. (2017). Modulation of low shear stressinduced eNOS multisite phosphorylation and nitric oxide production via protein kinase and ERK1/2 signaling. *Mol Med Rep, 15*(2), 908-914. doi:10.3892/mmr.2016.6060

Koyasu, S., Kobayashi, M., Goto, Y., Hiraoka, M., & Harada, H. (2018). Regulatory mechanisms of hypoxia-inducible factor 1 activity: Two decades of knowledge. *Cancer Sci, 109*(3), 560-571. doi:10.1111/cas.13483

Kruger-Genge, A., Blocki, A., Franke, R. P., & Jung, F. (2019). Vascular Endothelial Cell Biology: An Update. *Int J Mol Sci, 20*(18). doi:10.3390/ijms20184411

Kumar, S., Kumar, A., Pathania, A. S., Guru, S. K., Jada, S., Sharma, P. R., . . . Malik, F. (2013). Tiron and trolox potentiate the autophagic cell death induced by magnolol analog Ery5 by activation of Bax in HL-60 cells. *Apoptosis, 18*(5), 605-617. doi:10.1007/s10495-013-0805-y

Laddha, A. P., & Kulkarni, Y. A. (2020). NADPH oxidase: A membrane-bound enzyme and its inhibitors in diabetic complications. *Eur J Pharmacol, 881*, 173206. doi:10.1016/j.ejphar.2020.173206

Lawler, J. (2022). Counter regulation of tumor angiogenesis by vascular endothelial growth factor and thrombospondin-1. *Semin Cancer Biol, 86*(Pt 2), 126-135. doi:10.1016/j.semcancer.2022.09.006

Lawler, P. R., & Lawler, J. (2012). Molecular basis for the regulation of angiogenesis by thrombospondin-1 and -2. *Cold Spring Harb Perspect Med, 2*(5), a006627. doi:10.1101/cshperspect.a006627

Lee, I. H., Kawai, Y., Fergusson, M. M., Rovira, II, Bishop, A. J., Motoyama, N., . . . Finkel, T. (2012). Atg7 modulates p53 activity to regulate cell cycle and survival during metabolic stress. *Science, 336*(6078), 225-228. doi:10.1126/science.1218395

Lee, S. J., Kim, H. P., Jin, Y., Choi, A. M., & Ryter, S. W. (2011). Beclin 1 deficiency is associated with increased hypoxia-induced angiogenesis. *Autophagy, 7*(8), 829-839. doi:10.4161/auto.7.8.15598

Lee, S. J., Sekimoto, T., Yamashita, E., Nagoshi, E., Nakagawa, A., Imamoto, N., . . . Yoneda, Y. (2003). The structure of importin-beta bound to SREBP-2: nuclear import of a transcription factor. *Science, 302*(5650), 1571-1575. doi:10.1126/science.1088372

Li, K. C., Wang, C. H., Zou, J. J., Qu, C., Wang, X. L., Tian, X. S., . . . Cui, T. (2020). Loss of Atg7 in Endothelial Cells Enhanced Cutaneous Wound Healing in a Mouse Model. *J Surg Res, 249*, 145-155. doi:10.1016/j.jss.2019.12.004

Li, T. Y., Sun, Y., Liang, Y., Liu, Q., Shi, Y., Zhang, C. S., . . . Lin, S. C. (2016). ULK1/2 Constitute a Bifurcate Node Controlling Glucose Metabolic Fluxes in Addition to Autophagy. *Mol Cell, 62*(3), 359-370. doi:10.1016/j.molcel.2016.04.009

Li, X., Ye, Y., Zhou, X., Huang, C., & Wu, M. (2015). Atg7 enhances host defense against infection via downregulation of superoxide but upregulation of nitric oxide. *J Immunol, 194*(3), 1112-1121. doi:10.4049/jimmunol.1401958

Li, Y. Y., Lam, S. K., Mak, J. C., Zheng, C. Y., & Ho, J. C. (2013). Erlotinib-induced autophagy in epidermal growth factor receptor mutated non-small cell lung cancer. *Lung Cancer, 81*(3), 354-361. doi:10.1016/j.lungcan.2013.05.012

Liang, P., Jiang, B., Li, Y., Liu, Z., Zhang, P., Zhang, M., . . . Xiao, X. (2018). Autophagy promotes angiogenesis via AMPK/Akt/mTOR signaling during the recovery of heat-denatured endothelial cells. *Cell Death Dis, 9*(12), 1152. doi:10.1038/s41419-018-1194-5

Liang, X. H., Jackson, S., Seaman, M., Brown, K., Kempkes, B., Hibshoosh, H., & Levine, B. (1999). Induction of autophagy and inhibition of tumorigenesis by beclin 1. *Nature, 402*(6762), 672-676. doi:10.1038/45257

Lipinski, M. M., Zheng, B., Lu, T., Yan, Z., Py, B. F., Ng, A., . . . Yuan, J. (2010). Genome-wide analysis reveals mechanisms modulating autophagy in normal brain aging and in Alzheimer's disease. *Proc Natl Acad Sci U S A, 107*(32), 14164-14169. doi:10.1073/pnas.1009485107

Liu, J., Bi, X., Chen, T., Zhang, Q., Wang, S. X., Chiu, J. J., . . . Jiang, F. (2015). Shear stress regulates endothelial cell autophagy via redox regulation and Sirt1 expression. *Cell Death Dis, 6*, e1827. doi:10.1038/cddis.2015.193

Liu, J., Fan, L., Wang, H., & Sun, G. (2016). Autophagy, a double-edged sword in anti-angiogenesis therapy. *Med Oncol, 33*(1), 10. doi:10.1007/s12032-015-0721-9

Lu, L., Payvandi, F., Wu, L., Zhang, L. H., Hariri, R. J., Man, H. W., . . . Bartlett, J. B. (2009). The anti-cancer drug lenalidomide inhibits angiogenesis and metastasis via multiple inhibitory effects on endothelial cell function in normoxic and hypoxic conditions. *Microvasc Res, 77*(2), 78-86. doi:10.1016/j.mvr.2008.08.003

Lu, Q., Xie, Z., Yan, C., Ding, Y., Ma, Z., Wu, S., . . . Zou, M. H. (2018). SNRK (Sucrose Nonfermenting 1-Related Kinase) Promotes Angiogenesis In Vivo. *Arterioscler Thromb Vasc Biol, 38*(2), 373-385. doi:10.1161/ATVBAHA.117.309834

Luo, X., Hu, Y., He, S., Ye, Q., Lv, Z., Liu, J., & Chen, X. (2019). Dulaglutide inhibits high glucose- induced endothelial dysfunction and NLRP3 inflammasome activation. *Arch Biochem Biophys, 671*, 203-209. doi:10.1016/j.abb.2019.07.008

Lynch, C. M., Kinzenbaw, D. A., Chen, X., Zhan, S., Mezzetti, E., Filosa, J., . . . Didion, S. P. (2013). Nox2-derived superoxide contributes to cerebral vascular dysfunction in diet-induced obesity. *Stroke, 44*(11), 3195-3201. doi:10.1161/STROKEAHA.113.001366

Madamanchi, N. R., Li, S., Patterson, C., & Runge, M. S. (2001). Reactive oxygen species regulate heat-shock protein 70 via the JAK/STAT pathway. *Arterioscler Thromb Vasc Biol, 21*(3), 321-326. doi:10.1161/01.atv.21.3.321

Maes, H., Kuchnio, A., Peric, A., Moens, S., Nys, K., De Bock, K., . . . Carmeliet, P. (2014). Tumor vessel normalization by chloroquine independent of autophagy. *Cancer Cell, 26*(2), 190-206. doi:10.1016/j.ccr.2014.06.025

Masoud, G. N., & Li, W. (2015). HIF-1alpha pathway: role, regulation and intervention for cancer therapy. *Acta Pharm Sin B, 5*(5), 378-389. doi:10.1016/j.apsb.2015.05.007

Matsui, Y., Kyoi, S., Takagi, H., Hsu, C. P., Hariharan, N., Ago, T., . . . Sadoshima, J. (2008). Molecular mechanisms and physiological significance of autophagy during myocardial ischemia and reperfusion. *Autophagy, 4*(4), 409-415. doi:10.4161/auto.5638

Mauthe, M., & Reggiori, F. (2016). ATG proteins: Are we always looking at autophagy? *Autophagy, 12*(12), 2502-2503. doi:10.1080/15548627.2016.1236878

Melincovici, C. S., Bosca, A. B., Susman, S., Marginean, M., Mihu, C., Istrate, M., . . . Mihu, C. M. (2018). Vascular endothelial growth factor (VEGF) - key factor in normal and pathological angiogenesis. *Rom J Morphol Embryol, 59*(2), 455-467.

Mentzer, S. J., & Konerding, M. A. (2014). Intussusceptive angiogenesis: expansion and remodeling of microvascular networks. *Angiogenesis, 17*(3), 499-509. doi:10.1007/s10456-014-9428-3

Merchant, J. L., Bai, L., & Okada, M. (2003). ZBP-89 mediates butyrate regulation of gene expression. *J Nutr, 133*(7 Suppl), 2456S-2460S. doi:10.1093/jn/133.7.2456S

Michel, T., & Vanhoutte, P. M. (2010). Cellular signaling and NO production. *Pflugers Arch, 459*(6), 807-816. doi:10.1007/s00424-009-0765-9

Mizushima, N. (2007). Autophagy: process and function. *Genes Dev, 21*(22), 2861-2873. doi:10.1101/gad.1599207

Mizushima, N. (2020). The ATG conjugation systems in autophagy. *Curr Opin Cell Biol, 63*, 1-10. doi:10.1016/j.ceb.2019.12.001

Montezano, A. C., & Touyz, R. M. (2012). Reactive oxygen species and endothelial function--role of nitric oxide synthase uncoupling and Nox family nicotinamide adenine dinucleotide phosphate oxidases. *Basic Clin Pharmacol Toxicol, 110*(1), 87-94. doi:10.1111/j.1742-7843.2011.00785.x

Mortensen, M., Ferguson, D. J., Edelmann, M., Kessler, B., Morten, K. J., Komatsu, M., & Simon, A. K. (2010). Loss of autophagy in erythroid cells leads to defective removal of mitochondria and severe anemia in vivo. *Proc Natl Acad Sci U S A, 107*(2), 832-837. doi:10.1073/pnas.0913170107

Mu, J., Zhang, D., Tian, Y., Xie, Z., & Zou, M. H. (2020). BRD4 inhibition by JQ1 prevents high-fat diet-induced diabetic cardiomyopathy by activating PINK1/Parkin-mediated mitophagy in vivo. *J Mol Cell Cardiol, 149*, 1-14. doi:10.1016/j.yjmcc.2020.09.003

Nagy, J. A., Chang, S. H., Shih, S. C., Dvorak, A. M., & Dvorak, H. F. (2010). Heterogeneity of the tumor vasculature. *Semin Thromb Hemost, 36*(3), 321-331. doi:10.1055/s-0030-1253454

Nakatogawa, H. (2020). Mechanisms governing autophagosome biogenesis. *Nat Rev Mol Cell Biol, 21*(8), 439-458. doi:10.1038/s41580-020-0241-0

Napolitano, G., & Ballabio, A. (2016). TFEB at a glance. *J Cell Sci, 129*(13), 2475-2481. doi:10.1242/jcs.146365

Newsholme, P., Cruzat, V. F., Keane, K. N., Carlessi, R., & de Bittencourt, P. I., Jr. (2016). Molecular mechanisms of ROS production and oxidative stress in diabetes. *Biochem J, 473*(24), 4527-4550. doi:10.1042/BCJ20160503C

Newsholme, P., Haber, E. P., Hirabara, S. M., Rebelato, E. L., Procopio, J., Morgan, D., . . . Curi, R. (2007). Diabetes associated cell stress and dysfunction: role of mitochondrial and non-mitochondrial ROS production and activity. *J Physiol, 583*(Pt 1), 9-24. doi:10.1113/jphysiol.2007.135871

Niiyama, H., Huang, N. F., Rollins, M. D., & Cooke, J. P. (2009). Murine model of hindlimb ischemia. *J Vis Exp*(23). doi:10.3791/1035

Nishikawa, T., & Araki, E. (2007). Impact of mitochondrial ROS production in the pathogenesis of diabetes mellitus and its complications. *Antioxid Redox Signal, 9*(3), 343-353. doi:10.1089/ars.2006.1458

Niu, C., Chen, Z., Kim, K. T., Sun, J., Xue, M., Chen, G., . . . Li, X. (2019). Metformin alleviates hyperglycemia-induced endothelial impairment by downregulating autophagy via the Hedgehog pathway. *Autophagy, 15*(5), 843-870. doi:10.1080/15548627.2019.1569913

Nowotny, K., Jung, T., Hohn, A., Weber, D., & Grune, T. (2015). Advanced glycation end products and oxidative stress in type 2 diabetes mellitus. *Biomolecules, 5*(1), 194-222. doi:10.3390/biom5010194

Nussenzweig, S. C., Verma, S., & Finkel, T. (2015). The role of autophagy in vascular biology. *Circ Res, 116*(3), 480-488. doi:10.1161/CIRCRESAHA.116.303805

Onnis, B., Rapisarda, A., & Melillo, G. (2009). Development of HIF-1 inhibitors for cancer therapy. *J Cell Mol Med, 13*(9A), 2780-2786. doi:10.1111/j.1582-4934.2009.00876.x

Ouyang, C., You, J., & Xie, Z. (2014). The interplay between autophagy and apoptosis in the diabetic heart. *J Mol Cell Cardiol, 71*, 71-80. doi:10.1016/j.yjmcc.2013.10.014

Ozaki, M., Kawashima, S., Yamashita, T., Hirase, T., Namiki, M., Inoue, N., . . . Yokoyama, M. (2002). Overexpression of endothelial nitric oxide synthase accelerates atherosclerotic lesion formation in apoE-deficient mice. *J Clin Invest, 110*(3), 331-340. doi:10.1172/JCI15215

Paez-Ribes, M., Allen, E., Hudock, J., Takeda, T., Okuyama, H., Vinals, F., . . . Casanovas, O. (2009). Antiangiogenic therapy elicits malignant progression of tumors to increased local invasion and distant metastasis. *Cancer Cell, 15*(3), 220-231. doi:10.1016/j.ccr.2009.01.027

Palazon, A., Tyrakis, P. A., Macias, D., Velica, P., Rundqvist, H., Fitzpatrick, S., . . . Johnson, R. S. (2017). An HIF-1alpha/VEGF-A Axis in Cytotoxic T Cells Regulates Tumor Progression. *Cancer Cell, 32*(5), 669-683 e665. doi:10.1016/j.ccell.2017.10.003

Pardali, E., & ten Dijke, P. (2009). Transforming growth factor-beta signaling and tumor angiogenesis. *Front Biosci (Landmark Ed), 14*(13), 4848-4861. doi:10.2741/3573

Park, E. J., Lee, Y. M., Oh, T. I., Kim, B. M., Lim, B. O., & Lim, J. H. (2017). Vanillin Suppresses Cell Motility by Inhibiting STAT3-Mediated HIF-1alpha mRNA Expression in Malignant Melanoma Cells. *Int J Mol Sci, 18*(3). doi:10.3390/ijms18030532

Parra-Izquierdo, I., Castanos-Mollor, I., Lopez, J., Gomez, C., San Roman, J. A., Sanchez Crespo, M., & Garcia-Rodriguez, C. (2019). Lipopolysaccharide and interferon-gamma team up to activate HIF-1alpha via STAT1 in normoxia and exhibit sex differences in

human aortic valve interstitial cells. *Biochim Biophys Acta Mol Basis Dis, 1865*(9), 2168-2179. doi:10.1016/j.bbadis.2019.04.014

Parzych, K. R., & Klionsky, D. J. (2014). An overview of autophagy: morphology, mechanism, and regulation. *Antioxid Redox Signal, 20*(3), 460-473. doi:10.1089/ars.2013.5371

Pattison, J. S., Osinska, H., & Robbins, J. (2011). Atg7 induces basal autophagy and rescues autophagic deficiency in CryABR120G cardiomyocytes. *Circ Res, 109*(2), 151-160. doi:10.1161/CIRCRESAHA.110.237339

Pestana, C. R., Oishi, J. C., Salistre-Araujo, H. S., & Rodrigues, G. J. (2015). Inhibition of autophagy by chloroquine stimulates nitric oxide production and protects endothelial function during serum deprivation. *Cell Physiol Biochem, 37*(3), 1168-1177. doi:10.1159/000430240

Piguet, A. C., Majumder, S., Maheshwari, U., Manjunathan, R., Saran, U., Chatterjee, S., & Dufour, J. F. (2014). Everolimus is a potent inhibitor of activated hepatic stellate cell functions in vitro and in vivo, while demonstrating anti-angiogenic activities. *Clin Sci (Lond), 126*(11), 775-784. doi:10.1042/CS20130081

Portilla-Fernandez, E., Ghanbari, M., van Meurs, J. B. J., Danser, A. H. J., Franco, O. H., Muka, T., . . . Dehghan, A. (2019). Dissecting the association of autophagy-related genes with cardiovascular diseases and intermediate vascular traits: A population-based approach. *PLoS One, 14*(3), e0214137. doi:10.1371/journal.pone.0214137

Potente, M., Gerhardt, H., & Carmeliet, P. (2011). Basic and therapeutic aspects of angiogenesis. *Cell, 146*(6), 873-887. doi:10.1016/j.cell.2011.08.039

Prabhu, S. D., & Frangogiannis, N. G. (2016). The Biological Basis for Cardiac Repair After Myocardial Infarction: From Inflammation to Fibrosis. *Circ Res, 119*(1), 91-112. doi:10.1161/CIRCRESAHA.116.303577

Przybylski, M. (2009). A review of the current research on the role of bFGF and VEGF in angiogenesis. *J Wound Care, 18*(12), 516-519. doi:10.12968/jowc.2009.18.12.45609

Pugh, C. W., & Ratcliffe, P. J. (2003). Regulation of angiogenesis by hypoxia: role of the HIF system. *Nat Med, 9*(6), 677-684. doi:10.1038/nm0603-677

Qiao, Z., Xu, Z., Xiao, Q., Yang, Y., Ying, J., Xiang, L., & Zhang, C. (2020). Dysfunction of ATG7-dependent autophagy dysregulates the antioxidant response and contributes to oxidative stress-induced biological impairments in human epidermal melanocytes. *Cell Death Discov, 6*, 31. doi:10.1038/s41420-020-0266-3

Rabinowitz, J. D., & White, E. (2010). Autophagy and metabolism. *Science, 330*(6009), 1344-1348. doi:10.1126/science.1193497

Rajappa, M., Saxena, P., & Kaur, J. (2010). Ocular angiogenesis: mechanisms and recent advances in therapy. *Adv Clin Chem, 50*, 103-121.

Ribatti, D. (2009). Endogenous inhibitors of angiogenesis: a historical review. *Leuk Res, 33*(5), 638-644. doi:10.1016/j.leukres.2008.11.019

Rius, J., Guma, M., Schachtrup, C., Akassoglou, K., Zinkernagel, A. S., Nizet, V., . . . Karin, M. (2008). NF-kappaB links innate immunity to the hypoxic response through transcriptional regulation of HIF-1alpha. *Nature, 453*(7196), 807-811. doi:10.1038/nature06905

Roca-Agujetas, V., de Dios, C., Leston, L., Mari, M., Morales, A., & Colell, A. (2019). Recent Insights into the Mitochondrial Role in Autophagy and Its Regulation by Oxidative Stress. *Oxid Med Cell Longev, 2019*, 3809308. doi:10.1155/2019/3809308

Rohlenova, K., Goveia, J., Garcia-Caballero, M., Subramanian, A., Kalucka, J., Treps, L., . . . Carmeliet, P. (2020). Single-Cell RNA Sequencing Maps Endothelial Metabolic

Plasticity in Pathological Angiogenesis. *Cell Metab, 31*(4), 862-877 e814. doi:10.1016/j.cmet.2020.03.009

Rosenfeldt, M. T., O'Prey, J., Morton, J. P., Nixon, C., MacKay, G., Mrowinska, A., . . . Ryan, K. M. (2013). p53 status determines the role of autophagy in pancreatic tumour development. *Nature, 504*(7479), 296-300. doi:10.1038/nature12865

Ruart, M., Chavarria, L., Campreciós, G., Suarez-Herrera, N., Montironi, C., Guixe-Muntet, S., . . . Hernandez-Gea, V. (2019). Impaired endothelial autophagy promotes liver fibrosis by aggravating the oxidative stress response during acute liver injury. *J Hepatol, 70*(3), 458-469. doi:10.1016/j.jhep.2018.10.015

Russo, T. A., Banuth, A. M. M., Nader, H. B., & Dreyfuss, J. L. (2020). Altered shear stress on endothelial cells leads to remodeling of extracellular matrix and induction of angiogenesis. *PLoS One, 15*(11), e0241040. doi:10.1371/journal.pone.0241040

Saitoh, T., Fujita, N., Jang, M. H., Uematsu, S., Yang, B. G., Satoh, T., . . . Akira, S. (2008). Loss of the autophagy protein Atg16L1 enhances endotoxin-induced IL-1beta production. *Nature, 456*(7219), 264-268. doi:10.1038/nature07383

Sandoo, A., van Zanten, J. J., Metsios, G. S., Carroll, D., & Kitas, G. D. (2010). The endothelium and its role in regulating vascular tone. *Open Cardiovasc Med J, 4*, 302-312. doi:10.2174/1874192401004010302

Schaaf, M. B., Garg, A. D., & Agostinis, P. (2018). Defining the role of the tumor vasculature in antitumor immunity and immunotherapy. *Cell Death Dis, 9*(2), 115. doi:10.1038/s41419-017-0061-0

Schaaf, M. B., Houbaert, D., Mece, O., To, S. K., Ganne, M., Maes, H., & Agostinis, P. (2019). Lysosomal Pathways and Autophagy Distinctively Control Endothelial Cell Behavior to Affect Tumor Vasculature. *Front Oncol, 9*, 171. doi:10.3389/fonc.2019.00171

Schwartz-Roberts, J. L., Cook, K. L., Chen, C., Shajahan-Haq, A. N., Axelrod, M., Warri, A., . . . Clarke, R. (2015). Interferon regulatory factor-1 signaling regulates the switch between autophagy and apoptosis to determine breast cancer cell fate. *Cancer Res, 75*(6), 1046-1055. doi:10.1158/0008-5472.CAN-14-1851

Semenza, G. L. (2003). Targeting HIF-1 for cancer therapy. *Nat Rev Cancer, 3*(10), 721-732. doi:10.1038/nrc1187

Semenza, G. L. (2014). Hypoxia-inducible factor 1 and cardiovascular disease. *Annu Rev Physiol, 76*, 39-56. doi:10.1146/annurev-physiol-021113-170322

Senger, D. R., & Davis, G. E. (2011). Angiogenesis. *Cold Spring Harb Perspect Biol, 3*(8), a005090. doi:10.1101/cshperspect.a005090

Shen, N., Zhang, R., Zhang, H. R., Luo, H. Y., Shen, W., Gao, X., . . . Shen, J. (2018). Inhibition of retinal angiogenesis by gold nanoparticles via inducing autophagy. *Int J Ophthalmol, 11*(8), 1269-1276. doi:10.18240/ijo.2018.08.04

Singh, K. K., Lovren, F., Pan, Y., Quan, A., Ramadan, A., Matkar, P. N., . . . Verma, S. (2015). The essential autophagy gene ATG7 modulates organ fibrosis via regulation of endothelial-to-mesenchymal transition. *J Biol Chem, 290*(5), 2547-2559. doi:10.1074/jbc.M114.604603

Sobczak, M., Dargatz, J., & Chrzanowska-Wodnicka, M. (2010). Isolation and culture of pulmonary endothelial cells from neonatal mice. *J Vis Exp*(46). doi:10.3791/2316

Society for Vascular Surgery Lower Extremity Guidelines Writing, G., Conte, M. S., Pomposelli, F. B., Clair, D. G., Geraghty, P. J., McKinsey, J. F., . . . Society for Vascular, S. (2015). Society for Vascular Surgery practice guidelines for atherosclerotic occlusive disease of

the lower extremities: management of asymptomatic disease and claudication. *J Vasc Surg, 61*(3 Suppl), 2S-41S. doi:10.1016/j.jvs.2014.12.009

Sodha, N. R., Clements, R. T., Boodhwani, M., Xu, S. H., Laham, R. J., Bianchi, C., & Sellke, F. W. (2009). Endostatin and angiostatin are increased in diabetic patients with coronary artery disease and associated with impaired coronary collateral formation. *Am J Physiol Heart Circ Physiol, 296*(2), H428-434. doi:10.1152/ajpheart.00283.2008

Song, P., Rudan, D., Zhu, Y., Fowkes, F. J. I., Rahimi, K., Fowkes, F. G. R., & Rudan, I. (2019). Global, regional, and national prevalence and risk factors for peripheral artery disease in 2015: an updated systematic review and analysis. *Lancet Glob Health, 7*(8), e1020-e1030. doi:10.1016/S2214-109X(19)30255-4

Sowers, J. R., Epstein, M., & Frohlich, E. D. (2001). Diabetes, hypertension, and cardiovascular disease: an update. *Hypertension, 37*(4), 1053-1059. doi:10.1161/01.hyp.37.4.1053

Sprott, D., Poitz, D. M., Korovina, I., Ziogas, A., Phieler, J., Chatzigeorgiou, A., . . . Klotzsche-von Ameln, A. (2019). Endothelial-Specific Deficiency of ATG5 (Autophagy Protein 5) Attenuates Ischemia-Related Angiogenesis. *Arterioscler Thromb Vasc Biol, 39*(6), 1137-1148. doi:10.1161/ATVBAHA.119.309973

Stegmann, T. J. (1998). FGF-1: a human growth factor in the induction of neoangiogenesis. *Expert Opin Investig Drugs, 7*(12), 2011-2015. doi:10.1517/13543784.7.12.2011

Subramani, J., Kundumani-Sridharan, V., & Das, K. C. (2021). Chaperone-Mediated Autophagy of eNOS in Myocardial Ischemia-Reperfusion Injury. *Circ Res, 129*(10), 930-945. doi:10.1161/CIRCRESAHA.120.317921

Sukriti, S., Tauseef, M., Yazbeck, P., & Mehta, D. (2014). Mechanisms regulating endothelial permeability. *Pulm Circ, 4*(4), 535-551. doi:10.1086/677356

Sukseree, S., Schwarze, U. Y., Gruber, R., Gruber, F., Quiles Del Rey, M., Mancias, J. D., . . . Eckhart, L. (2020). ATG7 is essential for secretion of iron from ameloblasts and normal growth of murine incisors during aging. *Autophagy, 16*(10), 1851-1857. doi:10.1080/15548627.2019.1709764

Sung, S. J., Kim, H. K., Hong, Y. K., & Joe, Y. A. (2019). Autophagy Is a Potential Target for Enhancing the Anti-Angiogenic Effect of Mebendazole in Endothelial Cells. *Biomol Ther (Seoul), 27*(1), 117-125. doi:10.4062/biomolther.2018.222

Suzuki, K., Kirisako, T., Kamada, Y., Mizushima, N., Noda, T., & Ohsumi, Y. (2001). The pre-autophagosomal structure organized by concerted functions of APG genes is essential for autophagosome formation. *EMBO J, 20*(21), 5971-5981. doi:10.1093/emboj/20.21.5971

Sziksz, E., Pap, D., Lippai, R., Beres, N. J., Fekete, A., Szabo, A. J., & Vannay, A. (2015). Fibrosis Related Inflammatory Mediators: Role of the IL-10 Cytokine Family. *Mediators Inflamm, 2015*, 764641. doi:10.1155/2015/764641

Takeshita, S., Zheng, L. P., Brogi, E., Kearney, M., Pu, L. Q., Bunting, S., . . . Isner, J. M. (1994). Therapeutic angiogenesis. A single intraarterial bolus of vascular endothelial growth factor augments revascularization in a rabbit ischemic hind limb model. *J Clin Invest, 93*(2), 662-670. doi:10.1172/JCI117018

Tal, M. C., Sasai, M., Lee, H. K., Yordy, B., Shadel, G. S., & Iwasaki, A. (2009). Absence of autophagy results in reactive oxygen species-dependent amplification of RLR signaling. *Proc Natl Acad Sci U S A, 106*(8), 2770-2775. doi:10.1073/pnas.0807694106

Tao, Z., Shi, A., & Zhao, J. (2015). Epidemiological Perspectives of Diabetes. *Cell Biochem Biophys, 73*(1), 181-185. doi:10.1007/s12013-015-0598-4

Taraboletti, G., Rusnati, M., Ragona, L., & Colombo, G. (2010). Targeting tumor angiogenesis with TSP-1-based compounds: rational design of antiangiogenic mimetics of endogenous inhibitors. *Oncotarget, 1*(7), 662-673. doi:10.18632/oncotarget.101108

Tekabe, Y., Anthony, T., Li, Q., Ray, R., Rai, V., Zhang, G., . . . Johnson, L. L. (2015). Treatment effect with anti-RAGE F(ab')2 antibody improves hind limb angiogenesis and blood flow in Type 1 diabetic mice with left femoral artery ligation. *Vasc Med, 20*(3), 212-218. doi:10.1177/1358863X14568337

Tetzlaff, F., & Fischer, A. (2018). Human Endothelial Cell Spheroid-based Sprouting Angiogenesis Assay in Collagen. *Bio Protoc, 8*(17), e2995. doi:10.21769/BioProtoc.2995

Thomas, R. L., & Gustafsson, A. B. (2013). Mitochondrial autophagy--an essential quality control mechanism for myocardial homeostasis. *Circ J, 77*(10), 2449-2454. doi:10.1253/circj.cj-13-0835

Tian, W., Li, W., Chen, Y., Yan, Z., Huang, X., Zhuang, H., . . . Feng, D. (2015). Phosphorylation of ULK1 by AMPK regulates translocation of ULK1 to mitochondria and mitophagy. *FEBS Lett, 589*(15), 1847-1854. doi:10.1016/j.febslet.2015.05.020

Torisu, T., Torisu, K., Lee, I. H., Liu, J., Malide, D., Combs, C. A., . . . Finkel, T. (2013). Autophagy regulates endothelial cell processing, maturation and secretion of von Willebrand factor. *Nat Med, 19*(10), 1281-1287. doi:10.1038/nm.3288

Tousoulis, D., Kampoli, A. M., Tentolouris, C., Papageorgiou, N., & Stefanadis, C. (2012). The role of nitric oxide on endothelial function. *Curr Vasc Pharmacol, 10*(1), 4-18. doi:10.2174/157016112798829760

Towler, M. C., & Hardie, D. G. (2007). AMP-activated protein kinase in metabolic control and insulin signaling. *Circ Res, 100*(3), 328-341. doi:10.1161/01.RES.0000256090.42690.05

Tsao, C. W., Aday, A. W., Almarzooq, Z. I., Alonso, A., Beaton, A. Z., Bittencourt, M. S., . . . Martin, S. S. (2022). Heart Disease and Stroke Statistics-2022 Update: A Report From the American Heart Association. *Circulation, 145*(8), e153-e639. doi:10.1161/CIR.0000000000001052

Ueno, T., Masuda, N., Kamigaki, S., Morimoto, T., Saji, S., Imoto, S., . . . Toi, M. (2019). Differential Involvement of Autophagy and Apoptosis in Response to Chemoendocrine and Endocrine Therapy in Breast Cancer: JBCRG-07TR. *Int J Mol Sci, 20*(4). doi:10.3390/ijms20040984

van Royen, N., Piek, J. J., Buschmann, I., Hoefer, I., Voskuil, M., & Schaper, W. (2001). Stimulation of arteriogenesis; a new concept for the treatment of arterial occlusive disease. *Cardiovasc Res, 49*(3), 543-553. doi:10.1016/s0008-6363(00)00206-6

Walchli, T., Pernet, V., Weinmann, O., Shiu, J. Y., Guzik-Kornacka, A., Decrey, G., . . . Schwab, M. E. (2013). Nogo-A is a negative regulator of CNS angiogenesis. *Proc Natl Acad Sci U S A, 110*(21), E1943-1952. doi:10.1073/pnas.1216203110

Wang, H. J., Wei, J. Y., Liu, D. X., Zhuang, S. F., Li, Y., Liu, H., . . . Chen, Y. H. (2018). Endothelial Atg7 Deficiency Ameliorates Acute Cerebral Injury Induced by Ischemia/Reperfusion. *Front Neurol, 9*, 998. doi:10.3389/fneur.2018.00998

Wang, Q., Liang, B., Shirwany, N. A., & Zou, M. H. (2011). 2-Deoxy-D-glucose treatment of endothelial cells induces autophagy by reactive oxygen species-mediated activation of the AMP-activated protein kinase. *PLoS One, 6*(2), e17234. doi:10.1371/journal.pone.0017234

Wang, Y., Lu, X., Wang, X., Qiu, Q., Zhu, P., Ma, L., . . . Xu, X. (2021). atg7-Based Autophagy Activation Reverses Doxorubicin-Induced Cardiotoxicity. *Circ Res, 129*(8), e166-e182. doi:10.1161/CIRCRESAHA.121.319104

Wei, R., Wu, Q., Ai, N., Wang, L., Zhou, M., Shaw, C., . . . Kwok, H. F. (2021). A novel bioengineered fragment peptide of Vasostatin-1 exerts smooth muscle pharmacological activities and anti-angiogenic effects via blocking VEGFR signalling pathway. *Comput Struct Biotechnol J, 19*, 2664-2675. doi:10.1016/j.csbj.2021.05.003

Wen, Y., Zhou, X., Lu, M., He, M., Tian, Y., Liu, L., . . . Chen, X. (2019). Bclaf1 promotes angiogenesis by regulating HIF-1alpha transcription in hepatocellular carcinoma. *Oncogene, 38*(11), 1845-1859. doi:10.1038/s41388-018-0552-1

Wragg, J. W., Durant, S., McGettrick, H. M., Sample, K. M., Egginton, S., & Bicknell, R. (2014). Shear stress regulated gene expression and angiogenesis in vascular endothelium. *Microcirculation, 21*(4), 290-300. doi:10.1111/micc.12119

Wu, J., Contratto, M., Shanbhogue, K. P., Manji, G. A., O'Neil, B. H., Noonan, A., . . . Lee, R. (2019). Evaluation of a locked nucleic acid form of antisense oligo targeting HIF-1alpha in advanced hepatocellular carcinoma. *World J Clin Oncol, 10*(3), 149-160. doi:10.5306/wjco.v10.i3.149

Wu, J., Jin, Z., Zheng, H., & Yan, L. J. (2016). Sources and implications of NADH/NAD(+) redox imbalance in diabetes and its complications. *Diabetes Metab Syndr Obes, 9*, 145-153. doi:10.2147/DMSO.S106087

Wu, J., Lei, Z., & Yu, J. (2015). Hypoxia induces autophagy in human vascular endothelial cells in a hypoxia-inducible factor 1dependent manner. *Mol Med Rep, 11*(4), 2677-2682. doi:10.3892/mmr.2014.3093

Wu, W., Xu, H., Wang, Z., Mao, Y., Yuan, L., Luo, W., . . . Shen, Y. H. (2015). PINK1-Parkin-Mediated Mitophagy Protects Mitochondrial Integrity and Prevents Metabolic Stress-Induced Endothelial Injury. *PLoS One, 10*(7), e0132499. doi:10.1371/journal.pone.0132499

Wu, Y., Diab, I., Zhang, X., Izmailova, E. S., & Zehner, Z. E. (2004). Stat3 enhances vimentin gene expression by binding to the antisilencer element and interacting with the repressor protein, ZBP-89. *Oncogene, 23*(1), 168-178. doi:10.1038/sj.onc.1207003

Xie, Z., He, C., & Zou, M. H. (2011). AMP-activated protein kinase modulates cardiac autophagy in diabetic cardiomyopathy. *Autophagy, 7*(10), 1254-1255. doi:10.4161/auto.7.10.16740

Xu, H., Rahimpour, S., Nesvick, C. L., Zhang, X., Ma, J., Zhang, M., . . . Zhuang, Z. (2015). Activation of hypoxia signaling induces phenotypic transformation of glioma cells: implications for bevacizumab antiangiogenic therapy. *Oncotarget, 6*(14), 11882-11893. doi:10.18632/oncotarget.3592

Xu, J., Deng, Y., Ke, Y., Zhu, Y., Wang, P., Yu, Q., . . . Shi, B. (2022). Mutation of Beclin1 acetylation site at K414 alleviates high glucose-induced podocyte impairment in the early stage of diabetic nephropathy by inhibiting hyperactivated autophagy. *Mol Biol Rep, 49*(5), 3919-3926. doi:10.1007/s11033-022-07242-2

Xu, Q., Jiang, C., Rong, Y., Yang, C., Liu, Y., & Xu, K. (2015). The effects of fludarabine on rat cerebral ischemia. *J Mol Neurosci, 55*(2), 289-296. doi:10.1007/s12031-014-0320-9

Yamamoto, Y., Maeshima, Y., Kitayama, H., Kitamura, S., Takazawa, Y., Sugiyama, H., . . . Makino, H. (2004). Tumstatin peptide, an inhibitor of angiogenesis, prevents glomerular

hypertrophy in the early stage of diabetic nephropathy. *Diabetes, 53*(7), 1831-1840. doi:10.2337/diabetes.53.7.1831

Yan, L. J. (2018). Redox imbalance stress in diabetes mellitus: Role of the polyol pathway. *Animal Model Exp Med, 1*(1), 7-13. doi:10.1002/ame2.12001

Yan, Y., Wu, T., Zhang, M., Li, C., Liu, Q., & Li, F. (2022). Prevalence, awareness and control of type 2 diabetes mellitus and risk factors in Chinese elderly population. *BMC Public Health, 22*(1), 1382. doi:10.1186/s12889-022-13759-9

Yang, D., Livingston, M. J., Liu, Z., Dong, G., Zhang, M., Chen, J. K., & Dong, Z. (2018). Autophagy in diabetic kidney disease: regulation, pathological role and therapeutic potential. *Cell Mol Life Sci, 75*(4), 669-688. doi:10.1007/s00018-017-2639-1

Yang, L., Li, P., Fu, S., Calay, E. S., & Hotamisligil, G. S. (2010). Defective hepatic autophagy in obesity promotes ER stress and causes insulin resistance. *Cell Metab, 11*(6), 467-478. doi:10.1016/j.cmet.2010.04.005

Yin, Z., Pascual, C., & Klionsky, D. J. (2016). Autophagy: machinery and regulation. *Microb Cell, 3*(12), 588-596. doi:10.15698/mic2016.12.546

Youn, J. Y., Gao, L., & Cai, H. (2012). The p47phox- and NADPH oxidase organiser 1 (NOXO1)-dependent activation of NADPH oxidase 1 (NOX1) mediates endothelial nitric oxide synthase (eNOS) uncoupling and endothelial dysfunction in a streptozotocin-induced murine model of diabetes. *Diabetologia, 55*(7), 2069-2079. doi:10.1007/s00125-012-2557-6

Yun, C. W., & Lee, S. H. (2018). The Roles of Autophagy in Cancer. *Int J Mol Sci, 19*(11). doi:10.3390/ijms19113466

Zacharski, L. R., Shamayeva, G., & Chow, B. K. (2018). Iron reduction response and demographic differences between diabetics and non-diabetics with cardiovascular disease entered into a controlled clinical trial. *Metallomics, 10*(2), 264-277. doi:10.1039/c7mt00282c

Zeh, H. J., Bahary, N., Boone, B. A., Singhi, A. D., Miller-Ocuin, J. L., Normolle, D. P., . . . Lotze, M. T. (2020). A Randomized Phase II Preoperative Study of Autophagy Inhibition with High-Dose Hydroxychloroquine and Gemcitabine/Nab-Paclitaxel in Pancreatic Cancer Patients. *Clin Cancer Res, 26*(13), 3126-3134. doi:10.1158/1078-0432.CCR-19-4042

Zhang, J. X., Qu, X. L., Chu, P., Xie, D. J., Zhu, L. L., Chao, Y. L., . . . Chen, S. L. (2018). Low shear stress induces vascular eNOS uncoupling via autophagy-mediated eNOS phosphorylation. *Biochim Biophys Acta Mol Cell Res, 1865*(5), 709-720. doi:10.1016/j.bbamcr.2018.02.005

Zhang, S., Xu, H., Yu, X., Wu, Y., & Sui, D. (2017). Metformin ameliorates diabetic nephropathy in a rat model of low-dose streptozotocin-induced diabetes. *Exp Ther Med, 14*(1), 383-390. doi:10.3892/etm.2017.4475

Zhang, X., Cheng, X., Yu, L., Yang, J., Calvo, R., Patnaik, S., . . . Xu, H. (2016). MCOLN1 is a ROS sensor in lysosomes that regulates autophagy. *Nat Commun, 7*, 12109. doi:10.1038/ncomms12109

Zhang, Z., Apse, K., Pang, J., & Stanton, R. C. (2000). High glucose inhibits glucose-6-phosphate dehydrogenase via cAMP in aortic endothelial cells. *J Biol Chem, 275*(51), 40042-40047. doi:10.1074/jbc.M007505200

Zhao, L., Zhang, C. L., He, L., Chen, Q., Liu, L., Kang, L., . . . Huang, Y. (2022). Restoration of Autophagic Flux Improves Endothelial Function in Diabetes Through Lowering

Mitochondrial ROS-Mediated eNOS Monomerization. *Diabetes, 71*(5), 1099-1114. doi:10.2337/db21-0660

Zhao, R. Z., Jiang, S., Zhang, L., & Yu, Z. B. (2019). Mitochondrial electron transport chain, ROS generation and uncoupling (Review). *Int J Mol Med, 44*(1), 3-15. doi:10.3892/ijmm.2019.4188

Zheng, J., & Lu, C. (2020). Oxidized LDL Causes Endothelial Apoptosis by Inhibiting Mitochondrial Fusion and Mitochondria Autophagy. *Front Cell Dev Biol, 8*, 600950. doi:10.3389/fcell.2020.600950

Zhu, H. F., Wan, D., Luo, Y., Zhou, J. L., Chen, L., & Xu, X. Y. (2010). Catalpol increases brain angiogenesis and up-regulates VEGF and EPO in the rat after permanent middle cerebral artery occlusion. *Int J Biol Sci, 6*(5), 443-453. doi:10.7150/ijbs.6.443

Zhuang, S. F., Liu, D. X., Wang, H. J., Zhang, S. H., Wei, J. Y., Fang, W. G., . . . Chen, Y. H. (2017). Atg7 Regulates Brain Angiogenesis via NF-kappaB-Dependent IL-6 Production. *Int J Mol Sci, 18*(5). doi:10.3390/ijms18050968

Zhuang, Y., Li, Y., Li, X., Xie, Q., & Wu, M. (2016). Atg7 Knockdown Augments Concanavalin A-Induced Acute Hepatitis through an ROS-Mediated p38/MAPK Pathway. *PLoS One, 11*(3), e0149754. doi:10.1371/journal.pone.0149754

Zou, J., Fei, Q., Xiao, H., Wang, H., Liu, K., Liu, M., . . . Wang, N. (2019). VEGF-A promotes angiogenesis after acute myocardial infarction through increasing ROS production and enhancing ER stress-mediated autophagy. *J Cell Physiol, 234*(10), 17690-17703. doi:10.1002/jcp.28395

APPENDICES

Publications

1. **Hongmin Yao**, Jian Li, Zhixue Liu, Changhan Ouyang, Yu Qiu, Xiaoxu Zheng, Jing Mu, Zhonglin Xie. Ablation of endothelial Atg7 inhibits ischemia-induced angiogenesis by upregulating Stat1 that suppresses *Hif1a* expression. Autophagy. Published
2. Jian Li, **Hongmin Yao**, Fujie Zhao, Junqing An, Qilong Wang, Yadong Wang, Jing Mu, Xicong Tang, Zhixue Liu, Yu Qiu, Ming-hui Zou , Zhonglin Xie. Pycard deletion inhibits microRNA maturation and prevents neointima formation by promoting chaperone-mediated autophagic degradation of argonaute2 in adipose tissue. Autophagy. In revision.
3. Sean Michael Carr, **Hongmin Yao**, Ramprasath Tharmarajan, Jing Mu, Sanjiv Shrestha, Ping Song, Ming-hui Zou. Inhibition of FAK-actin pathway by Indoxyl sulfate Suppresses Angiogenesis and Arteriogenesis in a mouse model of chronic kidney disease. Arteriosclerosis, Thrombosis, and Vascular Biology. Submitted.
4. Hao Xing, Ningren Cui, **Hongmin Yao**, Christopher M. Johnson, Chun Jiang. Cloperastine reduces morphine-induced respiratory depression in rats: Potential mechanisms for GIRK channel inhibition in locus coeruleus neurons. J Cell Physiol. Submitted.
5. Chen Zhang, Cui Ma, **Hongmin Yao**, Lixin Zhang, Xiufeng Yu, Yumei Liu, Tingting Shen, Linlin Zhang, Fengying Zhang, Xinxin Chen, Daling Zhu. 12-Lipoxygenase and 12-hydroxyeicosatetraenoic acid regulate hypoxic angiogenesis and survival of pulmonary artery endothelial cells via PI3K/Akt pathway [J]. American Journal of Physiology-Lung Cellular and Molecular Physiology, 2018, 314(4): L606-L616.

6. Cui Ma, Chen Zhang, Mingfei Ma, Lixin Zhang, Linlin Zhang, Fengying Zhang, Yingli Chen, Fangyuan Cao, Minghui Li, Guangtian Wang, Tingting Shen, **Hongmin Yao**, Yumei Liu, Zhenwei Pan, Shasha Song & Daling Zhu. MiR-125a regulates mitochondrial homeostasis through targeting mitofusin 1 to control hypoxic pulmonary vascular remodeling. Journal of Molecular Medicine, 2017, 95(9): 977-993.
7. Cui Ma, Yun Liu, Yanyan Wang, Chen Zhang, **Hongmin Yao**, Jun Ma, Lei Zhang, Dandan Zhang, Tingting Shen, Daling Zhu. Hypoxia activates 15-PGDH and its metabolite 15-KETE to promote pulmonary artery endothelial cells proliferation via ERK 1/2 signalling [J]. British Journal of Pharmacology, 2014, 171(14): 3352-3363.